WIRELESS CONDITION BASED MONITORING OF GAS TURBINE ROTATING COMPONENTS

FINAL TECHNICAL REPORT

Reporting Period Start Date: October 1, 2010
Reporting Period End Date: March 30, 2014

Joshua McConkey, Nancy Ulerich, Alex Bevly, Cora Schillig, and Anand Kulkarni

June 30, 2014

Work Performed under DOE Cooperative Agreement No:

DE-FE0005666

Prepared by:

Siemens Energy, Inc.
4400 Alafaya Trail
Orlando, Florida 32826

Arkansas Power Electronics International, Inc.
535 West Research Center Boulevard
Fayetteville, Arizona 72701

DISCLAIMER

ACKNOWLEDGEMENTS

Siemens Energy, Inc. acknowledges the Department of Energy, National Energy Technology Laboratory, for their support in this challenging project. We appreciate the reviews, comments, and suggestions that enhanced our project, as well as the funding support.

Arkansas Power Electronics International, Inc. was responsible for the high temperature electronics board development.

Rove Technical Services developed the first generation electronic power transfer system that was installed for H-Class engine tests

The University of California at Berkley worked in a parallel program funded by Siemens within which they developed high temperature electronics components such as a Zener diode.

Siemens had many contributors to this program. David Mitchell initiated the program. Getnet Kidane was the Principle Investigator for the about the first 18 months of the project. Joshua McConkey was the project lead for the last 24 months of the project. Cora Schillig supported engine integration and materials assessments. Ramesh Subramanian was instrumental in obtaining the program, and he consulted on materials aspects throughout the program. Anand Kulkarni led the spray on sensor work. Alex Bevly developed many aspects of the wireless power supply electronics.

ABSTRACT

This is the final report on the program entitled “Condition Based Monitoring of Turbine Blades Demonstrated in H-Class Engine” of cooperative agreement DE-FE0005666 between the United States Department of Energy (DOE) and Siemens Energy, Inc. (Siemens). The program period was October 1, 2010 to March 30, 2014. This program developed high temperature wireless monitoring technology for online condition assessment of turbine blades via advances in wireless technology for high temperature gas turbine applications. The goal of this technology is to significantly improve gas turbine testing, validation, and on-line monitoring methods by allowing wireless transmittal of critical rotating part information such as temperature and strain, making such measurements inexpensive and easily accessible. High temperature versions of electronics, wireless magnetic power transfer systems, antennas, cables, and interconnects were successfully developed in this project. Laboratory and spin rig tests proved the functionality of components and the integrated system.

TABLE OF CONTENTS

LIST OF FIGURES

LIST OF TABLES

LIST OF ACRONYMS

AC	Alternating Current
APEI	Arkansas Power Electronics International
BJT	Bipolar Junction Transistor
CCS	Computer Controlled Supply
DC	Direct Current
DOE	Department of Energy
FFT	Fast Fourier Transform
FOD	Foreign Object Damage
FY	Fiscal Year
g	One Gravity Force, 9.8 m/s^2
GHz	Gigahertz
JFET	Junction Field Effect Transistor
kHz	Kilohertz
LTCC	Low Temperature Co-fired Ceramic
MHz	Megahertz
MOSFET	Metal-Oxide-Semiconductor Field-Effect Transistor
mW	Milliwatts
nF	Nanofarad
NPD	No Pull Data (in wire bond pull strength tests)
RF	Radio Frequency
SiC	Silicon Carbide
SIT	Static Induction Transistor
SNR	Signal to Noise Ratio
TTF	Time to Failure
V_{AC}	Voltage, Alternating Current
V_{DC}	Voltage, Direct Current
V_{DS}	Voltage between Drain and Source (on a transistor)
V_{RMS}	Voltage, Root Mean Square
UC	University of California
µF	Microfarad

EXECUTIVE SUMMARY

This report describes the activities of the program entitled “Condition Based Monitoring of Turbine Blades Demonstrated in H-Class Engine” of cooperative agreement DE-FE0005666 between the United States Department of Energy (DOE) and Siemens Energy, Inc. (Siemens). This program developed high temperature wireless monitoring technology for online condition assessment of turbine blades via advances in wireless technology for high temperature gas turbine applications. The goal of this technology is to significantly improve gas turbine testing, validation, and on-line monitoring methods by allowing wireless transmittal of critical rotating part information such as temperature and strain, making such measurements inexpensive and easily accessible.

Siemens Energy, Inc. initiated the development of advanced sensor compositions, thin film sensor deposition processes, and a high temperature wireless telemetry system before this project was initiated. Laboratory, rig, and engine testing demonstrated the feasibility of the concepts. This cooperative program allowed the progression of these concepts so that the components and system for a wireless sensor system achieved a Technical Readiness Level (TRL) 4.

Figure 1 illustrates how the wireless system is envisioned to be used to transmit sensor information from rotating turbine components to the instrumentation outside the engine casing. An external power supply (located outside the engine) generates a current in stationary,

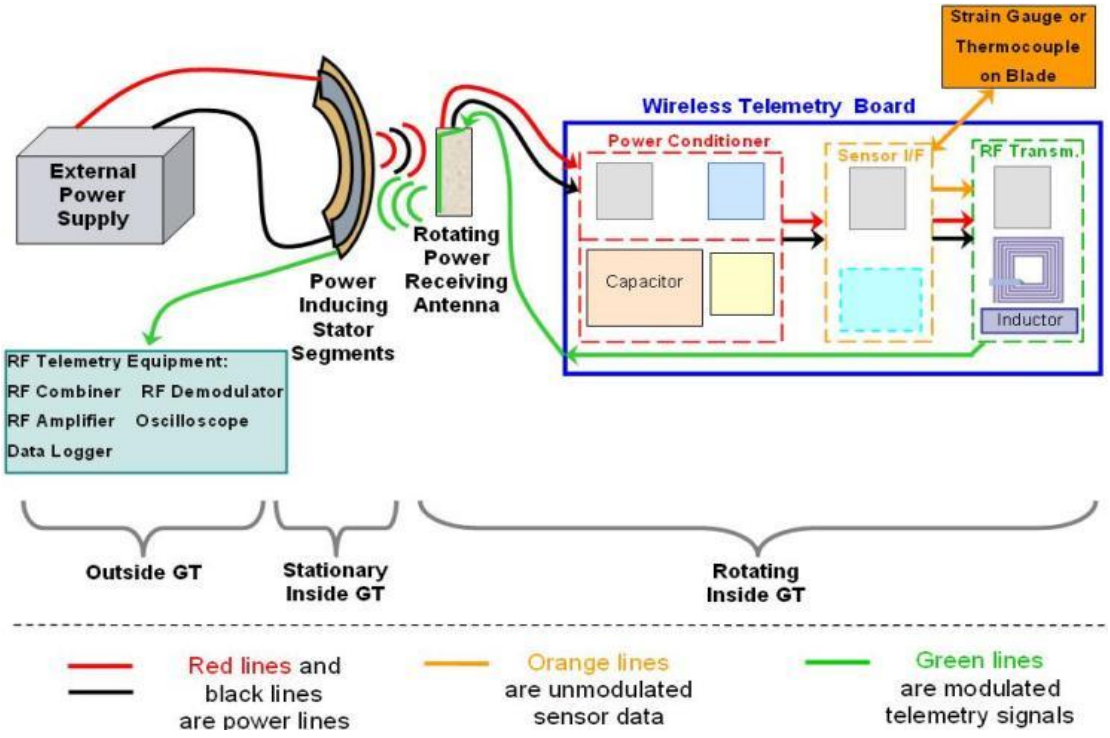

Figure 1: Wireless System Schematic

power-inducing stator segments (mounted on the stationary vane ring segments). The coils in this segment create a magnetic field. As the rotating power receiving antenna (located on the blade root) interacts with this magnetic field, it is inductively powered. This power is routed to the wireless telemetry board (located on the blade root). The wireless telemetry board communicates with temperature and strain sensors installed on the rotating blade. The wireless telemetry board also modulates the sensor data into an RF signal that is routed to the power receiving rotating antenna. The signal is then wirelessly transmitted to the stationary antenna embedded within the power inducing stator segments. This RF data is then routed outside the engine to instrumentation that stores the sensor data.

The harsh engine environment challenges this technology development. The wires connecting the external power supply must endure vibration and temperatures up to 600^{o}C. The power-inducing stator segments must endure significant vibration and temperatures up to 400^{o}C. Still, these conditions pale in comparison to the environment at the base of the blade. In addition to the vibration and 400^{o}C temperatures, those components also must endure g-loads of up 14,500g. Magnetics and electronics, in general, do not function at these temperatures. Many exotic materials, methods, and geometries were successfully implemented in our system development.

During this program, the following major accomplishments and research targets were achieved:

- A novel, high temperature magnetic inductive power supply was invented, implemented, and tested. It proved functional at temperatures exceeding 550°C and vibrations four times greater than that expected in large gas turbines.
- A wireless electronics board was manufactured that can function at temperatures up to 400°C. In order to develop this board, breakthroughs were made in wire bond strength, wire bond high temperature coatings, high temperature silicon carbide (SiC) transistors, and high temperature capacitors. Methods for increasing the board's resistance to temperature cycling fatigue and vibration-induced failure were invented and implemented.
- Thermal spray thermocouple sensors were implemented on large turbine blades.
- High temperature, high voltage, vibration-resistant wires were developed for carrying power to the inductive power supply inside the gas turbine.
- High temperature silicon carbide Zener diodes were manufactured at the University of California at Berkeley.
- Multiple furnace, vibration rig, and spin rig tests were performed on wireless system individual components and the integrated wireless monitoring system that assisted in development and achieved a TRL4 for the integrated system.

REPORT DETAILS

This program “Condition Based Monitoring of Turbine Blades Demonstrated in H-Class Engine” contained the following major technical tasks:

- Task 1 specifies the monitoring system integration approach and requirements.
- Task 2 performs scale up of thermal spray sensors, verifying properties of sensors on turbine blades, and manufacturing blades with sensors for H-Class engine testing.
- Task 3 develops and fabricates high temperature, high g-load wireless telemetry circuit boards for engine testing, and miniaturized circuit boards for spin tests at 450°C and 14,500g.
- Task 4 develops and fabricates a high temperature, high g-load wireless telemetry system comprised of induced power coils, a data transmission antenna, and an induced power receiver for use at 450°C and 14,500g.
- Task 5 develops and fabricates advanced silicon carbide (SiC) devices, matched transistor pairs, and integrated circuits.
- Task 6 prepares and performs demonstration tests of the system components in an H-class or equivalent gas turbine engine.

This report is split into three major sections: Experimental Methods, Results and Discussions, and Conclusions. In each of these sections, information will be presented as it pertains to each of the major tasks. Because many of the project tasks are independent in their development, this format allows the reader to follow the technical progress of each of the major tasks from the development of experimental methods, to results and discussions of tests, and finally to conclusions about the research. A final section is devoted to summary conclusions for the project as a whole (Section 3.7). If a reader wishes to follow the progress of the high temperature electronics board i.e., Task 3), for example, the information is found in Sections 1.3, 2.3, and 3.3.

1. EXPERIMENTAL METHODS

Experimental methods used in each task will be described in the following sections.

1.1 - TASK 1: DEVELOP CBM APPROACH FOR TURBINE BLADES

Task 1 specifies the monitoring system integration approach and requirements. This task defines the requirements of the data acquisition system and software that will integrate the wireless sensor data into the condition based maintenance system for remaining life predictions.

One of the most important parts of a turbine blade condition based monitoring system is the acquisition of temperature and dynamic strain from the surface of the blades. The development of the overall approach for obtaining the measurements from rotating turbine blades was conceptual in scope. Experimental methods for this development involved detailed assessments of the geometry and environment to define the engine's targeted installation points. Existing engine models and sensor readings were used to obtain expected temperatures, vibrations, strains, thermal expansions, g-loads, and chemical species concentrations for each potential installation point of each component of this wireless monitoring system. Optimal positions and routings were then chosen to assure placement of the wireless components in an optimum environment. Special consideration was also given to minimize the potential for foreign object debris (FOD) damage to the engine. Considerable analysis and design resources were devoted to securing components installed on rotating engine sections in order to preclude fragmentation and/or liberation.

The prototype version of this system is designed to be a standalone data collection system, for use in blade evaluation after validation tests. While post-test analysis is an important use of the data from this system, one key additional goal is to develop a real-time blade monitoring tool. Thus a methodology was developed to route the temperature and strain data in real time to the engine data collection system, effectively networking this remaining useful life (RUL) data. This approach will be discussed in detail in Section 2.1.

Once the blade surface measurements are obtained, one of the key uses of this data is the construction of 2D temperature and strain/vibration maps of rotating turbine blades. A methodology was developed to create 2D temperature maps on blades using infrared (IR) cameras. Because the infrared camera data is not accurate on an absolute scale, however, a methodology was developed for correcting these 2D maps using point thermocouple temperature measurements. These thermocouple measurements, made by the wireless system, will be used to define the temperature at a point or points on the blade. This thermocouple measurement would then be used to scale the IR camera data, making the 2D blade temperature maps more accurate. Similarly, strain gage data can be used to scale and further inform 3D blade vibration maps obtained from other data sources. These maps can then be used as empirical feedback mechanisms for computed

blade models. This data will also to be used to update remaining useful life (RUL) models. Because this project did not advance to the engine implementation stage, the blade mappings, model correction, and RUL model methodologies were not fully developed or implemented.

1.2 - TASK 2: SCALE-UP AND MANUFACTURING OF SPRAYED SENSORS

Task 2 performs scale up of thermal spray sensors, verifying properties of sensors on turbine blades and manufacturing blades with sensors for H-Class engine testing. The development of the sensor application methods was completed before this project began. During this program, the method was applied to large Row 4 turbine blades for an H-Class engine (see Figure 2).

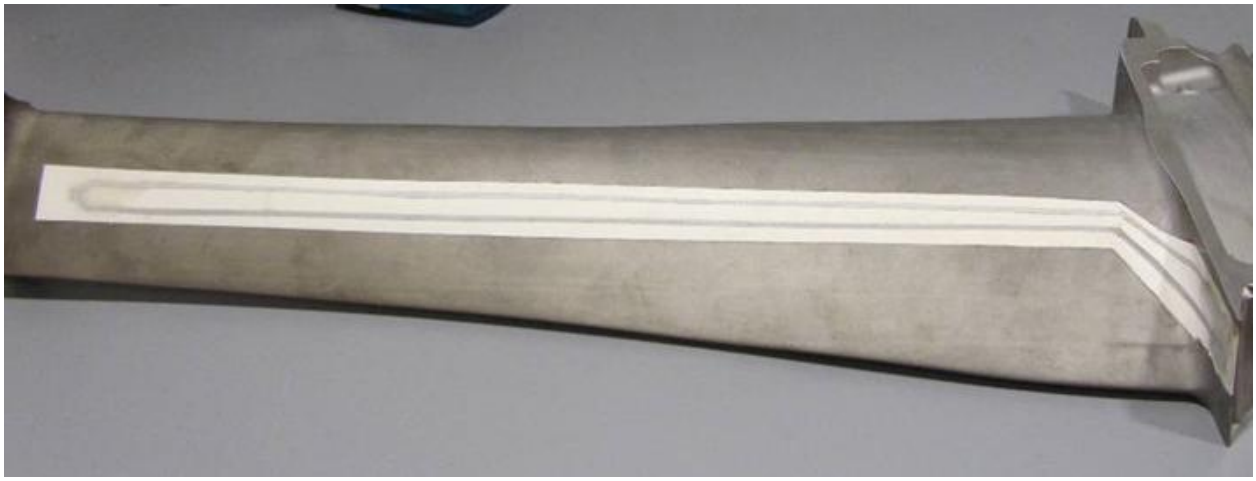

Figure 2: Spray-On Thermocouple Applied to Blade

The test methodology employed included installation of these blades with spray-on thermocouples into the H-Class engine. The Row 4 turbine blade row in the H-class engine was selected for demonstration because of ease of access to this row that would allow rotor instrumentation and disassembly at convenient phases in the engine tests. This blade row also allows larger spaces available for component installation. For this installation, the wireless telemetry system components must withstand temperatures up to 400ºC, and the g-load is approximately 14,500g. Row 4 turbine blades were instrumented with spray-on thermocouples and conventional strain gauges. Detailed installation and component drawings were produced for this installation, documenting the components and their locations, and design reviews were held.

Development of the strain gauge process occurred during Phase I of this project. The planned methodology of testing these devices was to install standard strain gages in proximity to the flame spray strain gages, and compare the results. The repeatability and hysteresis of the flame spray strain gages were tested. Unfortunately, consistent strain gauge performance was not produced with the spray on technique, so spray on strain

gages were not installed on engine blades. We planned to use standard strain gages with the wireless system in all lab, rig, and engine tests.

Unfortunately, the H-class Blade 4 engine test had to be cancelled because the first version of the power inducing stators did not survive the engine environment. Delays related to durability and availability of electronics boards prevented subsequent engine testing during this project. Engine validation could not, therefore, be completed. Bench tests measured the voltage produced as the spray-on thermocouple was exposed to different temperatures using a flame source and a standard thermocouple was used as a baseline measurement.

Methodologies of production, adhesion testing, and preliminary lifing were developed and performed by Siemens before this project was initiated. A description of that method, therefore, falls outside the scope of this report.

Because no engine test was accomplished, and accuracies were not sufficient, the spray-on sensor technologies were not scaled up or brought to high volume manufacturing.

1.3 - TASK 3: ROBUST 450^{O}C WIRELESS TELEMETRY CIRCUIT BOARD

Task 3 develops and fabricates high temperature, high g-load wireless telemetry circuit boards for engine testing, and miniaturized circuit boards for spin tests at 400°C and 14,500g. This task is subcontracted to Arkansas Power Electronics International, Inc. (APEI).

The experimental methodologies involved in creating and testing these complex electrical boards span many different areas of expertise. APEI performed the majority of this work on the subcomponent level; Siemens and APEI worked together to test the boards in an integrated fashion at high g-loads and temperatures. In this section, descriptions of testing procedures will begin at the lowest sub-component level, and then proceed to experimental methodologies for the larger components and integrated systems. The subcomponent experimentation focused on transistors, capacitors, inductors, and bond wire strengthening. The component-level testing involved board cracking investigations, temperature exposure tests, integration testing, and spin rig tests.

Silicon Carbide Transistor Testing Methodology

The most important component of the board is the silicon carbide transistors. These were obtained from third party vendors, but they are not off-the-shelf components, being custom-designed parts. A methodology was developed at APEI to measure the parameters of each custom-made transistor so that matching pairs could be found for board construction. This matching pair circuit geometry is necessary because only p-type transistors can currently be manufactured, and matching pair configuration is required for accurate amplification given that limitation. In addition to the parameter matching furnace testing, long term parameter testing was also performed on the transistors.

APEI used a high temperature probe station to obtain the current-voltage (I-V) curves over temperature for each silicon carbide transistor. The test setup utilized the Agilent B1505A power device analyzer / curve tracer in the APEI Electronics Assembly Laboratory. This system is used in conjunction with a hot plate to allow temperature range testing. For connection purposes, the devices were aligned in a grid on a piece of ceramic to facilitate probing the backside drain connection. Using the microscope mounted on the probe station, one probe was landed on each of the source and gate pads and another probe was landed on the ceramic substrate. The curve tracer was set up to run the characterization test at two different voltage from drain to source (V_{DS}) values, 25 V and 40 V, and then to auto-export the data for later analysis and matching. Once this process was complete for the entire grid of devices at room temperature, it was repeated at 300°C and 450°C. The devices were characterized in batches with a manageable grid size (approximately 15cm×15cm grids for this quantity) because of how crucial it is to maintain the identity of each device for later matching purposes. Example results of this testing for one type of silicon carbide transistor are shown in Figures 3 and 4. Results of this transistor testing are described in Section 2.3

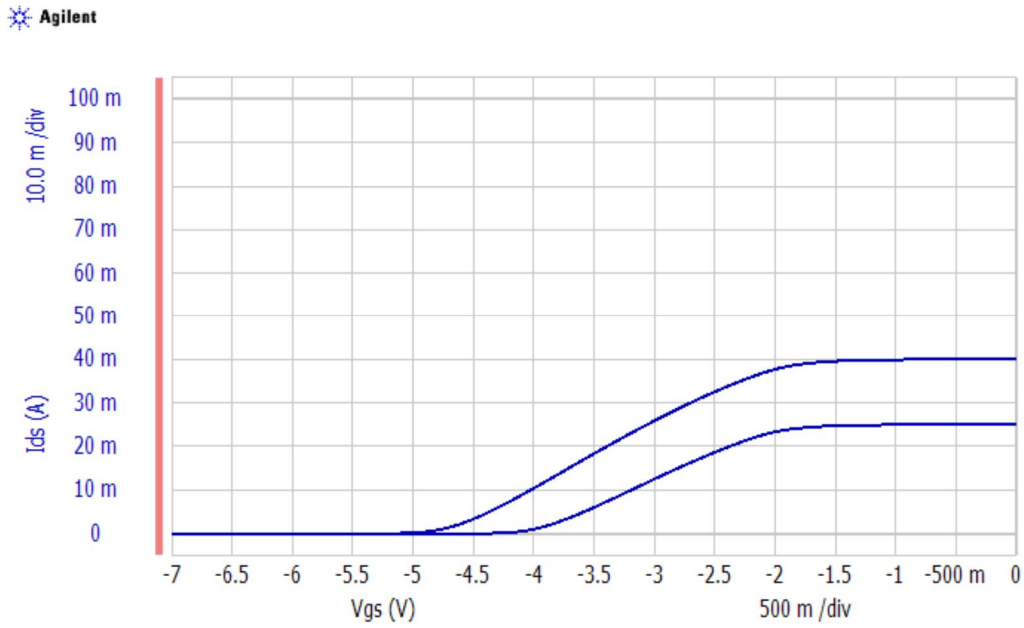

Figure 3: SiC Transistor I-V Curves at 25 & 40V at 25ºC

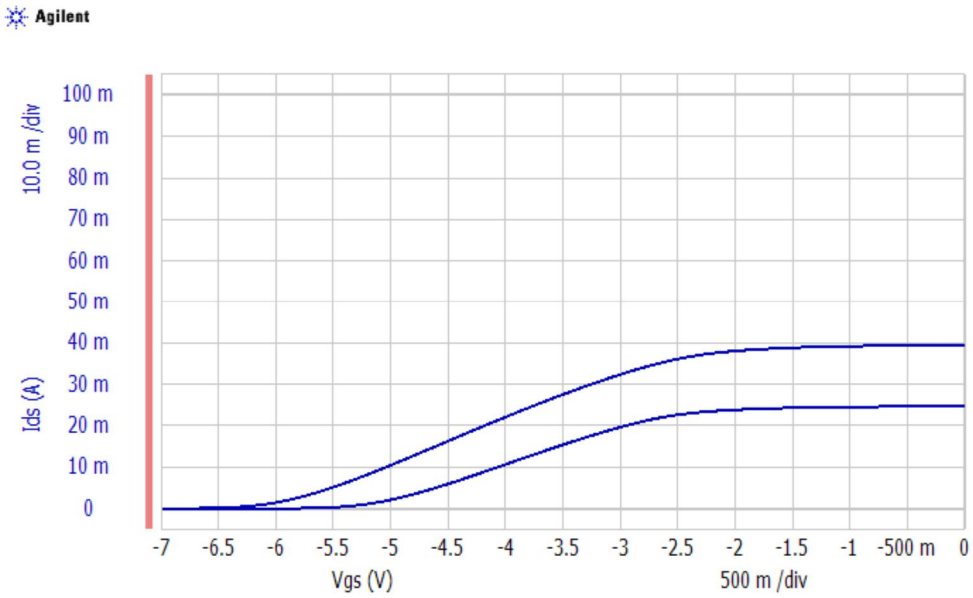

Figure 4: SiC Transistor I-V Curves at 25 & 40V at 450ºC

High Temperature Capacitor Testing Methodology

Another important component for the electronics boards is the capacitors. Extensive effort was put into procuring insulator-on-glass capacitors that provide consistent values and low current leakage over the entire temperature range. Another potential weakness of these components is aging-related increases to the current leakage. In order to compare different vendor offerings, APEI developed a low temperature co-fired ceramic (LTCC) furnace rig. LTCC is a ceramic widely used for high temperature electronics mounting. This rig had three connections for each capacitor, one for each of the two capacitor electrical ports and a ground connection. The capacitance of each element could, therefore, be measured, as well as the current leakage to ground. Figure 5 shows the layout of this APEI designed and fabricated capacitor test board, and Figure 6 shows a populated capacitor test board during testing in a furnace.

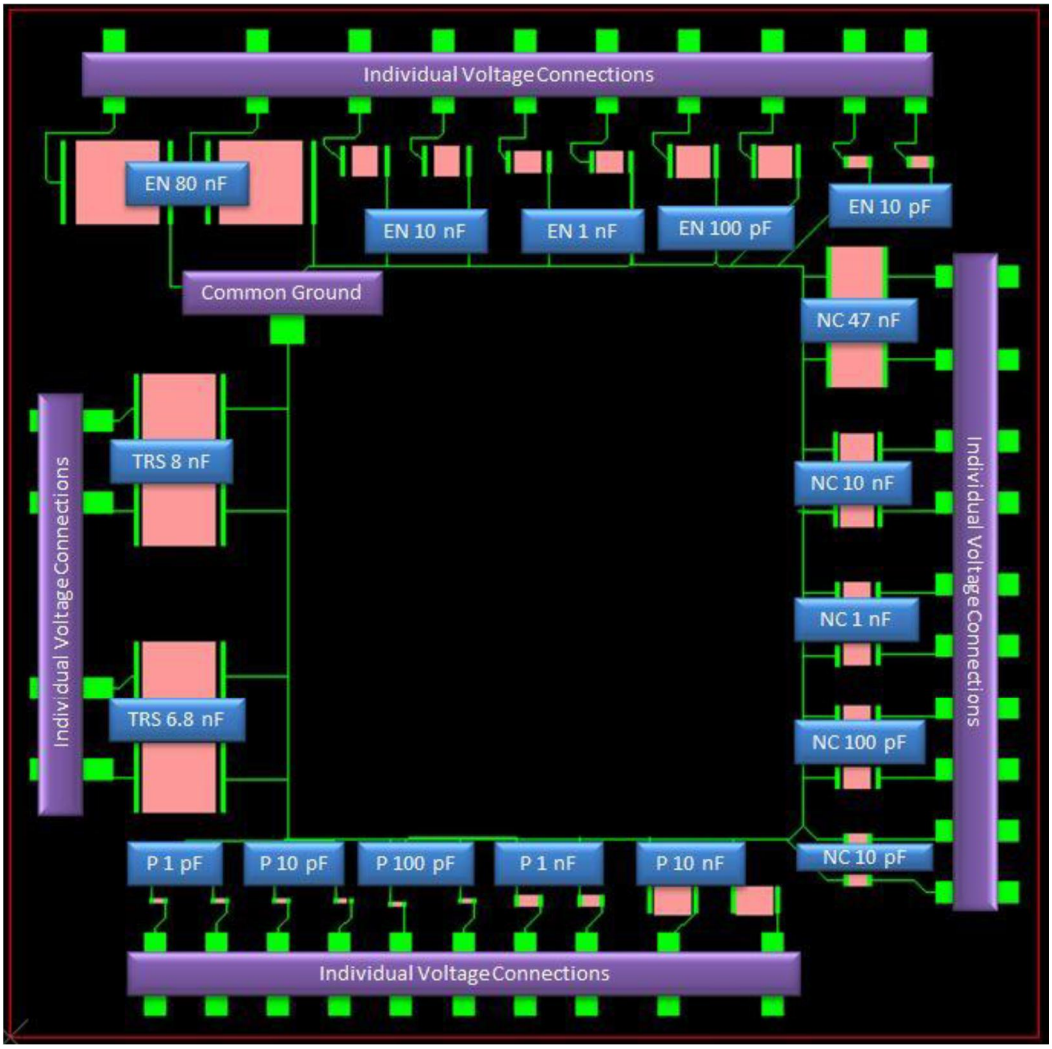

Figure 5: Capacitor Test Board Layout

After the LTCC board was produced, it was populated with the test capacitors. The capacitors were attached to the substrate using a ceramic potting compound and the electrical connections between the capacitors and the board were created using 1 mil gold wire bonds. Each lead wire was created using ~1m of 0.127mm diameter ceramic coated California Fine Wire. The lead wires were attached to the substrate using Pyroduct 597-A silver filled epoxy. The lead wires were routed through the top of the test furnace and attached to individual test channels on a breadboard switching matrix that was developed specifically for this test. This configuration is shown in Figure 6.

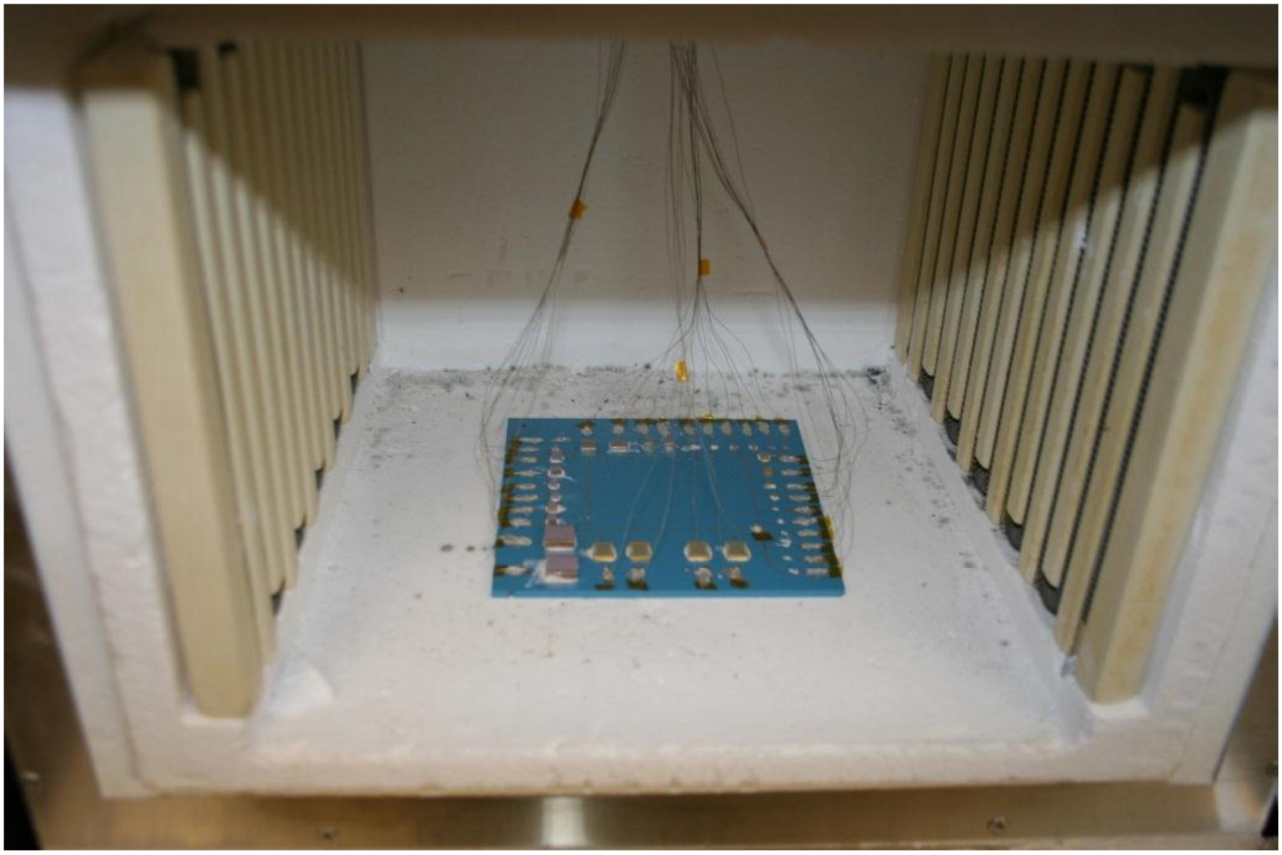

Figure 6: Populated Capacitor Test Board in Furnace

The schematic for the entire test setup is shown in Figure 7, while the physical switching matrix is shown in Figure 8. The system is controlled by a LabVIEW program via the NI 9104 digital output module and the 0-5V computer controlled supply (CCS). Each capacitor is connected to the 30V bias voltage though separate p-channel MOSFETs (part number ZVP3306A). The split 5V and 25V supplies used to achieve the bias voltage were necessary to properly bias the MOSFETs, so they could be driven with the 5V output from the digital module. During the majority of the testing, the CCS is kept at 0V to create a V_{GS} of -5V and ensure that the transistors are in the on-state. In this configuration, the bias voltage is applied across all the capacitors. Once every 10 minutes, the CCS is switched to 5V to create a V_{GS} = 0V and turn the MOSFETs off so that none of the capacitors are biased. The LabVIEW program uses the multiplexing circuitry to apply 0V to the gate of a single MOSFET, which biases the selected capacitor at 30V, at which time the ammeter measures the leakage current. The LabVIEW program reads the ammeter and records the leakage current in a log file. Over ~40 seconds, the setup switches to each capacitor and logs its leakage current. The CCS is then switched back to 0V to bias all the capacitors. It is important to keep the capacitors under bias for the maximum amount of time because it gives worst case stresses in the dielectric material.

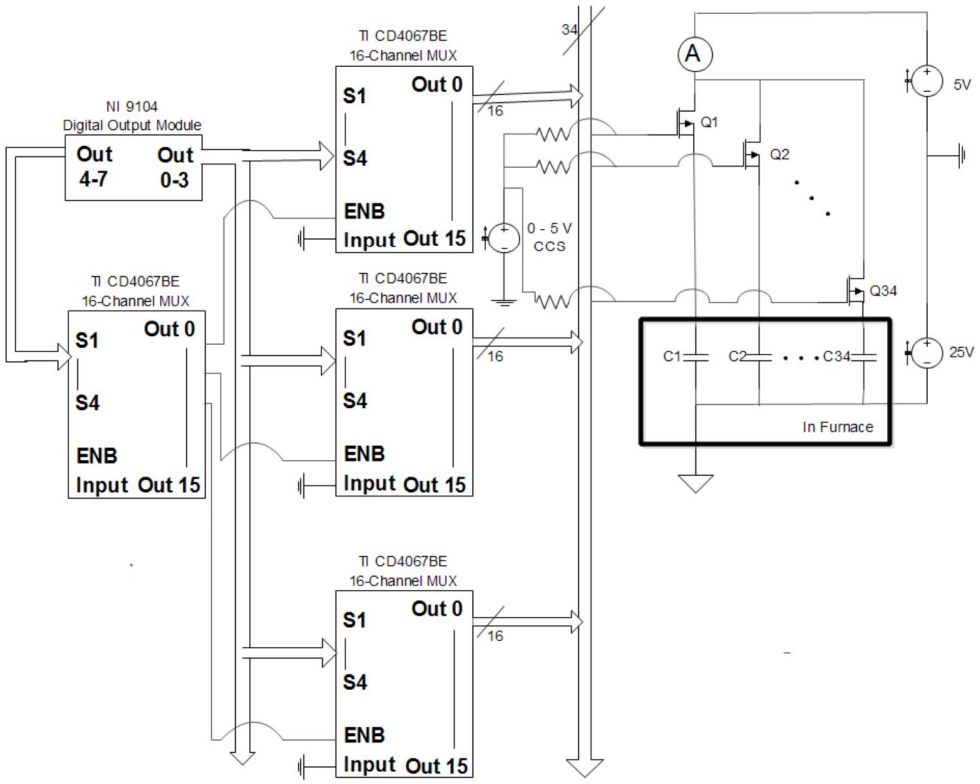

Figure 7: Capacitor Test Schematic

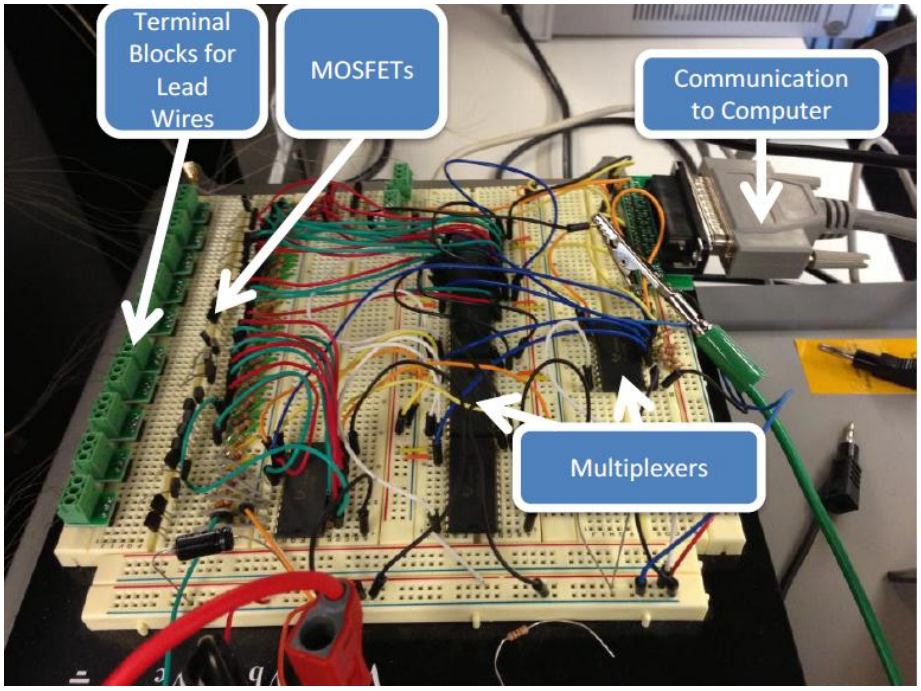

Figure 8: Capacitor Test Station Switching Matrix

The multiplexing circuit is driven by the digital output module, configured to provide two 4-bit output channels. The Texas Instruments CD4067BE 16-channel multiplexer was chosen to provide the switching capabilities. The first 4-bit output channel is used to operate the select pins on a single multiplexer, designated the drive multiplexer. The second 4-bit output channel is used to drive the select pins on three other multiplexers. The drive multiplexer is used to switch the enable pins on the other three multiplexers to set the active device. The input to the multiplexers is set to 0V to provide a low impedance path to ground for the gate of the desired MOSFET. All of the other multiplexer output pins (except the selected one) provide a high impedance path, so the gate voltages are driven through the pull-up resistors.

Results of this capacitor testing are described in Section 2.3

Inductor Encapsulation Testing Methodology

Many inductors on the electronics boards are implemented by applying one dimensional spirals of metallization on the Low Temperature Co-fired Ceramic (LTCC) substrate. When the board was exposed to large temperature variations, the thermal expansion differences between the LTCC and the gold metallization caused delamination of these long paths (see Figure 9). This resulted in loss of functionality of the board. A method of glass encapsulation was proposed to address this issue. In order to test whether this process solved the issue, a testing methodology was designed and implemented.

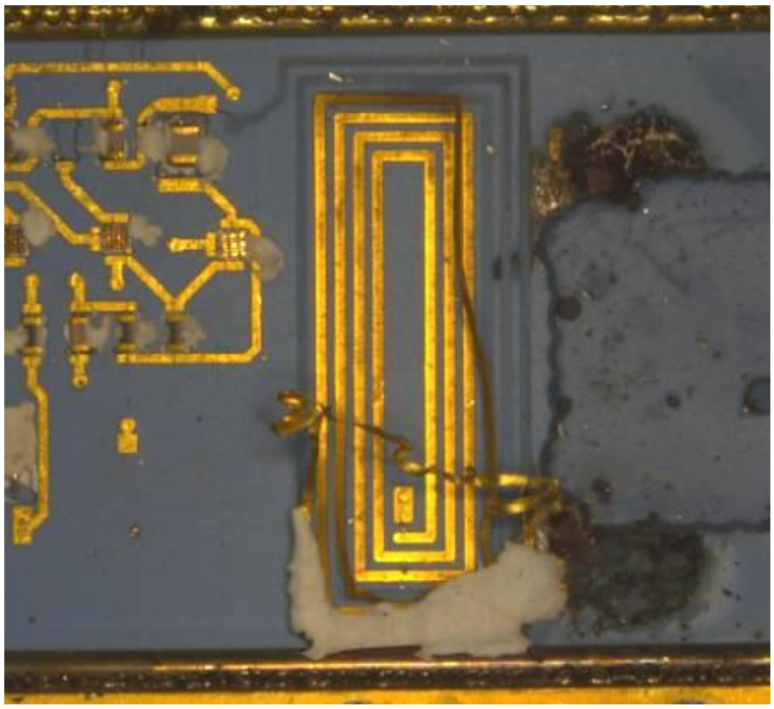

Figure 9: Delaminated Spiral Inductor on Electronics Board

For this task, APEI fabricated two separate large LTCC boards with a number metal trace spiral inductors on each (see Figure 10). The inductor traces were created by screen printing a gold thick film, DuPont TC502, onto the surface of the top ceramic layer. The layers were then laminated together and fired to create a single, monolithic substrate. Once the substrates were complete, the inductors were electroplated with approximately 25 microns of gold. Both boards utilized the same layout; a picture of the encapsulated version can be seen in Figure 10. One board was a control, and the other was treated with a glass encapsulant to protect the inductors from delamination.

APEI engineers created parameters for optimally applying and processing the encapsulant. After the gold-plating process was complete, the glass encapsulant was applied to the LTCC substrate as a post-fire paste via screen printing. Upon application, the substrate was then re-fired with a peak temperature of 850ºC to sinter the encapsulant. A zoomed-in comparison of an un-encapsulated versus an encapsulated inductor can be seen in Figure 10.

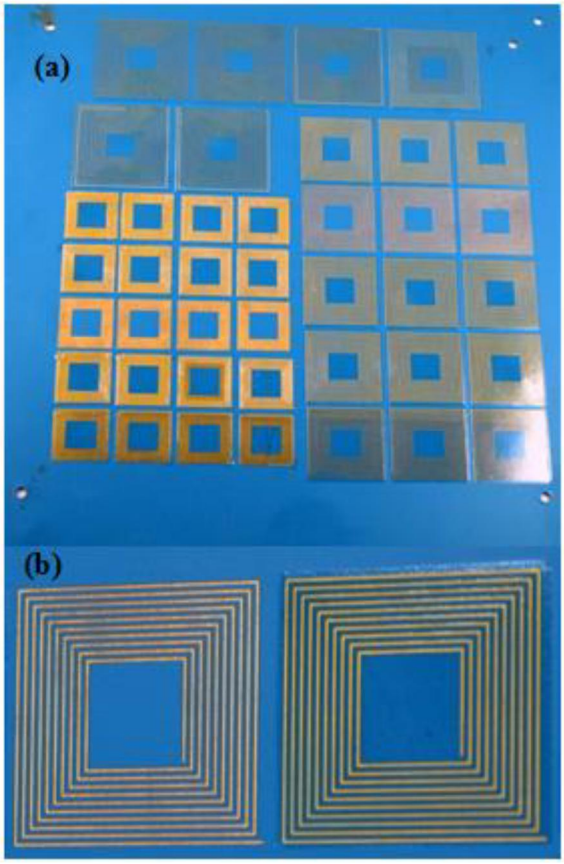

Figure 10: An Inductor Test Board (a) with Zoom-In Comparison View (b)

A thermal cycling setup and profile was created to ensure that the boards would experience a significant thermal shock. The testing was conducted in a Vulcan oven, with a thermocouple attached to each board for continual monitoring of each board's temperature. Both of the boards were cycled at the same time to ensure that they were

exposed to the same cycling profiles. The boards were heated to 450ºC. Once the maximum temperature was reached, the boards were thermally aged for 10 minutes. Once the hold time elapsed, the boards were removed from the oven and placed onto a large heat sink with an attached fan for rapid cooling to 40ºC. The cycle was then repeated. Both boards underwent a general visual inspection after every cycle, in order to note any changes. In addition to this general inspection, each individual inductor was inspected and photographed using APEI's Keyence VHX–400 digital microscope system every 10 cycles to provide multiple comparison points during the analysis.

A total of 100 thermal shocks were completed. Results of inductor delamination testing are discussed in Section 2.3.

Bond Wire Testing Methodology

In an engine environment, the electronics boards will see g-loads in excess of 14,000g. Extensive testing has shown that bond wire lifting and deformation is a major cause of board failure during these high g-load tests. There are a high number of bond wires on each board (~200), and the failure of even one of these may results in a major loss of functionality. In order to mitigate this risk, APEI performed a number of bond wire material improvements, bonding strength optimizations, and post-bond modifications.

After optimizing the bond wire material and the bond scrub strength, it was deemed necessary to further increase bond reliability via a specialized bond wire coating. This was expected to drastically increase the bond wire stiffness and pull strength, thereby mitigating bond wire deformation and lifting. This section will describe the methodology by which this new coating mechanism was tested. At first, it was unknown exactly how thick the bond wire coating should be. Two rounds of testing were completed.

For this initial testing, four LTCC substrates were produced and each was mounted in a metallic package; an example of the product is shown in Figure 11. Each board was bonded with 1000 test wire bonds. The bonds were created from 10µm x 20µm platinum ribbon. The wire bond settings for power, time, and force were kept consistent through the bonding process across each board. The length and loop height setting were controlled according to the wire bond group number shown with red background in Figure 11).

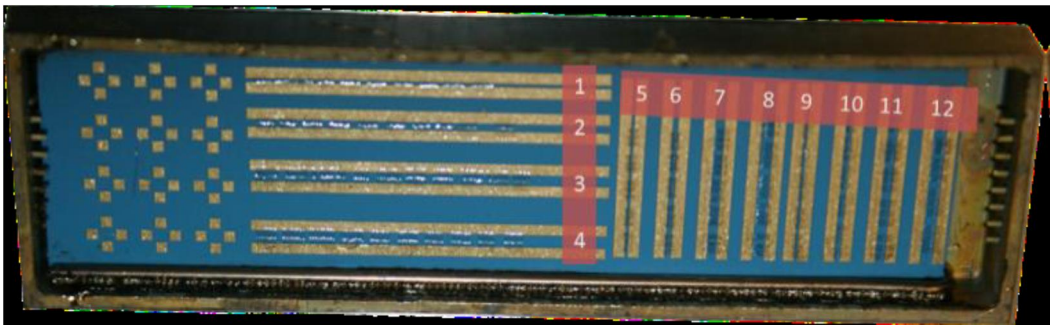

Figure 11: Bond Wire Test Board Mounted in Metallic Package

The pads in the plus sign (+) pattern on the left side of the board were used for conductivity tests. Two of each set were bonded together and the connectivity of these were checked after each set of thermal cycles. This test ensured that the thermal expansion of the bond wire coat did not separate the bond from the substrate. Table 1 shows the bond wire lengths, bonder settings, and the total number of bonds in each section that is enumerated in Figure 11.

Group	Center to Center Distance (mil)	WB Step Setting	WB Loop Setting	Total Number of Bonds
1	48.1	2.7	2.8	100
2	62.1	3.4	2.8	100
3	72.2	4.0	2.8	100
4	79.3	4.3	2.8	100
5	46.2	2.0	2.0	75
6	54.2	2.0	2.0	75
7	65.9	3.7	2.0	75
8	76.9	3.7	2.0	75
9	46.2	2.0	2.4	75
10	54.2	2.0	2.4	75
11	65.9	3.7	2.4	75
12	76.9	3.7	2.4	75

Table 1: Bond Wire Lengths, Bond Settings, and Numbers for Initial Test Board

After wire bonding, the boards were sent to a vendor for bond wire coating deposition. Each board was coated with a different thickness. Board 1 was coated with 2μm, Board 2 was coated with 5μm, Board 3 was coated with 12μm, and Board 4 was coated with 25μm. The original plan called for no 5μm board, and a 50μm board instead. Discussions with the vendor indicated coating anything over 25μm could be problematic, so it was replaced with the 5μm board. This type of coating takes place via chemical vapor deposition (CVD), so all exposed surfaces were uniformly coated. Figure 12 shows wire bonds in Group 4 of Board 4 before and after being coated with a layer 25μm thick.

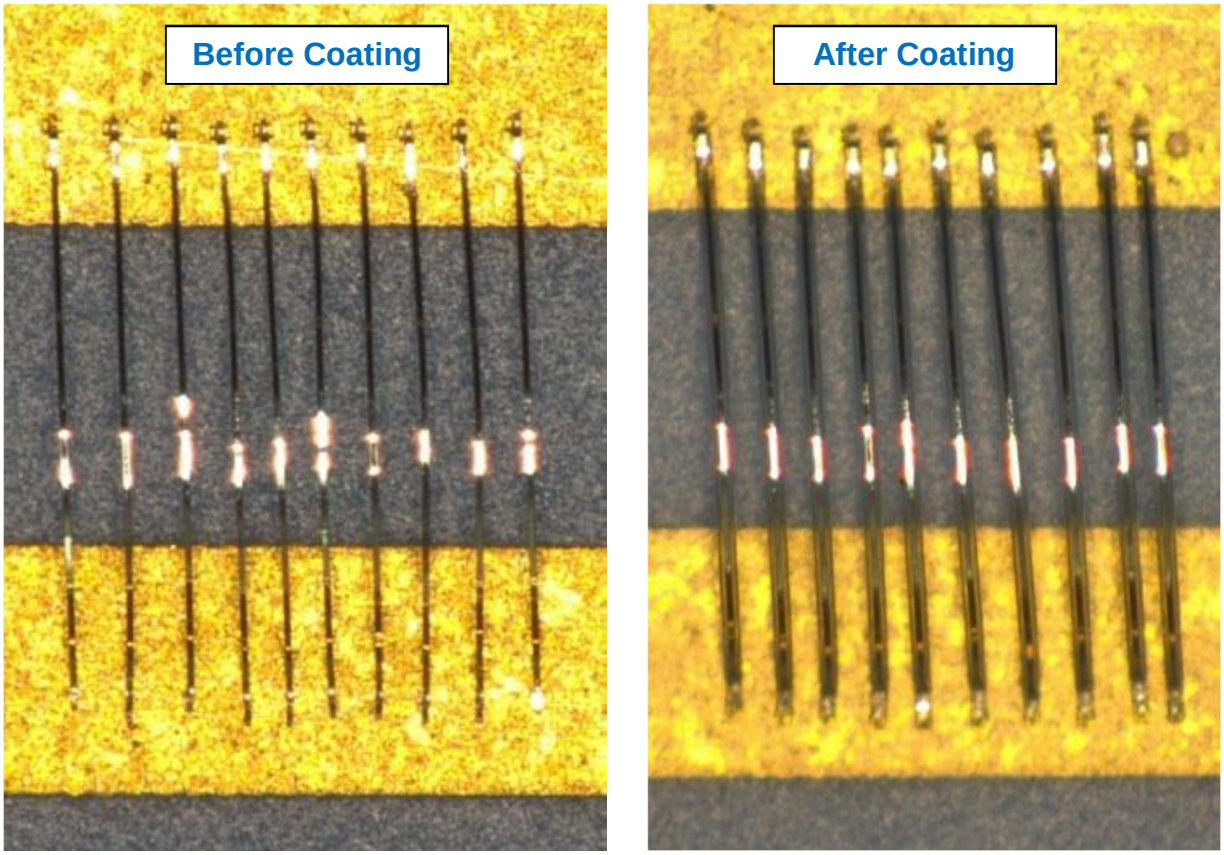

Figure 12: Bond Wires Before and After 25µm Coating

The strength of the wire bonds was determined through pull testing using a Dage 4000 multipurpose reliability tester. Pull tests were performed on wire bonds from each group on each board before coating, after coating, and after every 10 thermal cycles up to 50 total cycles.

The thermal cycling took place in a computer-controlled Vulcan box furnace. The furnace automatically cycled between 450°C and 50°C. The control thermocouple (TC) was spot welded to a previously used metallic package. This ensured that the thermal mass attached to the control was nearly identical to that of the boards under test. The board reached the maximum test temperature of 450°C in 20 minutes. The cool down time to reach 50°C was about 2.5 hours.

During this testing, it became clear that the selected coating did not survive temperatures up to 450ºC. The known engine environment at the electronics board installation point had recently been shown via advanced modelling to reach temperatures of only 385ºC. The combined goal of these tasks was to explore the effects of coating wire bonds. The initial task tested coated wire bonds with respect to thermal cycling. The thermal cycle testing indicated that the coating initially increased the strength of the wire bonds, but after repeated 450°C exposure, the coating provided no measurable increase in bond strength. The original goal of the current task was to determine if the coating would

increase the integrity of the wire bonds during g-loading. The results from the first thermal cycle tests necessitated adding additional thermal cycle testing.

A second thermal cycle experiment was performed to determine if the coating could be beneficial to Siemen's applications with the lower operating temperature (380 – 400°C), as further engine modelling in 2013 indicated that the maximum temperature the board would see in the engine was close to 385 °C instead of the originally modelled 450°C. The initial testing indicated that the most effective coating thicknesses were greater than 5µm, but no greater than 12µm. Coatings less than 5µm did not significantly increase the bond strength, but coatings greater than 12µm added significant mass to the wire bond that caused sagging at higher temperatures and such excess mass was thought to possibly be detrimental during g-loading. Two test boards were coated with 8µm and two test boards were coated with 12µm of the material. One set of boards was thermal cycled at APEI, Inc. facilities and the other was sent to Aerodyn Engineering in Indianapolis for spin testing.

For this wire bond strength test, five LTCC substrates were produced and each was mounted into a metallic package using a laser welded bezel. Each board was bonded with 400 test wire bonds. The wire bonds intended for thermal cycle testing were created from 10µm X20 µm platinum (Pt) ribbon. Half of the wire bonds intended for spin testing were created from the same PT ribbon. The other half were created using 25µm gold (Au) wire. Previous heated spin tests of Au wire bonds revealed that Au is an unsuitable material for high-temperature, g-loaded electronics. Pt wire bonds do not readily deform when subjected to 400 °C and 14,000 g's; therefore, the addition of the Au wire bonds was necessary to help determine the coating's effectiveness. The Pt wire bonds were still necessary on the spin test boards to determine if the coating added too much mass and therefore deteriorated g-load performance. Wire bond settings for length and loop height were kept consistent for every wire bond during the test. The settings for force, time, and ultrasonic power were determined by the material of the bond (Pt or Au).

After wire bonding, the boards were coated. Boards TC-12 and ST-12 were coated to a thickness of 12µm. Boards TC-8 and ST-8 were coated to a thickness of 8µm. The coating takes place via chemical vapor deposition (CVD), so every exposed surface was uniformly coated. Figure 13 shows uncoated wire bonds on ST-12 and wire bonds in the same group after 12µm of coating. One control board was left uncoated to have a direct comparison for the coating's effect on pull strength.

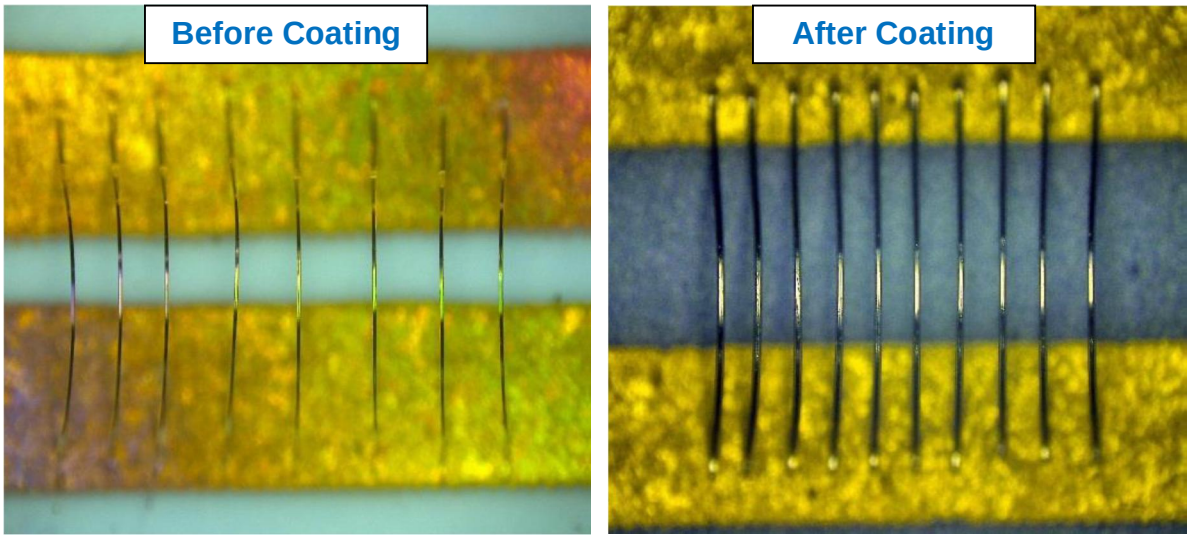

Figure 13: Bond Wires Before and After 12µm Coating

The strength of the wire bonds was determined through pull testing using a Dage 4000 multipurpose reliability tester. Pull tests were performed on 50 wire bonds from each thermal cycle board (TC-8 and TC-12) and the control board (C) before coating, after coating, and after every 10 thermal cycles up to 50 total cycles.

The thermal cycling took place in computer-controlled Vulcan box furnace. The furnace automatically cycled between 400 °C and 50 °C. The control thermocouple (TC) was spot welded to a previously used metallic board package. This ensured that the thermal mass attached to the control was nearly identical to that of the boards under test. The board reached the maximum test temperature of 400 °C in 15 minutes. The cool down time to reach 50 °C was about 2.25 hours.

The spin test took place in Aerodyn Engineering's spin test rig. Boards ST-8 and ST- 12 both underwent spin testing. Microscope photographs were taken at 100X before and after spin testing to inspect for wire deformation.

Results of wire bond strength testing are discussed in Section 2.3.

Integrated Electronics Board Furnace Testing Methodology

Once the boards are fully assembled, they are tested in a laboratory setting. This section describes the methodology for measuring the functions of the board over temperatures from 25ºC to above 400ºC

The bench tests were performed using a hot plate setup. The transmitted frequency versus reference thermocouple temperature curve used for calibration is shown in Figure 14. What appears to be hysteresis in the data is most likely a difference in heating and cooling rates between the transmitter board and the reference thermocouple. The polynomial regression used for later test interpretation is shown red. The time to heat up

to 450°C was about 32 minutes and the cool down time back to 70°C was 62 minutes. The board encodes temperature information via changes in frequency. To test this calibration data during operation, a large ceramic block was added between the seal plate and the hot plate in order to change the thermal properties of the system. A similar methodology was used to measure the functionality of the strain gage board.

Results of the board temperature tests are discussed in Section 2.3.

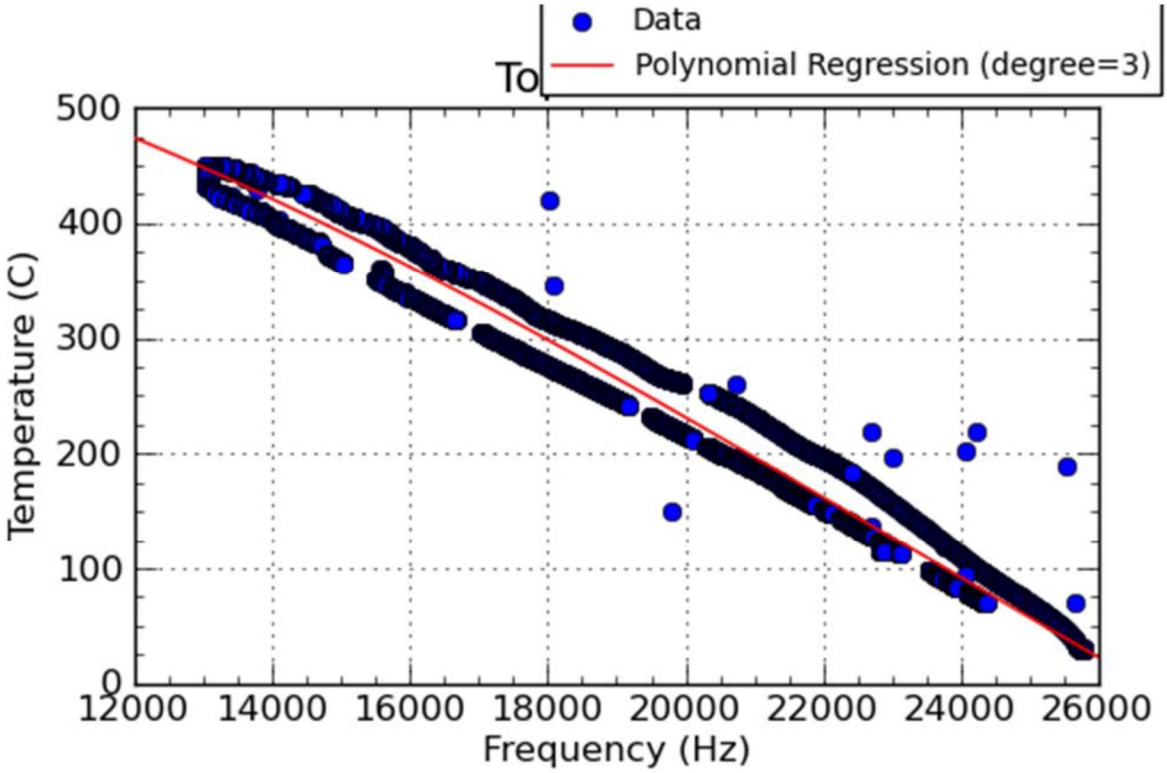

Figure 14: Frequency vs. Temperature Collected for Thermocouple Board Calibration

Integrated Electronics Board Spin Rig Testing Methodology

In order to simulate the high g-loads the board is expected to see in an engine, spin rig tests were performed on the electronics boards. These spin tests were accomplished at the Aerodyn spin rig in Indianapolis, Indiana. The electronics boards were installed into their metallic packages and tested over temperature. Then these packages were wrapped in alumina fiber mesh for vibration protection, and wrapped in high temperature tape in order to keep the fiber mesh in place (see Figure 15). This was then inserted into the custom seal plate. This seal plate has a mechanical interface with the electronics board which is identical to the engine installation. The wrapped board is covered with a metallic lid which is bolted in place.

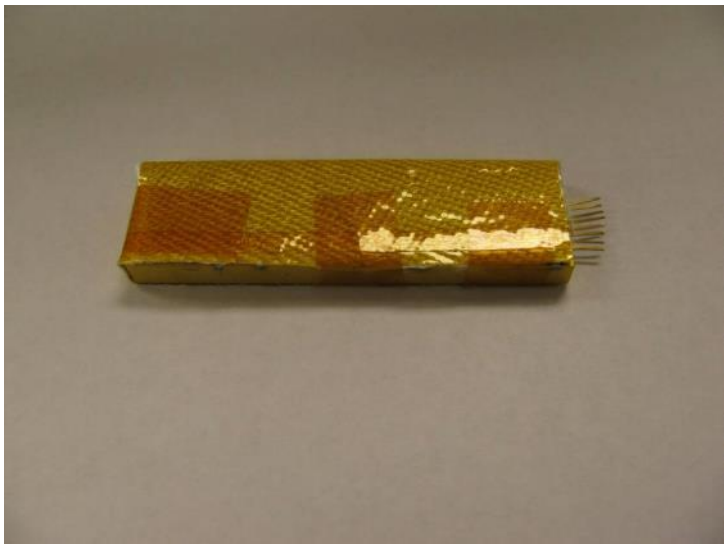

Figure 15: Electronics Board Wrapped in Alumina Mesh and Tape

Preliminary integration testing was performed by supplying APEI with a metallic seal plate (extremely similar to engine installation geometry) containing a magnetic receiver. This interfaces with the electronic board, providing it power. The electronics board transmits its radio frequency (RF) data signal to the magnetic receiver. An external magnetic power supply sends power to the magnetic receiver. In this way, testing was performed to ensure proper integration before the entire system was configured.
The seal plate is bolted to a spin disk which is mounted in the spin rig. One set of spin tests was performed solely to test the mechanical strength of bond wires. In this case, no electrical connections were made to the spinning test board. However, other tests were functional tests. In these cases, electrical connections are made with the board and routed across the spin disk and out of the spin rig via a slip ring. These electrical connections are used to monitor the functionality of the board during the spin test. See Figure 16 for an example of the electrical connections on the electronics board. When spun at full speeds, the g-load imparted to the electronics board approaches 14,500g. Therefore, the electrical connections must be reinforced with high temperature cement. Typical electrical connection configuration for a full system spin test is shown in Figure 17.

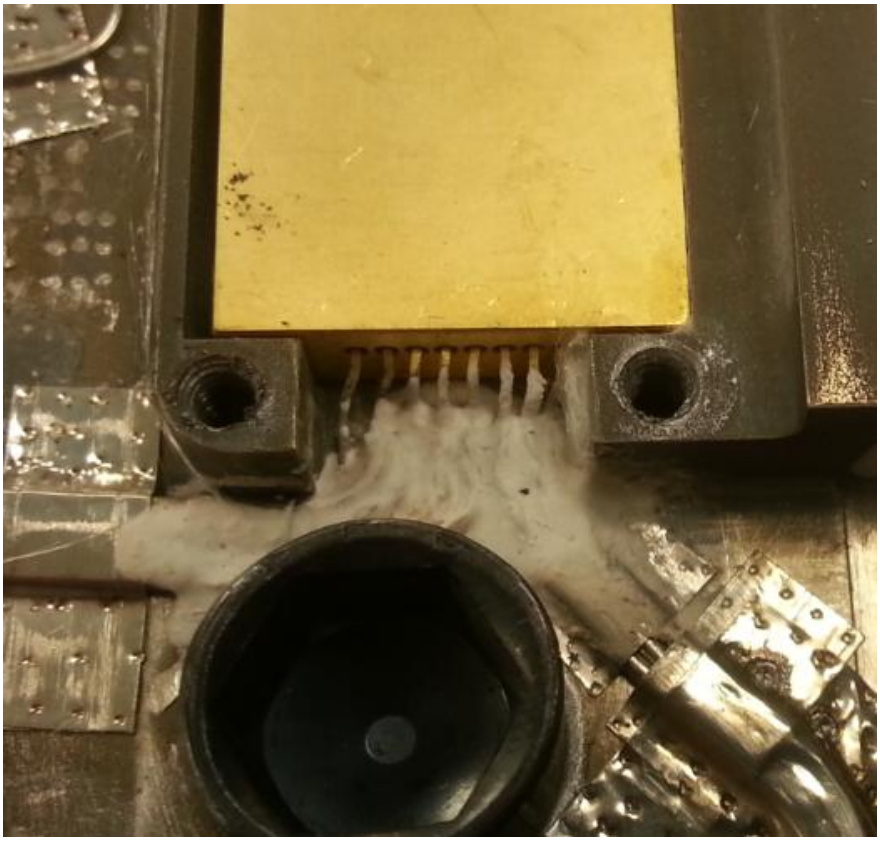

Figure 16: External Electrical Connections of Electrical Board on Seal Plate

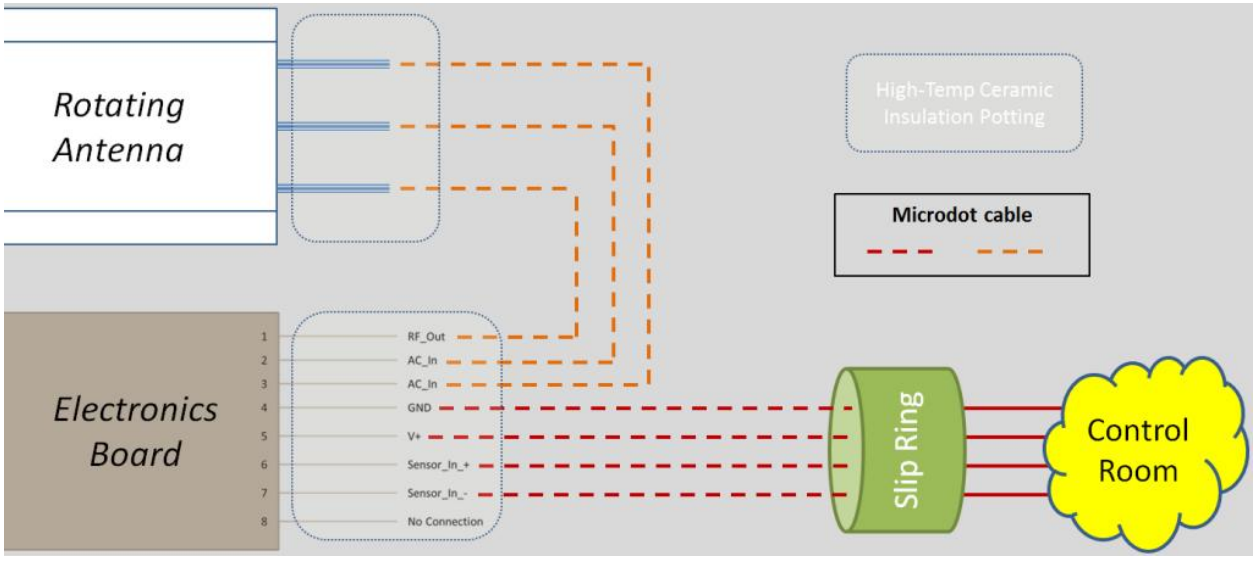

Figure 17: Seal Plate Connection Schematic for Full System Spin Test

The spin test rig at Aerodyn is also heated electrically, and is capable of reaching internal temperatures of 400ºC. Typical spin test procedure is to bring the rig to a slow speed

resulting in 500g, and increase the temperature from 25ºC to 350ºC or 400ºC. Then the speed is slowly increased and held at intervals of 500 or 1000g until the target of 14,500g is reached. A dwell at that speed then occurs. During this entire time, multiple parameters of the system are read in the control room and from supporting electronics. Table 2 lists the parameters measured during full system spin tests. SNR is signal to noise ratio, the measure of the strength of the RF carrier vs. the noise floor.

Data Source	Measurement
Spin Rig Control Instruments	Speed (g-load)
Spin Rig Control Instruments	Temperature
Thermocouple Board	Output RF Carrier & SNR
Thermocouple Board	Rectified Voltage
Thermocouple Board	Input Voltage (simulates TC)
Strain Gage Board	Output RF Carrier & SNR
Strain Gage Board	Rectified Voltage
Strain Gage Board	Input Voltage (simulates SG)
Power Supply	Input Power
Power Supply	Reflected Power
Power Supply	Input Current
Power Inducing Stator	Coil Impedance
Power Inducing Stator	Coil-RF Line Resistance
Power Inducting Stator	Coil-Ground Resistance

Table 2: Typical Measurements and Sources during a Full System Spin Rig Test

Results of all the electronics board spin tests are discussed in Section 2.3.

1.4 - TASK 4: ROBUST 450^{O}C WIRELESS TELEMETRY SYSTEM

This section describes the experimental methods used to test the wireless telemetry system. The wireless telemetry system discussed in this section involves two functionally different systems, the wireless power induction system and the RF telemetry antenna system. It does not include the wireless electronics board, though it does interface with the electronics board.

The wireless power induction system is responsible for transmitting electrical power from outside the engine to the stationary power inducing stators (via high temperature, vibration-resistant wiring), and then across an air gap to the rotating power receiving antenna. The power receiving antenna then routes this power to the wireless telemetry board (see Figure 18). The RF telemetry antenna system receives the modulated blade sensor RF telemetry signal from the wireless telemetry board, and routes it to an embedded RF dipole antenna which is embedded in the rotating power receiving antenna. The RF signal is then transmitted across the same air gap to the matched RF antenna which is embedded in the stationary power inducing stators. This match RF

stator antenna is connected to a high temperature, vibration-resistant wire which is routed out of the gas turbine to the RF demodulation and data recording equipment. The power induction system and the RF telemetry antenna system are co-located.

The rotating power antenna, the wireless telemetry boards, and the wires connecting them are held onto the root of the rotating blades in a custom-designed blade bracket (also called a seal plate). This blade bracket was designed to minimize the impact of the high g-load, high temperature, and high vibration environment on the rotating antenna, the wireless telemetry board, and their wires.

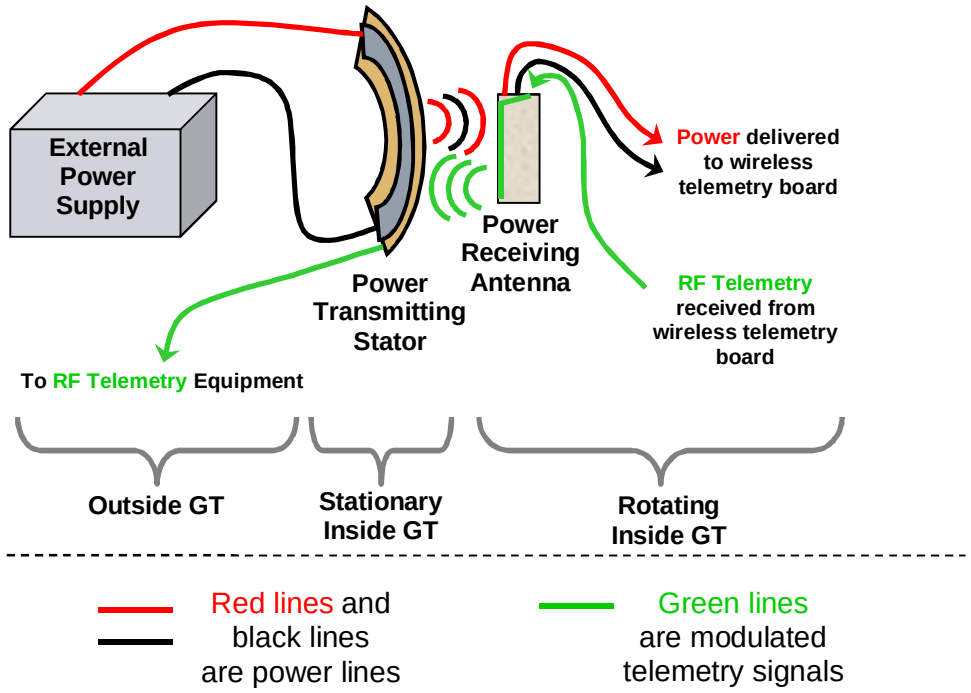

Figure 18: Schematic of the Wireless Power Induction System

Electrical Impedance Testing Methodology

The initial power supply was based on a highly resonant step-up transformer whose functionality was dependent on a strongly inductive load and exact matching. Testing of the independent functionality of this type of power supply was difficult. Due to limitations on power output, this first power supply was abandoned.

The power supply used during the majority of this project was an Electronics and Innovation (E&I) 1140 LA RF Power Amplifier. This off-the-shelf power supply has tightly specified amplifications parameters over the frequency and power range needed for this project. All lab tests confirmed that this device produced the outputs per specification and in agreement with its limited status readout display. Tests of output power used a

Tektronix CT1 AC current meter to measure output current and a Tektronix TDS 2002 Oscilloscope to measure output voltage.

The external power supply transfers maximum power to the power inducing stator coils when the impedance of the coils (very inductive) is matched to the output impedance of the external power supply (50 ohms, purely resistive). In order to accomplish this matching, a circuit of capacitors in series with an isolation transformer was created. In order to ensure the best possible matching a Wayne-Kerr 6500B Impedance Analyzer (Figure 19) was utilized. This device measures the impedance of the transformer, capacitors, and power coils in series with each other. Resistance, inductance, capacitance, reflected power, and signal phase changes were measured with this device over wide frequency ranges. This methodology was used very early in the design phase to select optimal coil geometries and lengths, to select optimal frequencies, to select optimal geometries of coils in relation to ground planes, to select correct transformer winding ratios, and to select the correct capacitor values for final matching. It was also useful for troubleshooting during failures and configuration mistakes.

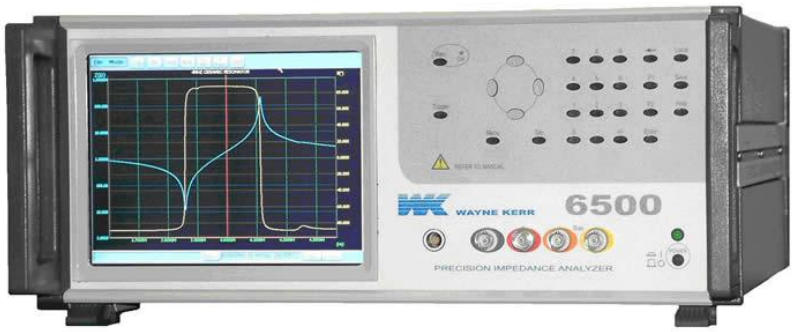

Figure 19: Wayne-Kerr 6500 B Impedance Analyzer (LCR Meter)

In the new planar coil design, there is significant capacitance from the coils to the grounded metal onto which they are mounted (see Figure 20). The impact of this capacitance is dependent on the frequency of AC power used to drive the coils and their proximity to the ground plane. Losses of up to 40% were suspected to be due to this unwanted capacitive path to ground. The AC current probe was used to confirm this loss by measuring the current between the ground plate and the laboratory ground. It was found that the inclusion of a transformer in series with the coils disrupted this capacitive ground loop by converting the single-ended output of the power supply into a differential voltage source. This differential voltage source change resulted in capacitive losses dropping from 40% to less than 5%. Thus, the robust methodology of AC current probes, oscilloscope voltage readings, and advanced impedance analysis resulted in enabling technology gains.

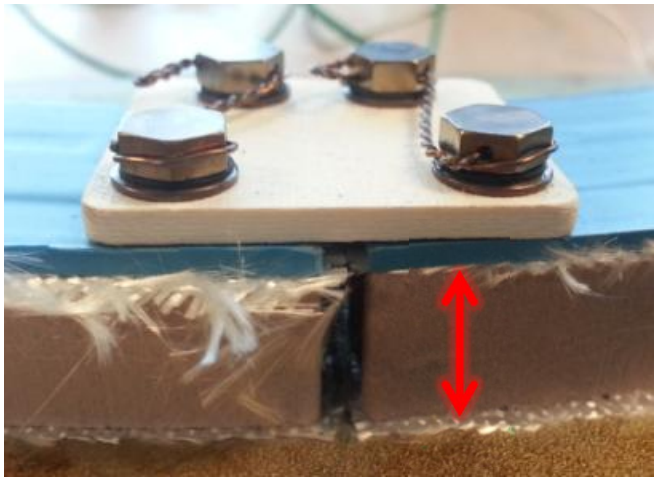

Figure 20: Capacitance Path (Red Arrow) Between Coils and Grounded Metal Backing

The same equipment was used to measure the properties of the power transmitting stator coils by themselves, as well as the embedded coils of the power receiving antenna. Figure 21 shows the power induction circuitry experimental setup.

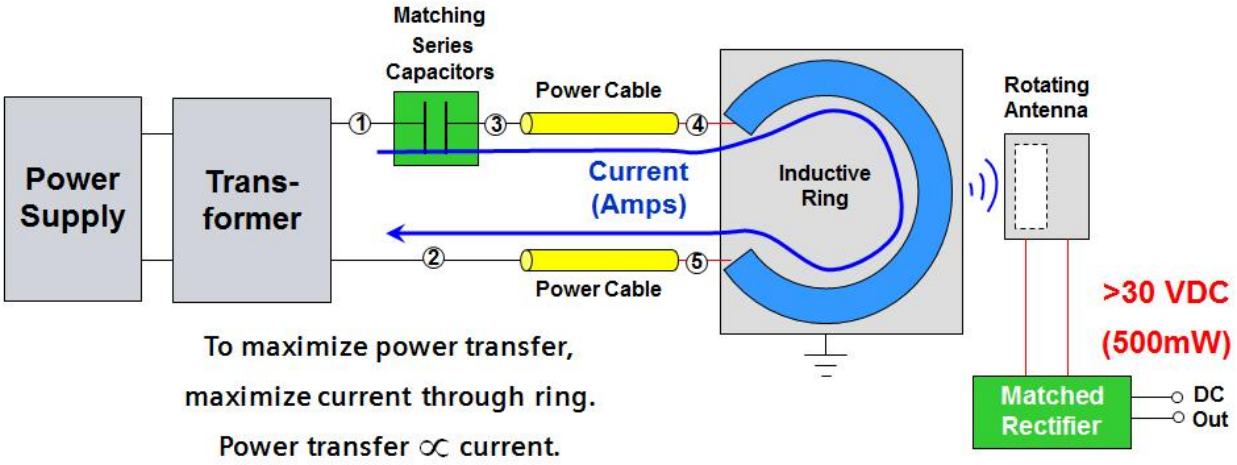

Figure 21: Schematic of Power Induction System Test Setup

The power coils were set in an oven and subjected to temperatures up to 600ºC while their impedance was periodically measured. The temperature within the furnaces was measured by two internal thermocouples which were kept in calibration annually. In order to make these measurements, fiberglass-insulated steel wires were compressively connected to the coil assembly. In order to measure the same parameters on the power receiving antenna, steel wires were silver soldered to the pins of the antenna. These insulated steel wires were feed outside the engine to the aforementioned measuring equipment.

Power Cable Testing Methodology

There were times that the steel wire connections were suspect. In order to determine whether this was an issue, alligator clips were used to connect to the power inducing coils, and the coils were placed on a hotplate. The hotplate and the majority of the coil were then covered in high temperature insulating material. The ends of the coils were kept cool enough to use the alligator clips (which cannot withstand temperatures above 250ºC), but the main section of the coils were able to be heated up to 400ºC. A Fluke 87A with thermocouple extension was used to point measure the temperature in this test. Thus it was shown that the steel wire/coil interface was indeed adding significantly to the series resistance. A stranded nickel wire was then selected for all future stator connections, with much better results.

Because of the high voltages and currents involved, shorting through insulation to ground was a major concern for the inductive power supply. Tests were performed on coils, lead wires, and longer power wires to allay these concerns. A Fluke 1587 Insulation Tester was used to measure between the center conductor and ground, and between the conductors of different sections of circuits. To test cable insulation over temperature, two cables were tightly wrapped around each other at least 15 times, and this twisted section was placed into an oven. The four ends of the two cables exited the oven. One end of each cable was connected to the insulation tester, while the other ends were kept far from each other, suspended in the air. The insulation resistance between the center conductors of the cables was then measured periodically as the oven was taken to high temperatures. The Fluke 1587 is capable of measuring at voltages up to 1000V while measuring current leakage below 1µA. This test gave the team the initial confidence in the cables under test. However, the Fluke 1587 is a DC voltage tester, while the system operates at high voltages at frequencies up to 1MHz. Therefore, other tests were performed using the E&I 1140 LA RF amplifier. This device displays the transmitted and reflected power. Circuits under test were matched to close to 50 ohms and placed in an oven. These circuits were driven by the RF amplifier. If a leakage occurred, it was evidence from the RF amplifier display. When matched well, the reflected power is close to zero watts. If a leakage occurs, this changed the impedance of the circuit and mismatches it, increasing the reflected power. Thus, circuit subcomponents and full assemblies were tested for insulation failures.

Power Transfer Testing Methodology

In order to characterize the power transfer between the power coils and the power receiver, it was necessary to do a number of tests with the power receiver placed in close proximity of the power coils. Early on, it was determined that the grounding and other electrical connections between the receiver had strong effects on the power transfer. Additionally, the presence of grounded metal also has strong effects on the power transfer. Therefore, the decision was made to create a test methodology which closely simulates the engine environment. In the engine, the power coils would be mounted on a large metallic structure which is grounded along with the rest of the engine. The rotating

sections, which are attached at the base of the blades, are also weakly grounded to the same earth ground. This strong/weak earth ground combination was not reliably repeatable in the lab. So tests were carried out with multiple combinations and strengths of grounds. The “strength” or “goodness” of a ground is inversely proportional to the resistance between the test point and true earth ground. By intentionally introducing a range of resistances between different ground surfaces, the following relationships were determined:

- The highest losses occurred when the stator coil metal backing is strongest.
- The highest losses occurred when the rotating coil metal backing is strongest.
- Losses were monotonically inversely proportional to the strength of the grounds as that strength is varied.
- If both the stator coil and rotating coil metal backings are grounded, it does not matter whether they are electrically connected otherwise.

Given these experimental data, we determined that the most pessimistic case would be a very strong ground connected to the stator metal backing, along with a very strong electrical connection between the stator metal backing and the rotating coil metal backing. A 2.54 cm copper mesh ground strap was, therefore, used to ground the stator coil metal backing to the lab ground. The rotating metal backing (which is an engine seal plate) is attached to the stator metal backing via metal cylindrical standoffs. All electrical tests on the system power transfer were carried out with the setup shown in Figure 22. Note that two of the bolts are not tightened down in this photo.

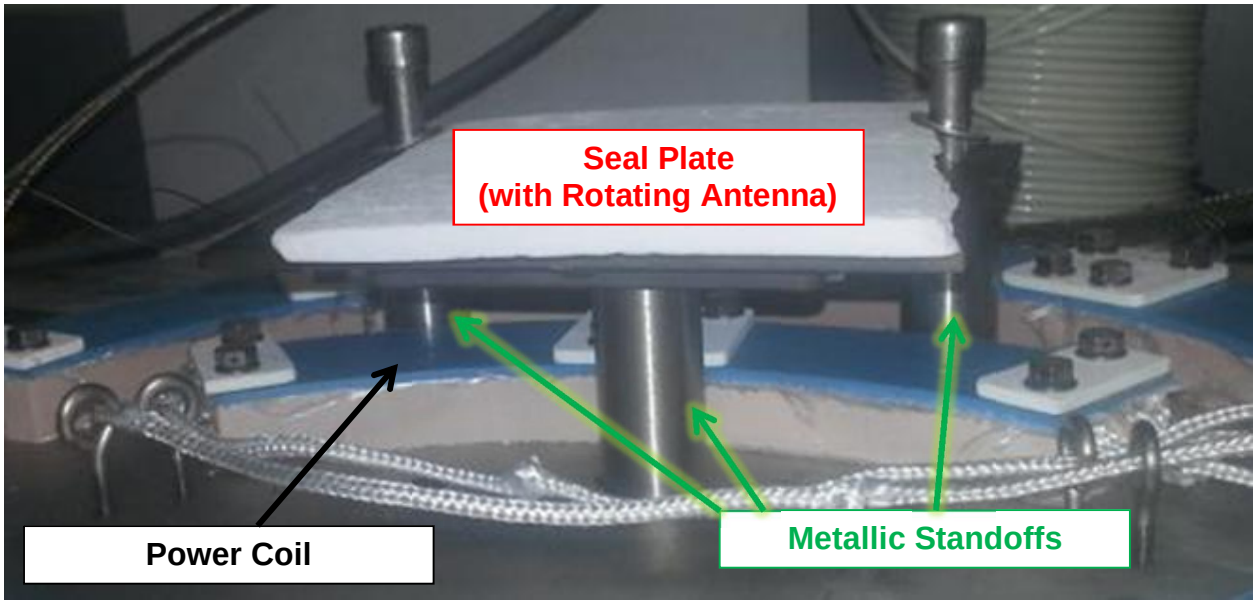

Figure 22: Seal Plate Installed Over Power Coil with Metallic Standoffs

The metallic standoffs served a second purpose of providing a very stable gap between the stator coils and the rotating power receiving coil seal plate. This seal plate was bolted and torqued into place for stability. This proved to be a mechanically reliable setup for lab furnace testing. Changing out the standoffs for those with different lengths also allowed the power transfer to be characterized at different gaps between the coils and the receiver.

A furnace dwell test was also performed on the inductive power system. During this test, High amounts of power (~300W) were continuously run through the circuit. The power transferred was continuously monitored during this test. Periodically, the power input was disconnected, and impedance measurements of the power coils were performed. Throughout the test, the furnace temperature was maintained at 400ºC. The purpose of this test was to simulate the dwell times the system must see in an engine during validation.

All furnace tests of the of the inductive power system mentioned in Section 2.4 were performed with the setup described above.

Vibration Testing Methodology

Vibration tests were also carried out on assemblies of the stator coils. These planar ceramic pieces were assembled in the same configuration that they would experience in a spin rig or engine test. A specialized metallic back plate was fabricated, and pieces were assembled with electrical connections protruding from the test article as shown in Figure 23.

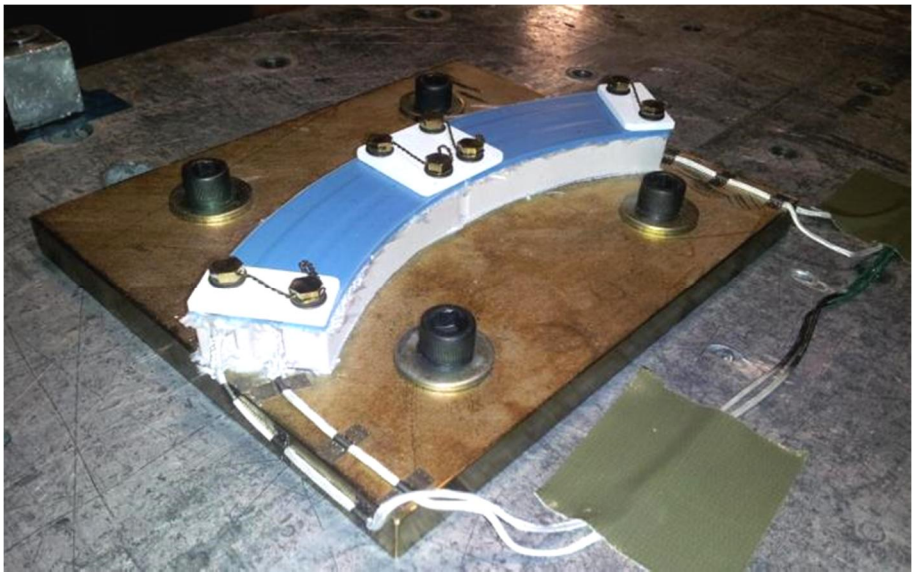

Figure 23: Power Coils Mounted on Vibration Plate

This test article was then taken to a lab which contains an electronically-controlled vibration table. The vibration profile of the tests was to have a major sinusoidal tone at

60Hz to match the major engine vibration mode. In addition, a lesser "rolling" sinusoidal tone which smoothly varies from 10 to 240Hz over the period of 2 minutes, then repeats continuously. This rolling tone is meant to simulate the range of frequencies at lower levels that the planar coils would have to endure in an engine environment. The energy at all these frequencies is designed to be significantly higher than the engine or spin rig vibration energies. Figure 24 illustrates the vibration profile graphically.

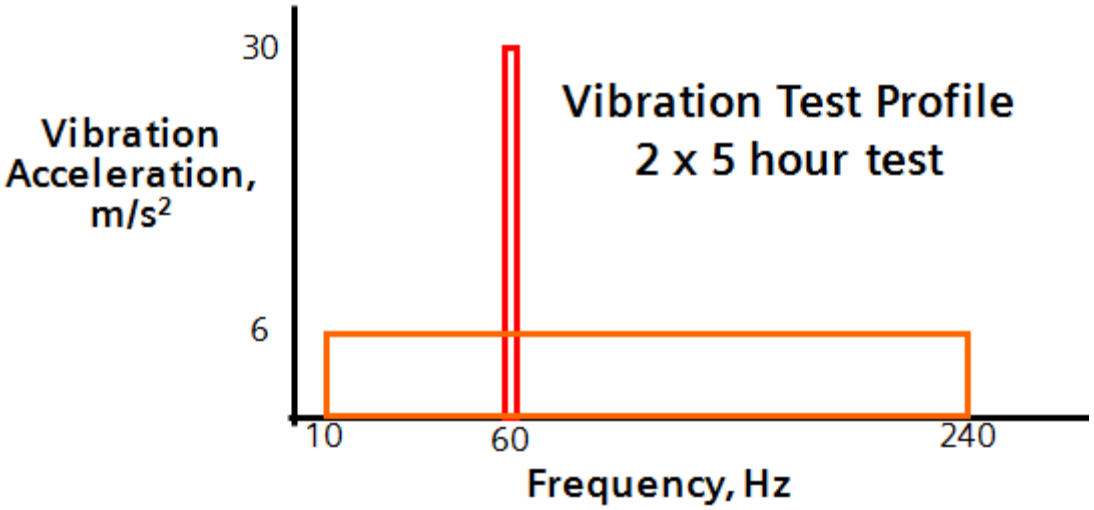

Figure 24: Vibration Profile for Planar Coils

These vibration tests occurred in three different dimensions: Normal to the plate and also in the two other orthogonal directions. Thus the plate was mounted in three different orientations on the same rig, as shown in Figure 25.

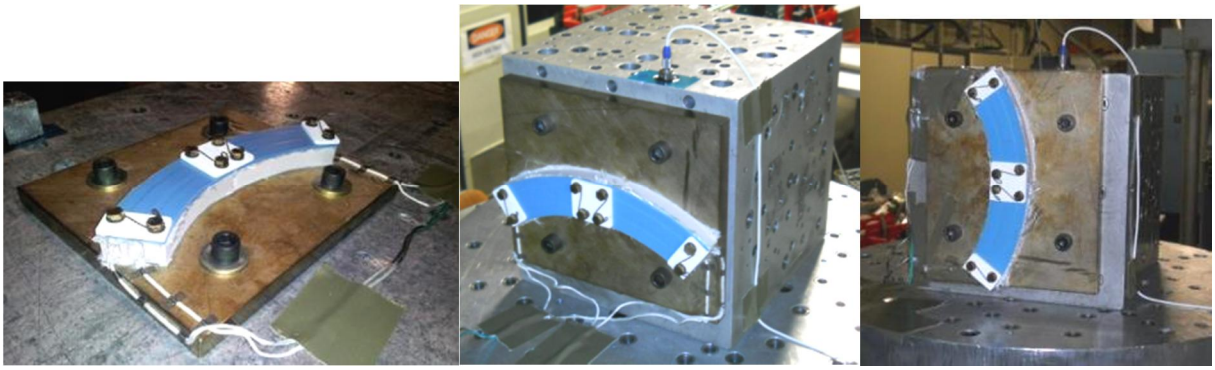

Figure 25: Three Different Orientations of Vibration Tests

Three different sets of vibration tests were performed on these coils. Electrical connections were monitored for continuity and isolation once per second throughout the tests. This data was recorded and reviewed after the test.

Radio Frequency (RF) Testing Methodology

In addition to wireless power transfer to the rotating components, this system is also responsible for the transmission of data from those rotating components to the stationary components and outside the engine. The wireless electronics board RF output has a direct connection to one of the pins of the rotating antenna. This connection goes to a monopole antenna inside the rotating antenna. This communicates wirelessly with the antenna line embedded in the power coils. Thus the data is transferred from rotating to stationary components. A high temperature cable communicates this signal from the stationary power coils to outside the engine.

In order to test this RF transfer circuit, a 70MHz tone was generated by Tektronix AFG 3102 Function Generator at a power of -20dBm. This is frequency and the lowest power expected to be emitted by the wireless electronics board. This was fed directly into the rotating antenna while it was in the power transfer configuration of being bolted onto the power coil assembly at an appropriate gap (usually 20mm). The transferred RF signal was then measured at the end of a 3.5m long high temperature shielded cable attached to the power coil's RF antenna port. This cable length simulates the length needed to exit a gas turbine in an expected installation configuration. This RF output was measured with a Tektronix 6.2GHz Field Spectrum Analyzer, and compared to the noise floor.

The RF center frequency was adjusted to cover the entire possible range of wireless telemetry board output frequencies (50-100MHz). This configuration was tested over temperature in an oven. It was also tested over a full range of temperatures while maximum power was delivered to the coils and measured on the rotating antenna, in order to measure the crosstalk between the power circuits and the RF circuit.

1.5 - TASK 5: ROBUST ADVANCED SILICON CARBIDE DEVICES

Task 5 develops and fabricates advanced silicon carbide (SiC) devices, matched transistor pairs, and integrated circuits. Siemens partnered with the University of California at Berkeley to develop advanced SiC devices.

The experimental methodologies used by the University of California at Berkeley were developed at times and with funding unrelated to this project. A brief description is made of the experimental methodologies for completeness.

High temperature measurements of novel silicon carbide electronics, including transistors, diodes, and energy scavengers, were mostly accomplished at the wafer level. That is, devices were fabricated on wafers, and prospective devices were measured on the wafer before the wafer was diced up to produce singular devices. For this purpose, a high temperature probe station was used for electrical evaluation. This probe station is capable of being calibrated to function over a temperature range of 0-550ºC. Thus voltages and currents could be measured on multiple ports of devices simultaneously, allowing measurements of inductance, capacitance, resistance, active amplification, and resonance. Heating was accomplished with electrical heating tables with active feedback. Dwell tests at high temperatures for hundreds of hours were performed in order to determine the aging of the devices. All of the above were used to measure metallic

adhesion and bond pad resistance for many of the devices. Testing was mostly done in regular atmosphere, though much of the processing occurred in controlled and sometimes inert gases.

In the case of piezoelectric energy scavengers, pressure variations were created using fan blades to interrupt a high pressure flow. This simulated the pressure variations at the blades of a gas turbine, and was applied to the diaphragms of the energy scavenging devices in order to produce small amounts of power.

X-ray diffraction, Raman scattering, and Raleigh scattering were used to measure doping and metallurgical properties of the devices under test. Cross sections were made of devices under test. Optical microscopes and scanning electron microscopes (SEMs) were used to evaluate etched profiles, diffusion, and coatings.

The results of all these tests are described in Section 2.5.

1.6 - TASK 6: SYSTEM INTEGRATION AND VALIDATION TESTING

Task 6 prepares and performs demonstration test of the system components and the integrated system. The validation plan included a variety of specifically designed laboratory tests on individual components, integrated spin testing of the components, and planned engine validation tests. Siemens charts technology development through assessing the Technology Readiness Level (TRL) of the system. Technology development proceeds by increasing test levels of the system and its components.

The wireless system components started the project at varied Technology Readiness Levels. The integrated system was judged, however to be at a TRL 2. Technology Readiness Level validation tests were performed first in low temperature laboratory tests, then high temperature laboratory tests, and finally in an integrated spin test that exposed the parts to the temperature and g-load. The philosophy of integration testing was to connect the system in increasing orders of complexity in non-challenging environments.

The wireless system passed a TRL 3 review through concept validation in lab tests. The TRL 3 testing included room temperature testing of performance without vibration. Details of these test methods were discussed in the component sections above.

The wireless system passed a TRL 4 review by showing functionality of components at environmental conditions closer to that expected in the engine. TRL 4 tests included high temperature testing in static ovens and lab vibration tests. Details of these test methods were discussed in the component sections above.

Many attempts were made to prove full system functionality in a heated spin test to obtain TRL 5. We were not, however, able to successfully achieve TRL 5.

Details of the system integration and validation testing results are given in Section 2.6.

Methodology for Selecting System Installation Point within the Gas Turbine

In this project, we planned to test the wireless sensor system in a turbine section of a large gas turbine. Rows 3 and 4 of the turbine section are moderate zones, with temperatures at the proposed installation points of less than 400ºC. Rows 1 and 2 are harsh zones, with temperatures significantly above this level. The harsher temperatures above 400ºC preclude the use of several key subcomponents and materials, so they are, therefore, outside the scope of this project. The focus of this project was to create a system that is functional in the turbine Row 3 and 4.

Subcomponent and System Integration Methodology

Many validation tests happened on the subcomponent level. Because of the harsh environment which the system must e**n**dure, extensive validation testing of all component materials, connections, vendor parts, and packaging were accomplished as early as possible As new component concepts arose during the system development, harsh environment tests of new materials, subcomponents, and combinations of these were re-performed to ensure proper and reliable function. After subcomponent and component testing, system integration testing occurred.

In integration testing, detailed specifications of the individual system components were developed, and then these characteristics were monitored in the test. Table 3 shows how

Specification Title	Min	Typical	Max
Wireless telemetry board Output telemetry frequency	50MHz	70MHz, various	100MHz
Wireless telemetry board Output telemetry power	-20dBm	-15dBm	NA
Wireless telemetry board Needed input voltage (over 1780Ω load)	$28.5V_{RMS}$	$35V_{RMS}$	$75V_{RMS}$
Wireless telemetry board Operating temperature	0ºC	350ºC	400ºC
Wireless telemetry board G-load (continuous)	0g	14,000g	16,000g
Wireless telemetry board Strain gage frequency error	NA	±1Hz	±3Hz
Wireless telemetry board Strain gage amplitude error	NA	±10%	±30%
Wireless telemetry board Thermocouple temperature error	NA	±4ºC	±8ºC

Table 3: Table of Some of the Input/Output Values for Electronics Board System Integration

the electronics board characteristics were tracked in lab and rig tests tabulating inputs, outputs, and their possible variations. By comparing the variable input/output (I/O) characteristics in tabular form, it became easy to make full evaluations of all the interconnections in the system. For high frequency connections, impedance matching and coordination occurred quite early. For instance, the receiving power load and optimal frequency of the electronics board was measured early on, and this exact load was used in all testing of the rotating antenna, which feeds power at specific frequencies into the electronics board.

2. RESULTS AND DISCUSSIONS

Results and discussions for each task will be described in the following sections.

2.1 - TASK 1: DEVELOP CBM APPROACH FOR TURBINE BLADES RESULTS

Task 1 specifies the monitoring system integration approach and requirements. This task evaluates and sets the requirements of the data acquisition system and software that will integrate the wireless sensor data into the condition based maintenance system for remaining life predictions.

An approach for networking component remaining useful life (RUL) data with Siemens Power Diagnostics engine monitoring system has was developed. Data integration into 2D area maps and incorporation into remaining life models was to be accomplished after engine testing was performed, but engine testing was not completed during this project due to issues with other system components. Engine test data obtained from this wireless telemetry system, point data and infrared 2D mapped data was planned to develop the part condition assessment.

Calibrating 2D Blade Maps with Wireless Point Data

In order to create 2D blade maps of temperature, one can either obtain many points of temperature data, or use a small number of points to calibrate a model. Because our concepts of this wireless system do not allow more than one to four sensor per blade, this wireless telemetry system alone cannot provide enough data on its own to create a full 2D map.

Siemens is, therefore, focused on a hybrid path for developing 2D blade temperature mapping. An IR camera will be used to capture a field of blade temperatures, and our wireless point sensors will be used to calibrate the values of that field. The IR camera system can show relative variations in temperature, but has relatively low absolute accuracy compared to thermocouples. The point thermocouple sensors from the wireless system will be used to calibrate and linearly scale the values attributed to the relative temperature map created by the IR camera.

The position of a temperature sensor on the blade is known from the sensor installation drawing. Since that point is exactly known, it can be mapped onto 2D and 3D data maps. Infrared camera images are grayscale temperature maps. Siemens has a system for aligning 2D infrared blade images onto 3D blade models, as illustrated in Figure 26.

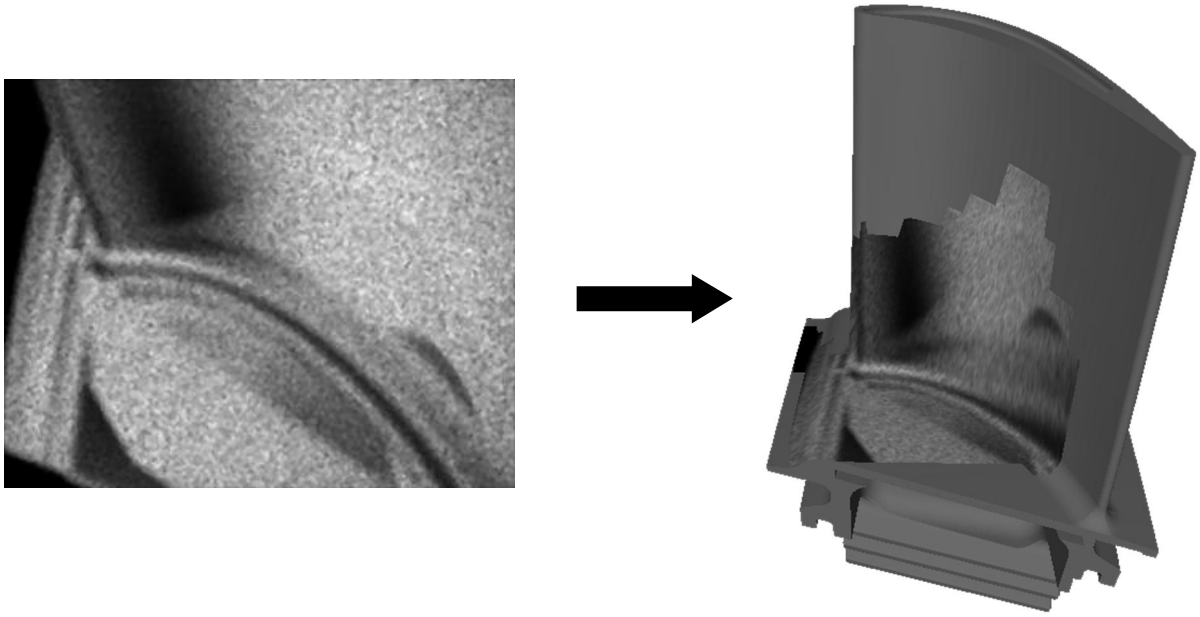

Figure 26: Siemens Infrared Temperature 2D Image Mapped onto a 3D Blade Model

In these images, the relative change in temperature over the blade has high accuracy, but the absolute value of temperature at each point has less accuracy than we expect to obtain from the wireless sensors. The wireless sensor data can, therefore, be used to calibrate the scale used to interpret the infrared temperature 2D and 3D models. First, the exact point of the temperature sensor is found on the model, as shown in Figure 27.

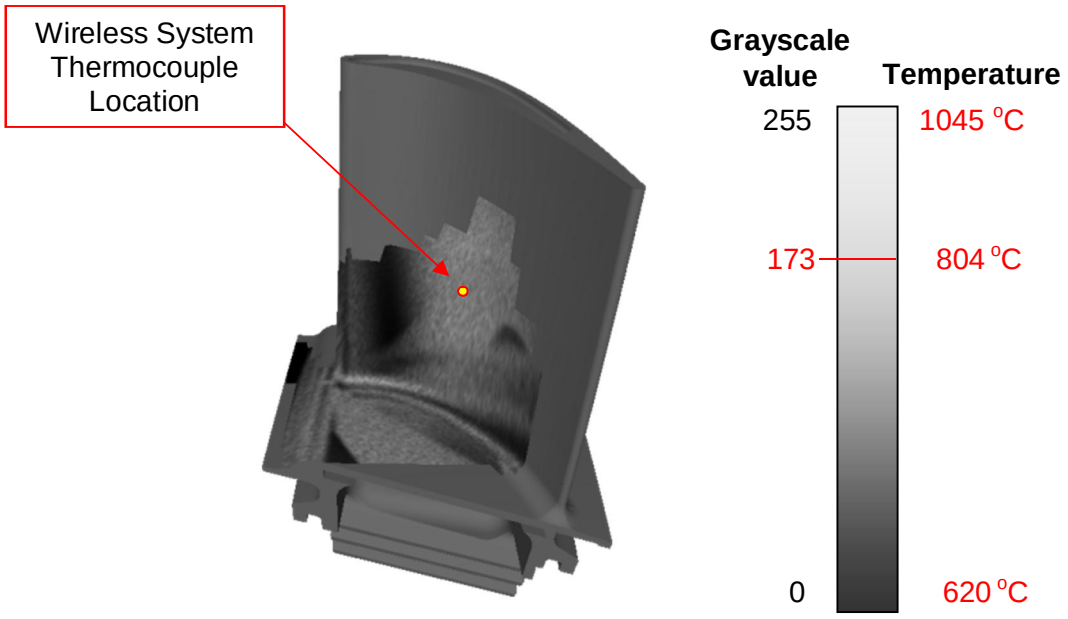

Figure 27: Locating the Temperature Sensor on the 3D Model

The example grayscale map is then sampled at that exact point, taking an average of the pixel values within 2mm of that sensor point. This average yields a specific grayscale value between 0 and 255, say 173. Currently, it is likely that the error in the infrared map is significant, and this color, 173, has the temperature value of 804°C. When we know that the temperature sensor reading from our wireless sensor, we can now perform a linear adjustment to the grayscale legend used to interpret the infrared grayscale temperature map as in Figure 28.

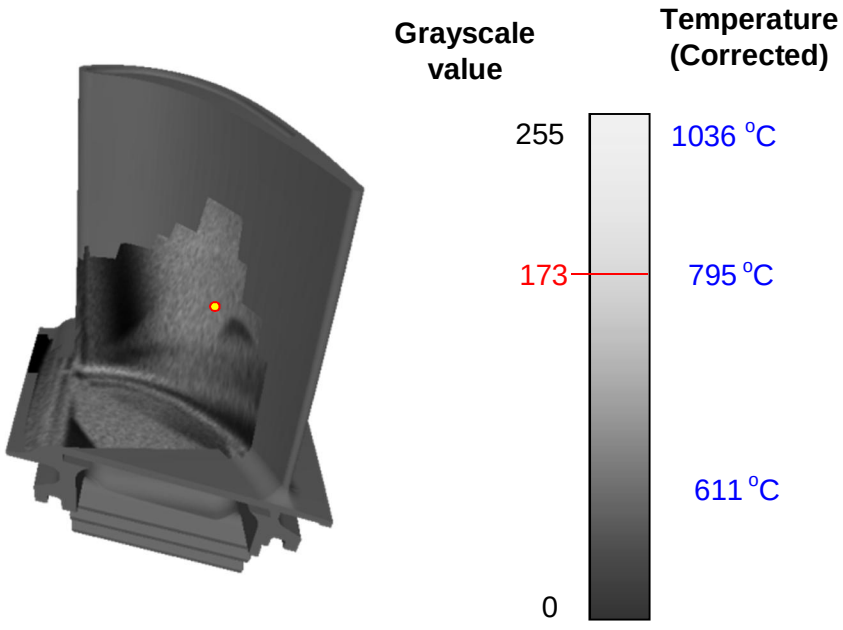

Figure 28: Locating the Temperature Sensor on the 3D Model

This adjusted temperature map can then be used to more accurately characterize the temperature at many points across the blade.

As a condition based monitoring (CBM) tool, this can be used in the following ways:

1) Real time analysis of the infrared camera data can be automatically scaled using wireless system point sensor data, or
2) Historical data from an infrared camera system can be used to set limits on the temperature at a certain point on the blade, given an established relationship of relative temperatures. Continuous monitoring of this point relative to these point temperature limits can be used to make decisions about blade life and other CBM contingencies.

For 2D strain blade mapping, a combination of strain models, noninvasive tip timing measurements, and the wireless point data will be used assess the rotating part. Modelled 2D strain mapping would be scaled with empirical point data (amplitude and frequency of strain) and results from tip timing data.

Sample rates of thermocouple and strain gauge point sensors were determined, and accuracy goals were set. These design goals are used as a basis for the wireless telemetry board circuit design. Because no integrated engine testing was accomplished during this project, this system was not realized and tested.

Networking Wireless Data into Existing Monitoring System

An important aspect of data analysis is the development of an approach to network Remaining Useful Life (RUL) data. A description of a design for bringing the wireless system data into the Siemens engine monitoring system follows.

The RF telemetry equipment outside the engine receives the RF data signal from the wireless system. This equipment is used to receive the RF signal, demodulate the data signal, and translate the data signal into temperature and strain data. The National Instruments equipment used to do this final translation has the capability of scaling the data to a 4-20mA current signal. Such 4-20mA signals are used by all standard Siemens diagnostics and control systems to read engine data. These new data signals will be incorporated into the recorded data stream, and can be made available remotely. Local or remote monitoring can then be accomplished, and blade temperature and strain data can be made available for Reliable Useful Life (RUL) analysis.

Specifically, the thermocouple signal can be scaled such that minimum and maximum temperatures can be linearly mapped to 4 and 20mA signals respectively. This simple solution is typical for thermocouple measurements, and would be handled by the telemetry system as a typical temperature reading.

For strain gauge data, pre-processing is required. There are two important aspects of the signal: amplitude and frequency. It is useful to know the frequencies of blade strain signals so that blade vibration frequencies can be obtained and compared to harmonics of interest. The peak amplitudes of that strain signal at those frequencies can tell us how strongly the blade is vibrating. With each blade, we are interested in a number of different modes of vibration, which manifest as different frequencies in the strain signal.

National Instruments provides processing subroutines called Virtual Instruments (VIs) which are capable of sampling the integrated amplitude and the average frequency. This is done once per second. Once the signal is demodulated and decoded into strain data at the RF telemetry equipment, the National Instruments system would use VIs to filter the signal into different frequency bands (e.g., 0-100Hz, 100-200Hz, 200-500Hz, 500-800Hz, and 800-1200Hz). A Fast Fourier Transform (FFT) is then performed on each band, and the frequency of the highest amplitude peak within each band would be reported, along with the maximum amplitude in that band. These frequencies and amplitudes are then scaled to 4-20mA signals and output to the Siemens diagnostics and control system.

Because most of the data processing occurs in software, the bands and signal scaling are completely reconfigurable, allowing for maximum flexibility and very quick reconfiguration. Figure 29 illustrates the approach. As this system is applied to different turbine or compressor rows, adjustments can be made to the parameters quickly and easily to match the frequency bands, strain amplitudes, and temperature amplitudes of interest

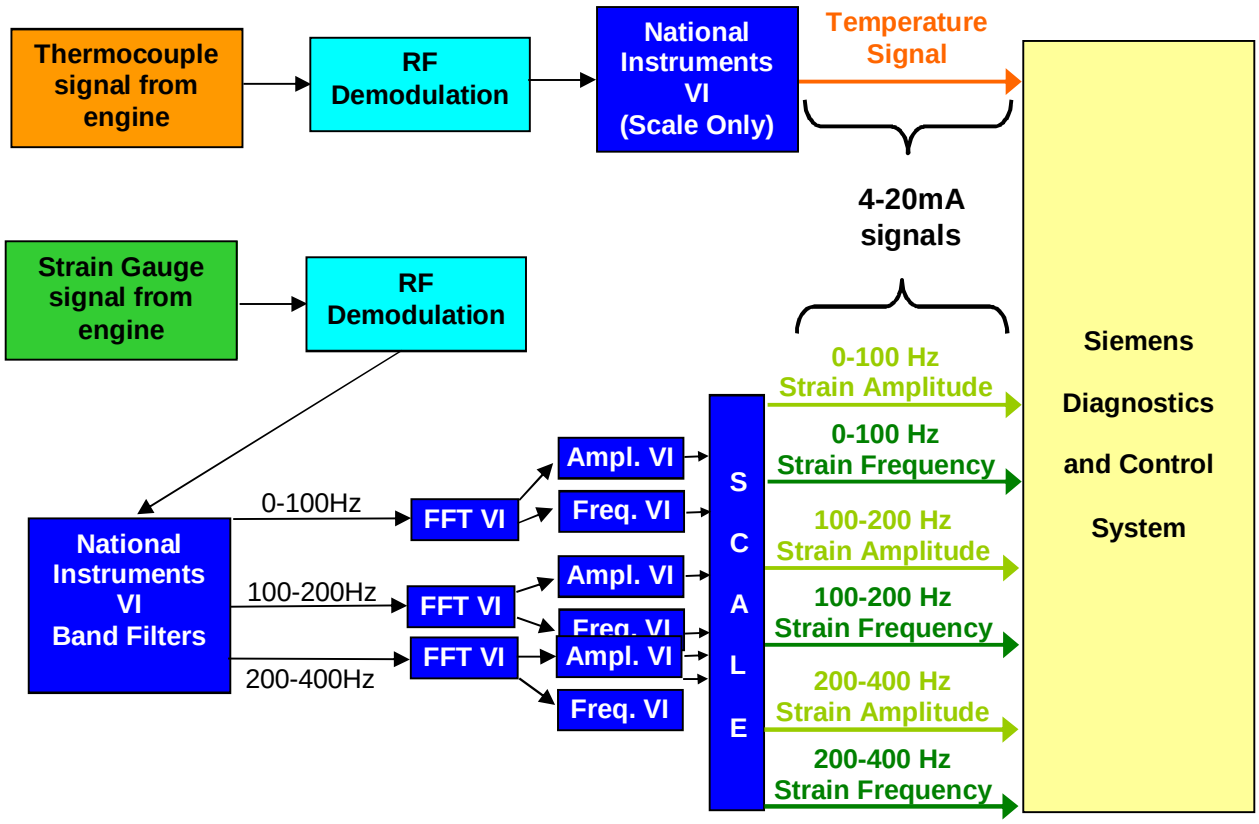

Figure 29: Approach to Network RUL Data to Siemens Power Diagnostics

Because technical issues with components of the wireless system precluded engine testing during this project, these CBM systems were not moved beyond the conceptualization and design stages. These systems are, however, overlaid on existing functional systems, future implementation is not expected to be difficult or time consuming.

2.2 - TASK 2: SCALE-UP & MANUFACTURING OF SPRAYED SENSORS RESULTS

Task 2 performs scale up of thermal spray sensors and manufacturing blades with sensors for H-Class engine testing. At the base of the blade, the imprinted sensor is connected to more conventional wire. This wire is routed to the wireless telemetry board mounted at the root of the blade. Siemens spray-on thermocouple technology offers a less accurate but more durable alternative to traditional thermocouples, and represents the only sensor-based method for directly measuring temperatures on blades for extended periods (greater than 100 hours). Figure 30 shows a close-up of spray-on thermocouple active region as installed on an H-class engine blade.

Figure 30: Close-up of Spray-On Thermocouple Applied to H-Class Blade

Spray-on thermocouples were successfully applied to Siemens engine test components. The Row 4 turbine blades in the H-class were selected for demonstration because of ease of access to this row that would allow rotor instrumentation and disassembly at convenient phases in the engine tests. This blade row also allows larger spaces available for component installation. The temperature that the wireless telemetry system components must withstand is approximately 400ºC, and the g-load is approximately 14,500g, making it the turbine blade row with the least harsh environment, and therefore a clear choice for initial system installation. Detailed installation and component drawings were produced for this installation, documenting the components and their locations.

Atmospheric plasma spraying procedures were used to apply thermocouples on three H-class Row 4 blades for an engine test. A robust manufacturing approach for thermocouple sensors had already been developed before this project was initiated, so that technology is not under the purview of this report, and will not be described in detail. Optical analysis of the spray trail reveals conformity and good adhesion. The blade was sectioned at different location to obtain information about layer thicknesses, cracks, and porosity (see Figure 31).

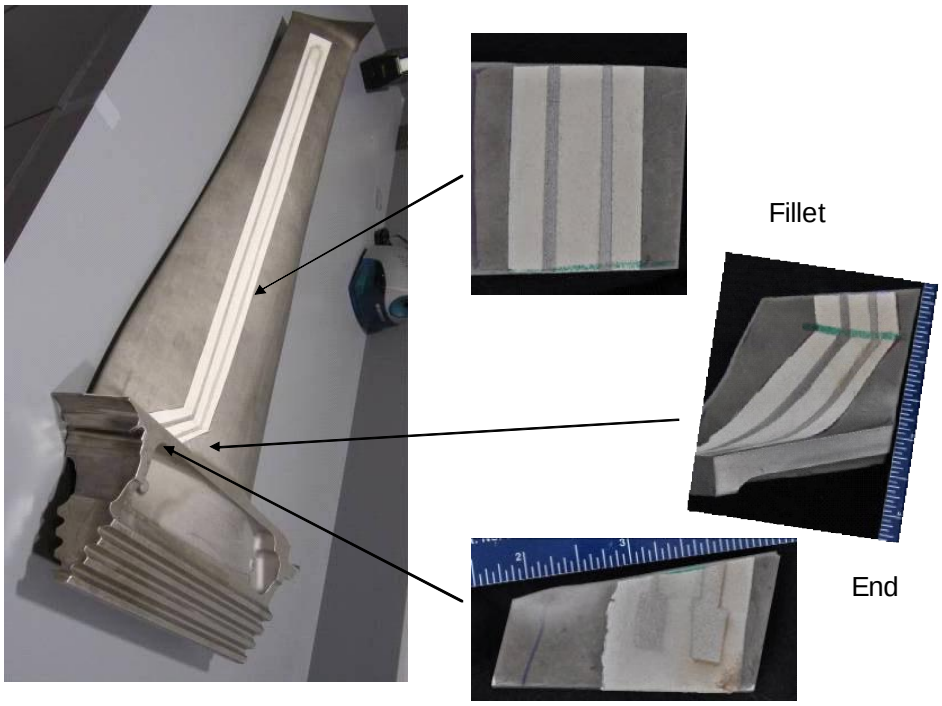

Figure 31: Cross-sections of a Spray-On Thermocouple on an H-class Blade

The effort to develop a strain gauge process did not meet with sufficient success. Consistent strain gauge resistances were not achieved with the available array of spray-on techniques, and this effort was suspended until another technological methodology becomes available. The plan for this project, therefore, was to use traditional strain gauges in the wireless technology demonstrations.

Testing of the H-class engine blade spray-on thermocouples was planned for a spring 2012 engine test. Other wireless system problems, however, caused the test to be cancelled before the blades were installed. Until the system is ready for another engine test, application of the sprayed-on thermocouples was halted.

2.3 - TASK 3: ROBUST 450^{O}C WIRELESS TELEMETRY CIRCUIT BOARD RESULTS

Task 3 develops and fabricates high temperature, high g-load wireless telemetry circuit boards for engine testing, and miniaturized circuit boards for spin tests at 400°C and 14,500g. This task is subcontracted to Arkansas Power Electronics International, Inc. (APEI).

The wireless telemetry board, the most complex component of the wireless system, resides at the base of rotating engine blades, where it must endure g-loads in excess of 14,500g and temperatures approaching 400^{o}C. It receives alternating current (AC) power from the rotating power receiving antenna. The board needs a minimum of 500mW in order to function, which necessitates an advanced and powerful magnetic power induction system. The wireless telemetry board conditions this power to a more useable

form for use by its on-board components. The on-board sensor interface subsystem communicates with a blade sensor via wired connections, reading the measurement data. This sensor data is then modulated to RF frequencies, and transmitted via antenna wire from the wireless transmitter board to the rotating power receiving antenna (which contains a small dipole RF antenna). This RF telemetry signal is then wirelessly sent to the stationary power inducting stators. From there it is sent out of the engine via high temperature cables, where the data is recovered.

Pre-DOE Project Work

Siemens development of this board began in 2006 at Arkansas Power Electronics International, Inc. (APEI). Because of the extremely challenging operating environment (400^{o}C and 14,500g), many new technologies, methodologies, and components had to be developed. By 2009, a working prototype existed that functioned during a low temperature, low g-load spin test. By March 2010, a prototype board functioned briefly at full g-load and a temperature of 420^{o}C, though it was not wirelessly powered and did not transmit its data wirelessly.

Summary of Electronics Board Spin Tests

Development since October 2010, when this DOE project began, has been significant. Many issues with the earlier prototypes have been resolved, while new issues have been revealed and characterized. Figure 32 shows two versions of this wireless transmitter boards that were developed: a type to be used with thermocouples and a type to be used with strain gauges. At the start of the project, the capabilities of this wireless transmitter board were minimal. Different sections of the electronics were still being integrated, and key subcomponents had not been fully characterized. Mechanical issues plagued the boards.

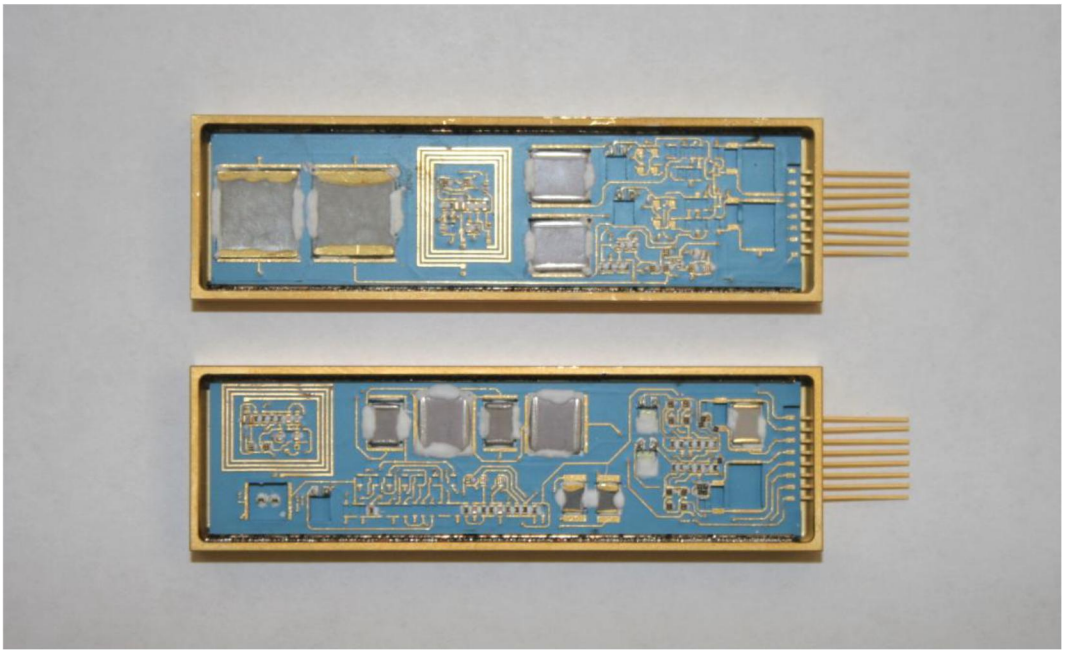

Figure 32: Image of Strain Gauge (Upper) and Thermocouple (Lower) Transmitter Boards

A summary of spin tests performed on the circuit boards is provided in Table 4. At the program's start, each spin test resulted in delaminated components or cracked boards. In the fall of 2010, an integrated design was achieved. All subcomponents were characterized and test boards were constructed. Mechanical tests initially failed, but packaging adjustments resulted in the first successful mechanical spin test at full g-load, with no cracking and no delaminating. In July 2011, for the first time, a transmitter board functioned at full g-load (14,500g) and full temperature (450^{o}C) for 1.5 hours, though it was not capable of being powered wirelessly, or transmitting its data wirelessly. In late 2011, a full g-load, full temperature mechanical spin test of two boards for 5 hours resulted in one board surviving with full functionality, and the other board lost only one of its 200 bonds. Upon repair of this bond, the board exhibited full functionality. In early 2012 two wireless transmitter boards were successfully wirelessly powered and data was wirelessly received during a spin test at full g-load for the very first time. Unfortunately, external connections on the spin disk failed, disconnecting the boards from power at full g-load. Analysis of the boards after this test showed that one board retained its functionality, but other boards exhibited delamination of an integrated inductor. This had not been seen before. It is believed that this occurred because these boards were temperature cycled during their calibration much more extensively than any other specimens to this point, and this temperature cycling caused the inductor to delaminate. Solutions to this issue were developed. These solutions are discussed in more detail below. External connection solutions were developed in order to make the connections to the wireless transmitter boards more robust under g-load conditions. Subsequent tests of specialty boards which focused just on the g-load and temperature impacts on bond wires or the inductors were then done in the spring of 2013 to test the solutions to these failure modes. In spring of 2014, a full g-load, full temperature spin rig test was performed on the entire system, which included two wireless electronics boards (one strain and one thermocouple board). Details of that test are discussed below.

Spin Test Date	Spin Test Description	Results & Analysis
April 2011	One thermocouple and one strain board, spun to 14,500g and 450^{o}C.	Both boards cracked due to lack of Nextel fabric
May/June 2011	Four thermocouple and four strain gauge boards spun to 14,500g and 450^{o}C, no electrical test.	All boards passed this mechanical test; no cracking.
July 2011	One thermocouple and one strain gauge board, powered by wired connection, for 14,500g, 450^{o}C functional test.	Thermocouple board damaged before spin test; Strain gauge board operated for 1.5 hours at full temperature and g-load; then failed due to lifted wire bond.

November 2011	One thermocouple and one strain gauge board - mechanical-only spin test at 14,500g and 450^{o}C.	Three wire bonds failed on thermocouple board. One wire bond failed on strain gauge board. Upon repair, both boards functioned nominally in bench tests.
January 2012	Two thermocouple boards and two strain gauge boards - fully functional, magnetically powered spin test at 14,500g and room temperature.	Both strain gauge boards survived test, and showed functionality at full g-load. Both thermocouple boards experienced delamination of RF inductor, causing failure. Issues with rotating antenna external connections prevented longer, high temperature testing.
March 2013	Inductors with glass encapsulation tested in spin test at 14,500g and 450ºC for 10 hours	No failures. Glass encapsulation a success.
April 2013	Bond Wire Test Boards with lesser coating spun at 17,000g and 400ºC.	Very good bond wire survival with little deformation. Polymer coating is a significant improvement in bond strength.
March 2014	Two fully functional thermocouple boards in full system test	One board functioned to 3000g; the other board functioned over 1 hour at 14,500g and 350ºC.

Table 4: Summary of Telemetry Board Spin Test Results

Early Thermocouple Board Development and Testing Results

In late 2010, thermocouple telemetry board designs for the H-class engine test were finalized. Figure 33 shows the strain gage schematic and board.

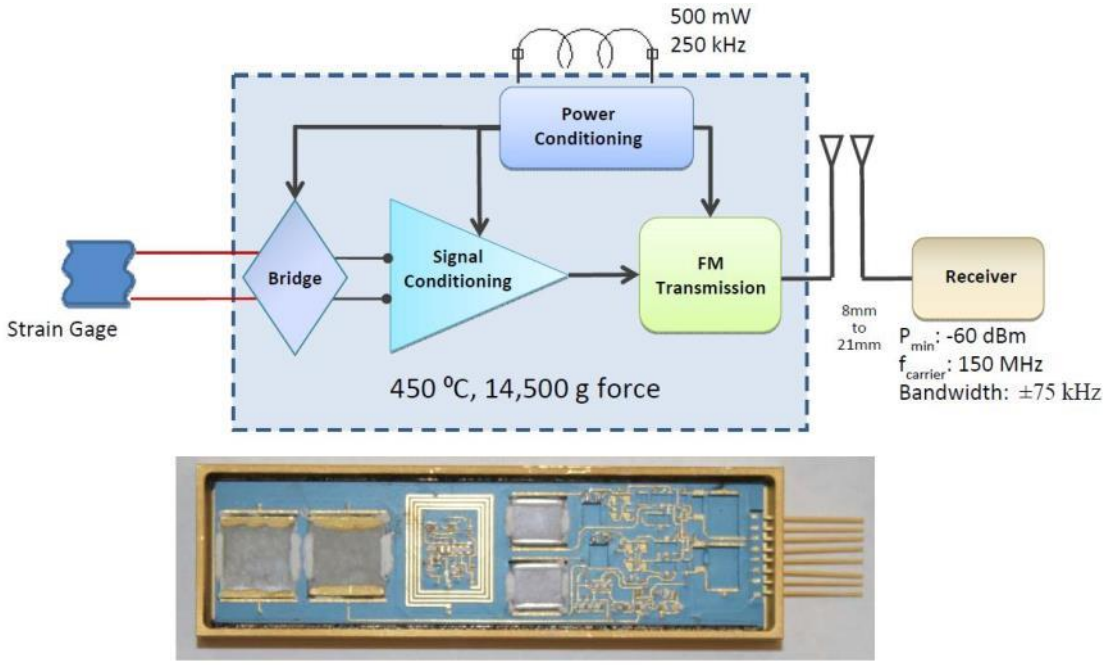

Figure 33: Strain Gauge Wireless Telemetry Board

A high temperature voltage regulator was implemented, tested, and incorporated into the boards. Bonding geometries and directions were optimized, resulting in much higher wire bond strengths, and bond failure rates were reduced by an order of magnitude. Mechanical tests that year showed that mechanical stability had been achieved (for both the thermocouple and strain gauge board versions): the boards no longer experienced cracking during g-load and temperature spin test. In order to achieve this mechanical stability, internal refinements to the package in which the boards are encased were implemented. Additionally, the package was wrapped in temperature-resistant material in order to cushion the package against vibrations; see Figure 34.

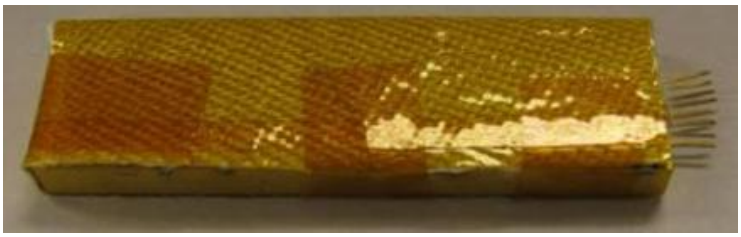

Figure 34: Telemetry Board Wrapped in Nextel Fiber and Kapton

Initial board fabrication was completed in August 2011. By the fall of 2011, calibrations of the thermocouple board were completed. A mechanical spin test was then performed

wherein a thermocouple wireless transmitter board was electrically tested before and after a full 450°C, 14,500g spin test. Three wire bonds (out of 200) failed during this test. Upon repair of the wire bonds, the board functioned nominally.

Further work was done to refine the wire bonding process, and two thermocouple wireless telemetry boards were produced for use in the H-class engine test. These boards were extensively calibrated during ten full thermal cycles to 450°C, producing stable calibration curves, such as the curve seen in Figure 35.

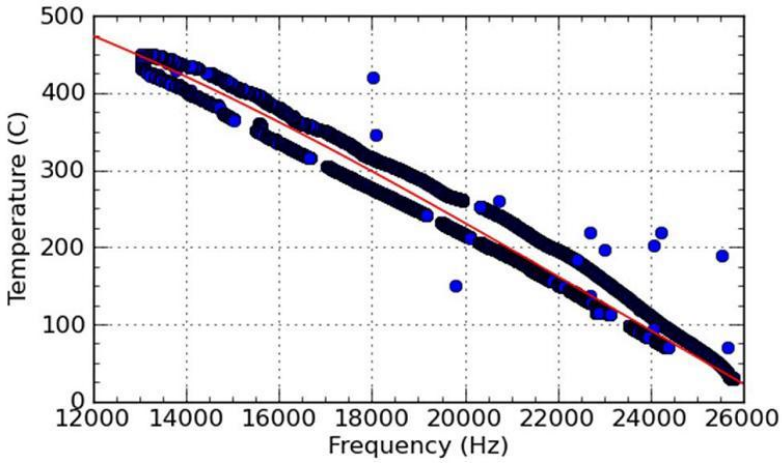

Figure 35: Calibration of Thermocouple Telemetry Board

The thermocouple boards survived these temperature tests, operating nominally up to about 420ºC. No lifted bonds were observed; however, preliminary signs of de-lamination of a spiral inductor were observed on both thermocouple boards. Repairs were made to this mechanical defect, and the boards were sent to be tested in a fully integrated high temperature g-load spin test.

Early Strain Gage Board Development and Testing Results

APEI refined the wire bonding process, and two strain gauge wireless telemetry boards were produced for use in the H-class engine test. These boards were extensively calibrated during 10 full thermal cycles to 450ºC resulting in stable calibration data shown in Figure 36. The boards survived these temperature tests, operating nominally up to about 420°C. No lifted bonds were observed; and no spiral inductor delamination was observed. The strain gauge boards were then sent to be tested in a fully integrated high temperature g-load spin test.

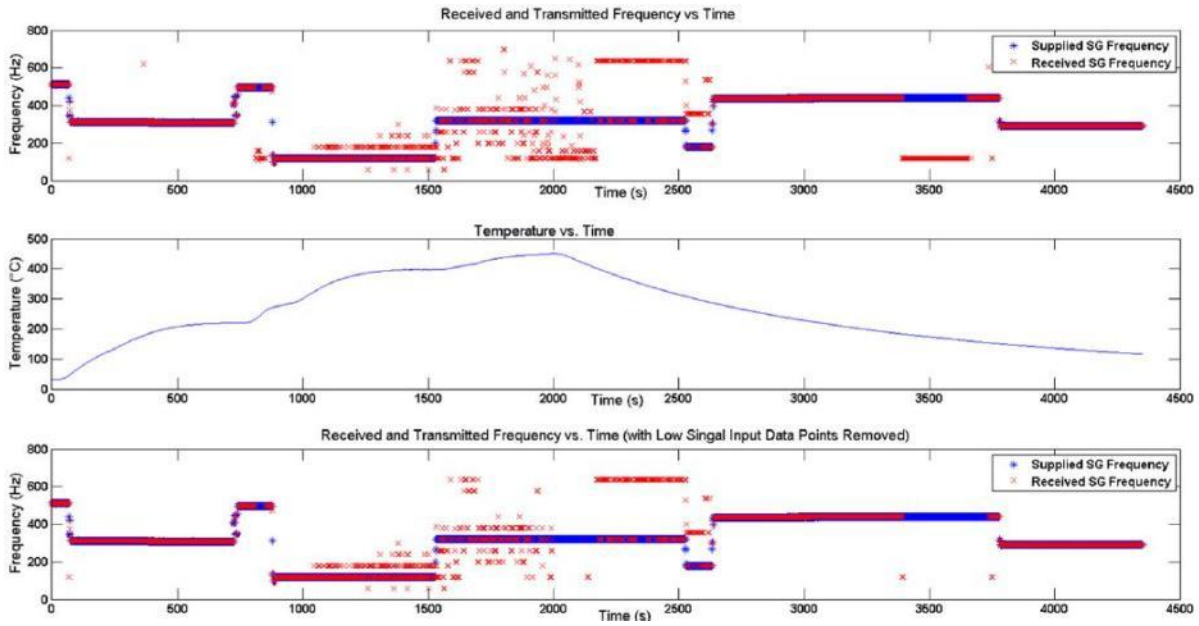

Figure 36: Calibration of Strain Gauge Telemetry Board

Attempted Incorporation of University of California at Berkeley Zener Diodes

Because of the need for wireless operation, a major concern of the board design is the nature of the power reception and data transmission. At the program's initiation, one of the biggest challenges to the form factor of the wireless telemetry system was the size of some passive components. APEI developed a new board layout which resulted in significant size reduction (30-40%) in board area.

In early 2011, the first generation of University of California and Berkeley Zener diodes was delivered to APEI for evaluation. Unfortunately, these diodes were not able to be wire-bonded due to metallization incompatibilities, and were not incorporated into the board designs, but they were evaluated electrically via probe stations. In early 2012, however, University of California at Berkeley delivered second generation Zener diodes to APEI that were designed for wire bonding, and exhibit improved electrical performance in UC Berkeley testing. These diodes were carefully evaluated at APEI, and are a target for future incorporation into APEI boards. The incorporation of these components will greatly reduce the complexity and area taken up by the power regulation circuitry on the board, allowing for design miniaturization.

Resolution of Board Cracking Issue

During the various spin tests of the wireless telemetry board, a number of different failures occurred such as board cracking, wire bond lifting, metallic trace delamination, and degradation of capacitors. During FY 2011, we resolved the board cracking issue by installing Nextel fiber inside and outside the board package. However the other problems remain potential sources of failure. Working with our subcontractor, Arkansas Power Engineering International (APEI), we developed a plan to mitigate these remaining issues in the coming months.

Resolution of Wire Bond Issues

During spin testing in January 2012, we observed a low, but unacceptable, rate of wire bond lifting (1 per 200 bonds). Each board has approximately 200 wire bonds. Because any lifted bond may rob the entire board of functionality, this failure rate is considered to be much too high. In order to mitigate this risk, Siemens contracted APEI to perform research into the use of coatings to strengthen wire bonding.

The solution chosen to mitigate this failure mode is coating the wire bonded boards with a thin coat of high temperature polymer in order to mechanically stabilize the wire bonds. In order to test this approach, four wire bond boards were created, each with 1,000 wire bonds, for a total of 4,000 wire bonds. Of these, 10% were tested for wire bond pull strength before polymer coating. These were initially coated with differing layers of this material: 2µm, 12µm, 25µm, and 50µm. One of the bond test boards (after coating) is shown in Figure 37.

Figure 37: Completed Bond Test Board (a) and a Close-up View of the Bonds (b)

Pull tests were performed on wire bonds from each group on each board before coating, after coating, and after every 10 thermal cycles up to 50 total cycles. The thermal cycling took place in computer-controlled Vulcan box furnace. The furnace automatically cycled between 450°C and 50°C. The control thermocouple (TC) was spot welded to a previously used metallic package. This ensured that the thermal mass attached to the control was nearly identical to that of the boards under test. The board reached the maximum test temperature of 450°C in 20 minutes. The cool down time to reach 50°C was about 2.5 hours.

Board # / Group #	Pre-Coat Pull Strength (g)				Post-Coat Pull Strength (g)				10 Cycles Pull Strength (g)				20 Cycles Pull Strength (g)				30 Cycles Pull Strength (g)				40 Cycles Pull Strength (g)				50 Cycles Pull Strength (g)			
	1	2	3	4	1	2	3	4	1	2	3	4	1	2	3	4	1	2	3	4	1	2	3	4	1	2	3	4
1	10.9	10.2	9.6	8.4	10.9	12.1	14.7	27.7	5.9	NPD	8.3	7.7	7.2	NPD	7.3	8.1	9.0	NPD	7.2	5.5	4.3	NPD	6.4	5.6	4.5	NPD	5.7	NPD
2	9.0	8.4	6.6	7.4	8.9	11.3	13.1	21.5	4.2	NPD	7.6	7.1	5.7	NPD	6.4	5.9	8.3	NPD	5.6	5.5	3.6	NPD	7.4	NPD	3.5	NPD	6.5	NPD
3	6.7	8.5	7.6	5.1	7.6	8.9	12.4	20.1	4.2	4.8	7.4	6.4	3.6	3.4	4.6	NPD	8.2	3.4	4.9	NPD	3.2	3.4	NPD	NPD	3.1	3.5	NPD	NPD
4	6.4	7.4	6.0	5.3	8.3	9.6	12.9	20.3	3.7	5.5	7.7	6.1	3.4	3.2	5.6	NPD	7.9	3.1	NPD	NPD	3.3	3.2	NPD	NPD	3.0	3.0	NPD	NPD
5	8.2	8.6	6.2	6.1	8.2	9.5	12.5	22.7	4.4	5.0	7.9	10.6	4.0	3.6	NPD	NPD	3.6	4.0	NPD	NPD	3.6	4.0	NPD	NPD	3.5	4.1	NPD	NPD
6	8.0	7.1	7.9	7.1	8.3	10.5	12.3	22.4	4.5	4.8	8.5	11.2	4.0	3.8	NPD	4.8	3.8	3.8	NPD	NPD	3.6	3.4	NPD	NPD	3.4	3.9	NPD	NPD
7	5.7	6.0	4.9	5.2	7.6	8.4	11.6	18.6	3.4	4.0	9.2	11.2	3.3	3.0	7.9	NPD	2.6	3.1	NPD	NPD	2.7	3.1	NPD	NPD	2.7	3.0	NPD	NPD
8	6.1	5.8	5.3	5.6	7.7	8.3	10.8	17.3	3.5	5.0	8.6	10.6	3.8	3.1	NPD	4.5	2.8	3.1	NPD	NPD	2.9	3.0	NPD	NPD	2.8	3.3	NPD	NPD
9	11.0	10.7	9.8	7.6	12.2	12.4	14.0	24.3	5.2	5.5	9.5	12.8	4.7	4.2	7.4	8.3	4.3	4.2	NPD	NPD	3.9	4.3	NPD	NPD	3.9	4.2	NPD	NPD
10	10.0	11.0	9.3	7.3	11.0	12.3	14.2	23.0	5.4	5.6	9.1	17.9	5.0	4.1	7.0	6.5	4.2	4.3	8.0	NPD	3.7	4.3	NPD	NPD	3.9	4.3	NPD	NPD
11	7.8	6.9	5.4	7.1	7.9	9.7	11.5	20.4	3.9	4.8	9.2	12.7	3.7	3.3	7.4	4.1	3.3	3.0	6.2	NPD	2.9	3.2	NPD	NPD	2.9	3.2	NPD	NPD
12	8.7	7.3	6.1	7.6	9.3	9.4	12.0	19.5	4.3	4.7	8.9	12.9	4.6	3.1	6.2	5.9	3.6	3.2	NPD	NPD	3.0	3.1	NPD	NPD	3.3	3.2	NPD	NPD

NPD = No Pull Data.

Table 5: Round 1 Wire Bond Pull Test Results

Table 5 summarizes the results of all the pull tests. There is no military standard for the strength of platinum wire bonds; however, as a reference, the military specification for 0.7 mil gold wire (which is larger than the Pt wire being used) is 1.6g. The initial pull strength before the coating shows all groups on all boards had pull strengths well above that specification. The effect of coating thickness becomes evident in reviewing the post-coat pull strengths. The 2µm coating (Board 1) provided little or no discernible benefit. At 5µm (Board 2) the mechanical support provided by the coating is apparent with increases in pull strength ranging from 5 – 48% depending on the group. As expected, the thicker coatings provided more support. The 12µm coating increased pull strengths from 43 – 137%, and the 24µm coating increased pull strengths from 156 – 294%. These dramatic increases in pull strength are in line with reports in the literature. After ten thermal cycles, the pull strengths dropped considerably. These drops are in-line with previous wire bond tests, so this result was expected. By comparing Boards 1 and 2 to Boards 3 and 4, it can be seen that the thicker coating is still supporting the wire bonds through 20 thermal cycles. After 30 thermal cycles, little can be discerned about Boards 3 and 4. Table 2 indicates that many groups start to have no pull data (NPD) after 20 thermal cycles. This occurred for a number of reasons. The thickest, 24µm coating on Board 4 began to pull away from the surface of the LTCC as shown in Figure 38. As a comparison, Figure 39 shows Board 3 after 20 thermal cycles with no delamination. As the coating peeled away from the surface, it lifted many of the wire bonds. This was the only board that experienced any delamination of the coating.

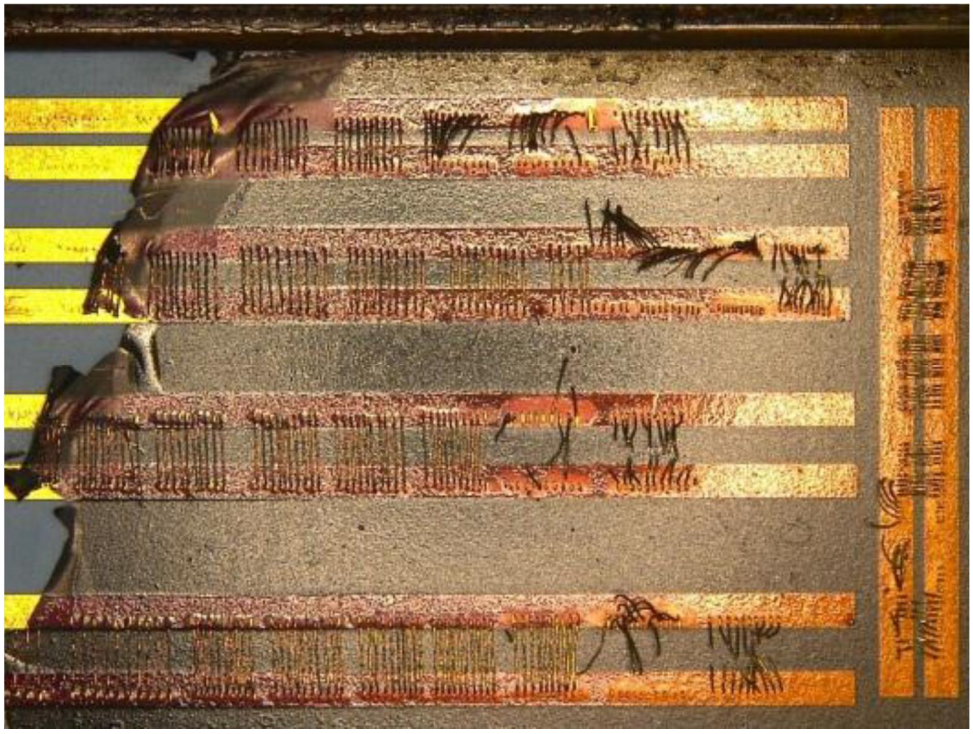

Figure 38: Board 4 after 20 Thermal Cycles up to 450ºC

Figure 39: Board 3 after 20 Thermal Cycles at 450ºC

Another issue caused NPD situations with Board 3 and exposed larger issues that will affect future test plans. It appears that the softening of the coating at higher temperatures causes it to weigh down the wire bonds and make them sag. This made it impossible to get the hook under the wire bonds for pull testing. This is especially problematic for g-loading applications. The sagging indicates that at high temperatures coating is no longer mechanically supporting the wire bond. In fact, the extra loading from the coating would likely cause the wire bonds to fail during centrifugal g-loading.

There was no sagging observed for Board 1 or Board 2, but the pull strengths indicate that the coating was also not providing any extra support after thermal cycling. The NPD data points on Board 2 come from testing error and were not coating related. The control TC used in the box furnace was already installed and had been previously used for thermal cycling, but at lower temperatures. There was a plastic coating on the TC that melted and dripped onto Board 2 during the first set of thermal cycles.

The first and most obvious conclusion from this test was that the coating cannot be used as a structural component at 450°C. While the initial gain in strength is promising, the material decomposes too rapidly and it is too soft at 450°C. According to the data sheet, the coating has a Young's Modulus of >80 MPa at 450°C, but this increases to >500 MPa at 377°C. Since this is a significant increase and Siemens' industrial turbine applications have maximum temperatures in that range, APEI recommends partially redoing the experiment at 400°C. Only two thicknesses will be used (8µm and 12µm) and there will be a reduction in the total number of wire bonds (for time and labor savings). During this testing, APEI will also prepare wire bond test boards for the spin test scheduled in Task 6. With the experience gained during this initial testing, redoing the test for 400 °C and preparing for the spin test was done. Analysis of engine models indicated that for Row 4 blade installation, the maximum temperature seen by the boards is slightly below 400ºC, instead of the initial estimation of 450ºC, an initial estimate which was made with a cruder approximation.

A second thermal cycle experiment was performed to determine if the polymer coating could be beneficial to Siemen's applications due to the lower operating temperature (380 – 400°C). This second thermal cycle testing was not originally planned in this program. To minimize the impact to the original schedule APEI, Inc. also performed the originally scheduled spin testing in parallel with this task. The initial testing indicated that the most effective coating thicknesses were greater than 5µm, but no greater than 12µm. Coatings less than 5µm did not significantly increase the bond strength, but coatings greater than 12µm added significant mass to the wire bond that caused sagging at higher temperatures and could be detrimental during g-loading. Two test boards were coated with 8µm and two test boards were coated with 12µm of polymer. One set of boards was thermal cycled at APEI, Inc. facilities and the other was sent to Aerodyn Engineering in Indianapolis for spin testing.

For this task, five LTCC substrates were produced and each was mounted into a metallic package using a laser welded bezel. Each board was bonded with 400 test wire bonds. The wire bonds intended for thermal cycle testing were created from 10µm X 20µm platinum (Pt) ribbon. Half of the wire bonds intended for spin testing were created from

the same PT ribbon. The other half were created using 25µm gold (Au) wire. Previous heated spin tests of Au wire bonds revealed that Au is an unsuitable material for high-temperature, g-loaded electronics. Figure 40 shows Au wire bonds that were deformed during heated spin testing.

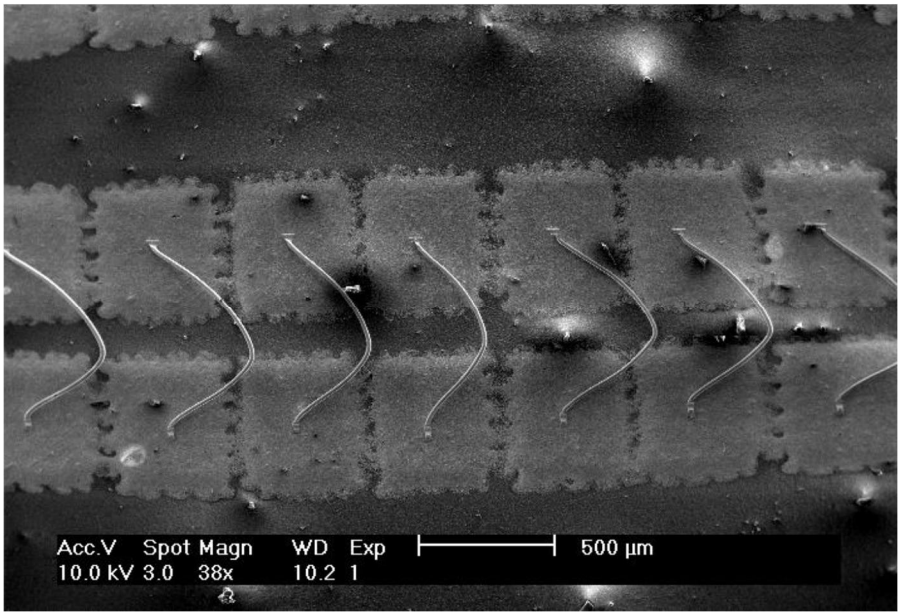

Figure 40: Au Wire Bonds After Spin Testing at 450ºC and 15,000g

Pt wire bonds do not readily deform when subjected to 450°C and 15,000g; therefore, the addition of the Au wire bonds was necessary to help determine the polymer coating's effectiveness. The Pt wire bonds were still necessary on the spin test boards to determine if the polymer coating added too much mass and therefore deteriorated g-load performance. Wire bond settings for length and loop height were kept consistent for every wire bond during the test. The settings for force, time, and ultrasonic power were determined by the material of the bond (Pt or Au). The settings for each material are summarized in Table 6.

Material	Bond	Power	Time	Force	Temperature (°C)
Platinum	1	0.82	4.6	0.0	300
	2	1.21	5.4	0.7	300
Gold	1	1.8	7.1	0.8	215
	2	2.27	7.4	1.5	215

Table 6: Bonder Settings Used To Create Bond Test Boards

After wire bonding, the boards were sent to a vendor for polymer deposition. Boards TC-12 and ST-12 were coated to a thickness of 12µm. Boards TC-8 and ST-8 were coated to a thickness of 8µm. This polymer coating takes place via chemical vapor deposition (CVD), so every exposed surface was uniformly coated. One control board was left uncoated to have a direct comparison for the coating's effect on pull strength.

The strength of the wire bonds was determined through pull testing using a Dage 4000 multipurpose reliability tester. Pull tests were performed on 50 wire bonds from each thermal cycle board (TC-8 and TC-12) and the control board (C) before coating, after coating, and after every 10 thermal cycles up to 50 total cycles.

The thermal cycling took place in computer-controlled Vulcan box furnace. The furnace automatically cycled between 400 °C and 50 °C. The control thermocouple was spot welded to a previously used metallic board package. This ensured that the thermal mass attached to the control was nearly identical to that of the boards under test. The board reached the maximum test temperature of 400 °C in 15 minutes. The cool down time to reach 50 °C was about 2.25 hours.

The spin test took place in Aerodyn Engineering's spin test rig. Boards ST- 8 and ST-12 both underwent spin testing. Microscope photographs were taken at 100X before and after spin testing to inspect for wire deformation.

The results from the thermal cycle testing to 400°C prove to be very promising and show that the 8µm polymer coating board exhibits a 355% improvement in strength over the control board, while the 12µm polymer coating board exhibits a 410% improvement in strength over the control board – both after a total of 50 cycles. Table 7 shows the averages of the pull test data for each of the three boards, after every 10 cycles. Therefore, this thermal cycling test indicates that the wire bond reliability may be significantly improved as a result of the polymer coating.

	TC-8	TC-12	C
Pre	8.436764	7.200764	8.4545
Post	13.44244	14.69565	-
10	13.6578	16.8784	7.218967
20	13.53128	17.26254	5.0591
30	13.37842	15.6731	3.545156
40	12.10376	16.83268	3.537767
50	12.32316	14.23264	3.4663

Table 7: Round 2 Heat Cycle Wire Bond Pull Strengths (C is Control Board)

The results from the boards that underwent spin testing, which experienced 400 °C and 17,000g for two hours, also prove to be promising. Au wire bonds were added to these boards to determine the ultimate effectiveness of the polymer coating. The polymer coating did not prevent the Au wire bonds on the spin test boards from deflecting due to g-load; however, they were not completely pressed against the substrate as in previous

spin tests with Au wire bonds. Additionally, the Au wire bonds with 12µm polymer did not deflect to the extent of those with the 8µm coating. Figure 41 shows the deflection of the 8µm bonds (left) compared to the 12µm bonds (right). These results indicate that the polymer was providing mechanical support to the bonds during g-loading.

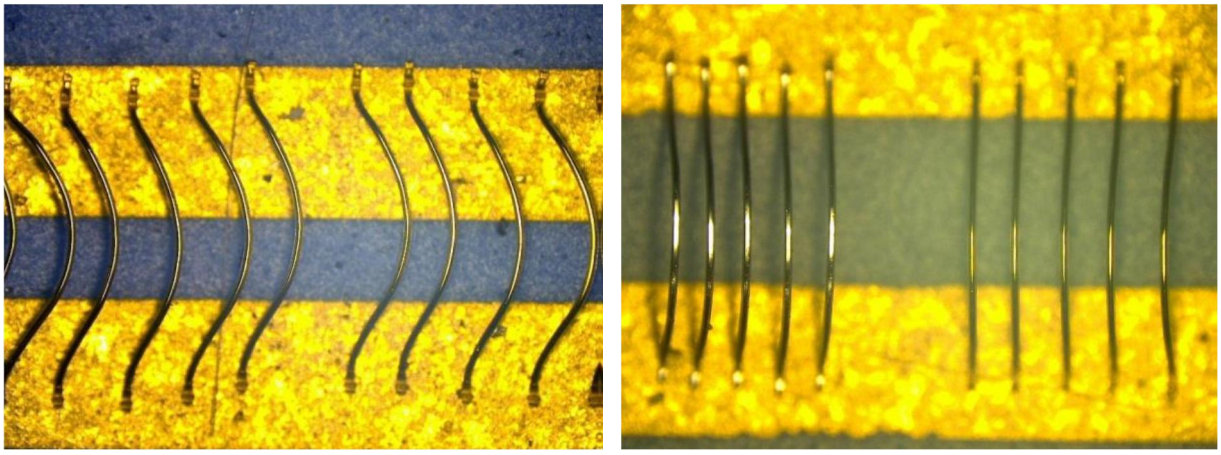

Figure 41: Deflection of Au Bonds Coated with 8um (Left) and 12um of Polymer (Right)

The Pt wire bonds demonstrate expected survivability of the harsh spin testing environment. The increase in pull strength (Table 8) after spin testing (compared to the post polymer coat thermal cycle board) is unexpected but is still within the statistical distribution of pull test results. Both boards successfully survived the spin testing and Figure 42 and 43 show the condition of the bonds after exposure to the spin test environment for 2 hours.

	ST-8	ST-12
Pre Coat	8.44	7.20
Post Coat	13.44	14.70
Post Spin	13.71	17.31

Table 8: Round 2 Spin Test Wire Bond Pull Strengths

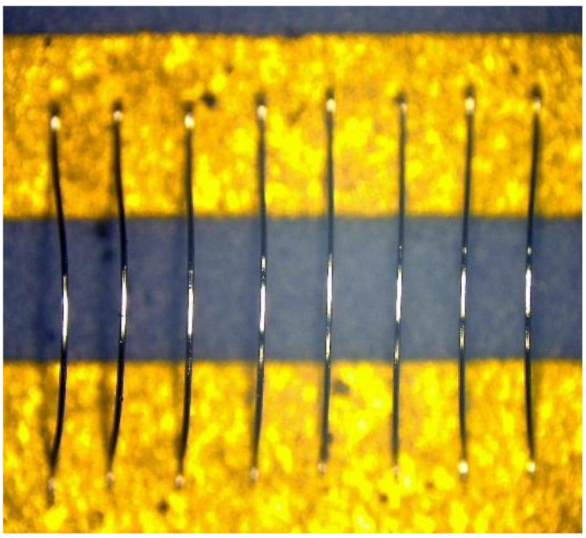

Figure 42: Pt Wire Bonds with 8um Coating after Spin Testing

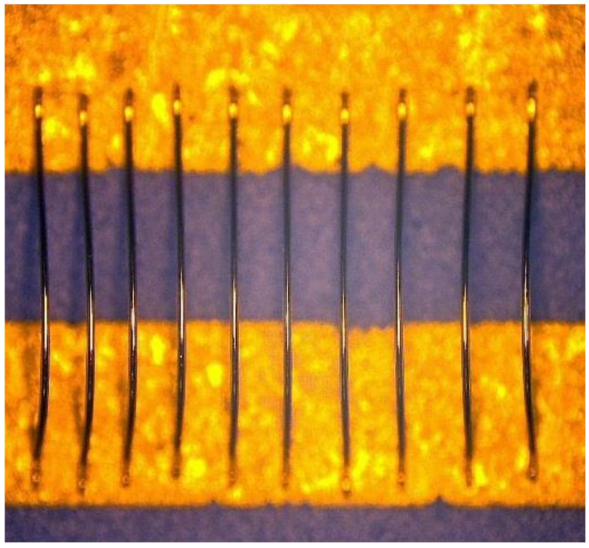

Figure 43: Pt Wire Bonds with 12um Coating after Spin Testing

Ultimately, the polymer coating has been shown to dramatically increase the integrity and reliability of platinum wire bonds. Even when exposed to the harsh environments of spin testing, the coating allowed the wire bonds to remain intact. For all boards constructed after April 2013, the 12µm polymer coating was utilized because of its ability to withstand spin testing, thermal cycling, and its ability to maintain continued high pull strength. During subsequent spin testing in the spring of 2014, no functional wire bond delamination was in evidence.

Resolution of Planar Trace Delamination Issue

Another issue that occurred in early spin tests is metal trace delamination within planar spiral inductors. Large metal traces were used to create planar inductors on the Low Temperature Co-fired Ceramic (LTCC) substrate of the wireless telemetry boards. Uniquely, these boards went through ten thermal cycles before the spin test as part of their calibration. It is believed that these thermal cycles weakened the bond between the surface metal and the LTCC substrate. During the spin tests in January to February 2012, the metallic traces delaminated. Beginning in spring 2012, a method to fix them problem was developed.

During thermal cycling and spin tests of the previous generation of wireless telemetry boards in early FY 2012, we observed damage to the planar inductors. The traces comprising the inductors lifted from the board and created open circuits, completely compromising the board functionality (see Figure 44). We believe the thermal mismatch between the gold traces and low temperature co-fired ceramic caused a weakening of the bond between them during thermal cycling. During subsequent spin testing, the g-loads and vibration broke those bonds, and the gold trace delaminated.

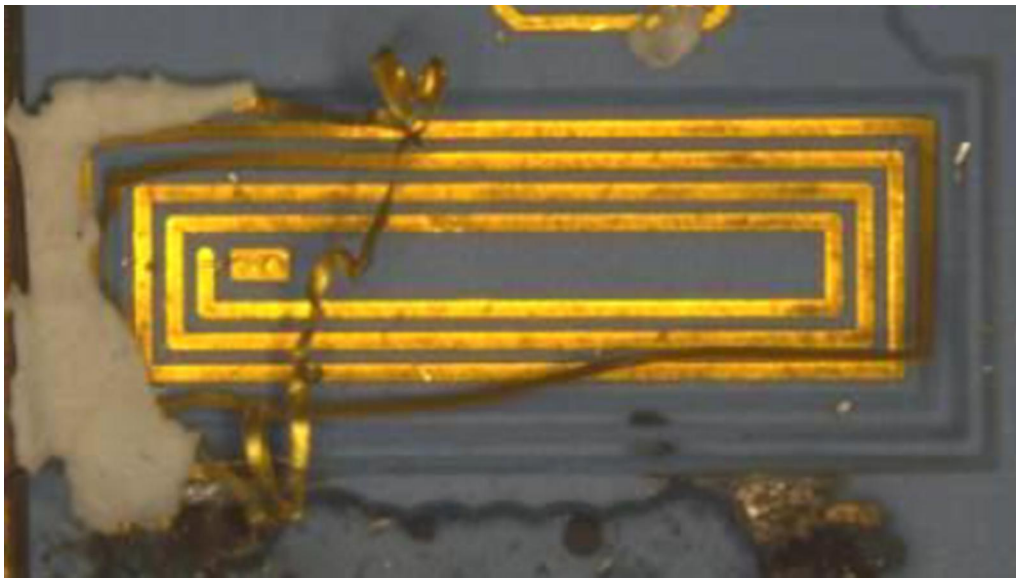

Figure 44: Close-up of Damaged Planar Inductor

Beginning in the summer of 2012, APEI Inc. developed and implemented a methodology of coating the planar inductors with a glass encapsulation. This is applied after the gold plating process, as a post-fire paste via screen printing. Upon application, the substrate was then re-fired at 850^{o}C in order to sinter the encapsulation. Figure 45 shows an un-encapsulated vs. encapsulated inductor.

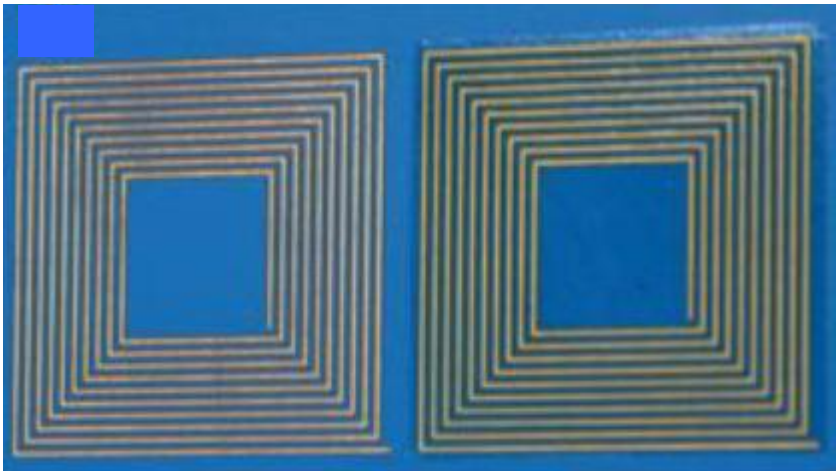

Figure 45: Unencapsulated (left) and Encapsulated (right) Inductors

To test this methodology, two boards, each with 41 inductors of several different geometries, were created. The inductors of one board were coated with the glass encapsulant, and the inductors of the other board were not. Each board was then subjected to thermal cycling to 450°C. During each thermal cycle, the board is heated to 450°C, held at that temperature for ten minutes, and removed from the oven to be placed on a heat sink for rapid thermal shock cooling to 40°C. An initial analysis was performed after 50 such cycles had been performed on each of these boards (out of the 100 cycles planned). Figure 46 shows the difference between the encapsulated (top) and un-

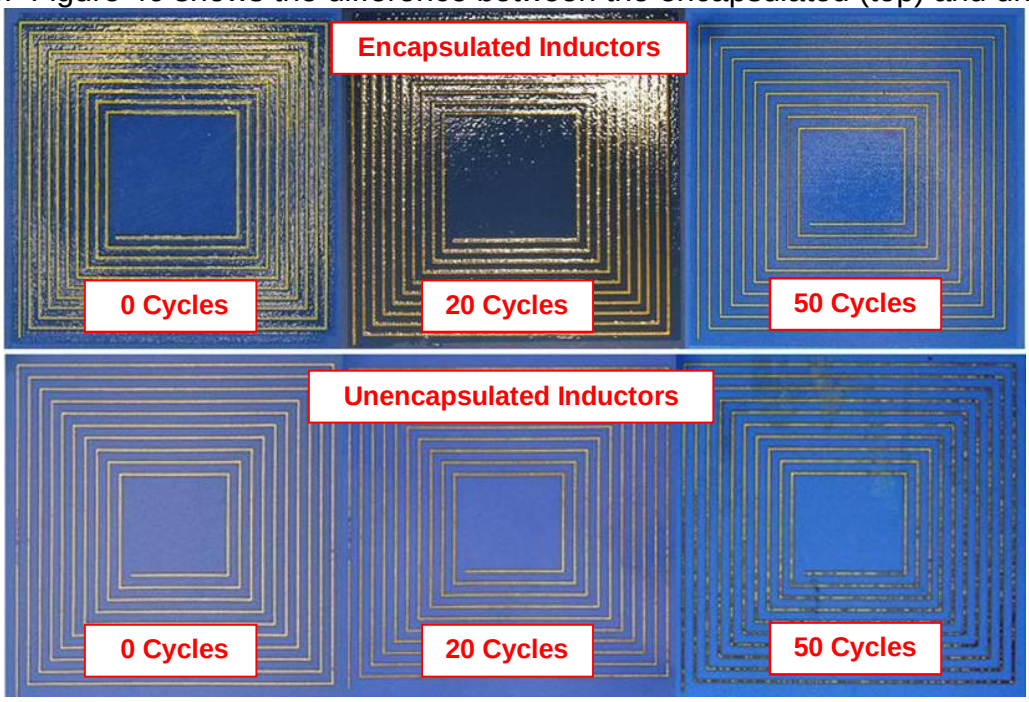

Figure 46: Thermal Cycle Performance of Encapsulated and Unencapsulated Inductors

encapsulated (bottom) inductors at 0, 20, and 50 cycles. In the bottom right, significant degradation of the inductor traces can be seen on the un-encapsulated inductor that has

experienced 50 cycles. This spotting was seen in inductors on wireless telemetry boards which later experienced delamination during spin testing.

One hundred thermal shocks were completed for both of the test boards. Both the encapsulated and unencapsulated boards were cycled together to ensure that the two boards were exposed to the same thermal profiles. Discoloration was noted upon the first inspection of the unencapsulated board. While this discoloration did not denote failure, previous experience by APEI engineers indicates that discoloration shows wear on the electrical traces and prolonged exposure to thermal cycling will yield eventual trace failure. Figure 47(a) shows the first sign of delamination of the traces after 60 cycles had been completed. The delamination is very evident and indicates a significant failure of the traces due to thermal cycling, which would render the inductor useless if used in a circuit design. The delamination seen on the unencapsulated inductor did not get significantly worse over the course of the last 40 cycles (Figure 47b); however, this is insignificant because the inductor would already be degraded and unusable in the circuit design as a result of the delamination. The unencapsulated failure can be contrasted with the replicate inductor (Figure 47c) on the encapsulation board for comparison purposes. It is important to note that the encapsulated board showed no signs of fatigue due to the thermal cycling process, throughout the duration of the testing.

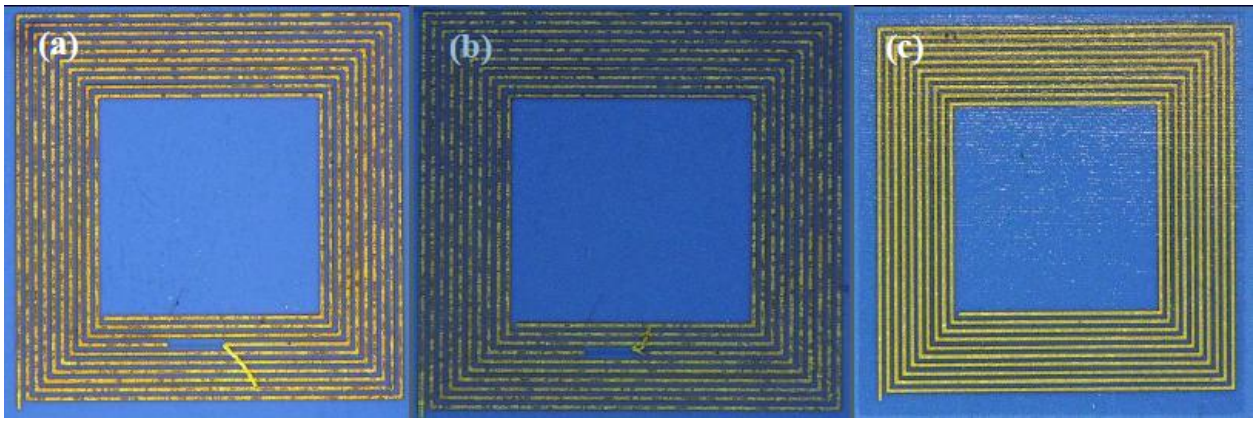

Figure 47: Unencapsulated at 60 (a) and 90 (b) Cycles, Encapsulated at 100 Cycles (c)

In addition to thermal shocking, APEI engineers investigated the effects of induced mechanical damage to the board to determine if the encapsulation method also performed well under extreme mechanical fatigue. Both of the boards were intentionally cracked so that the crack perforated several inductors. These boards were also thermal cycled under the aforementioned conditions. The unencapsulated boards showed delamination around the cracks after 20 thermal cycles. These delaminations became more significant over time, with increased thermal cycling, as seen in Figure 48. Not only did the electrical traces become degraded along the crack, but the LTCC substrate also showed significant wear along the crack. Delamination can be seen in both Figures 48 (b) and (c); it is shown to be isolated and just beginning in (b), while it becomes severe along the crack and quite significant in (c).

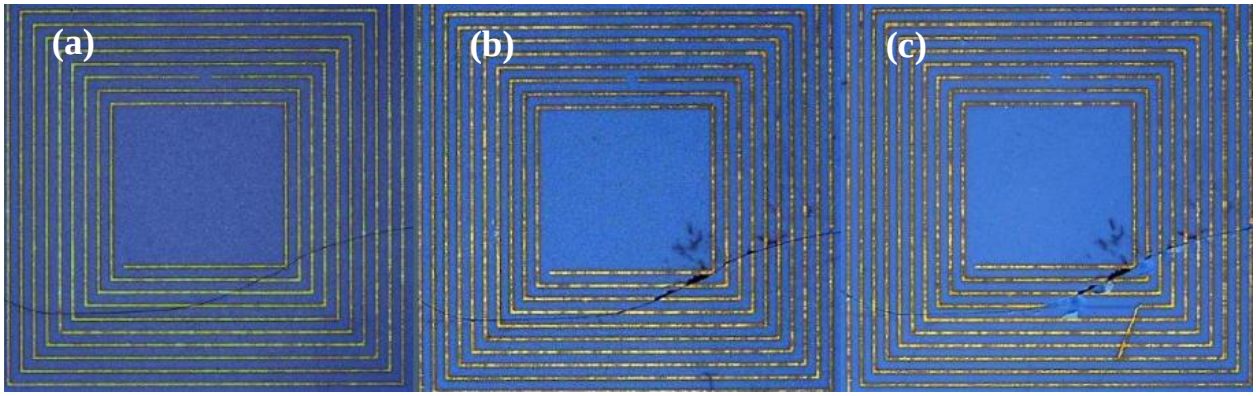

Figure 48: Unencapsulated at 10 (a), 50 (b), 100 (c) Cycles, Failing at Crack

In stark contrast to the failure of the un-encapsulated inductors, the glass encapsulant still protected the electrical traces from delamination – despite being mechanically compromised. The glass encapsulant did not show signs of additional cracking or fracturing along the initial break; rather, the encapsulant appeared to have a clean edge along the initial break. In fact, the encapsulation appears to lend the LTCC substrate additional support from further damage. The results can be seen in Figure 49.

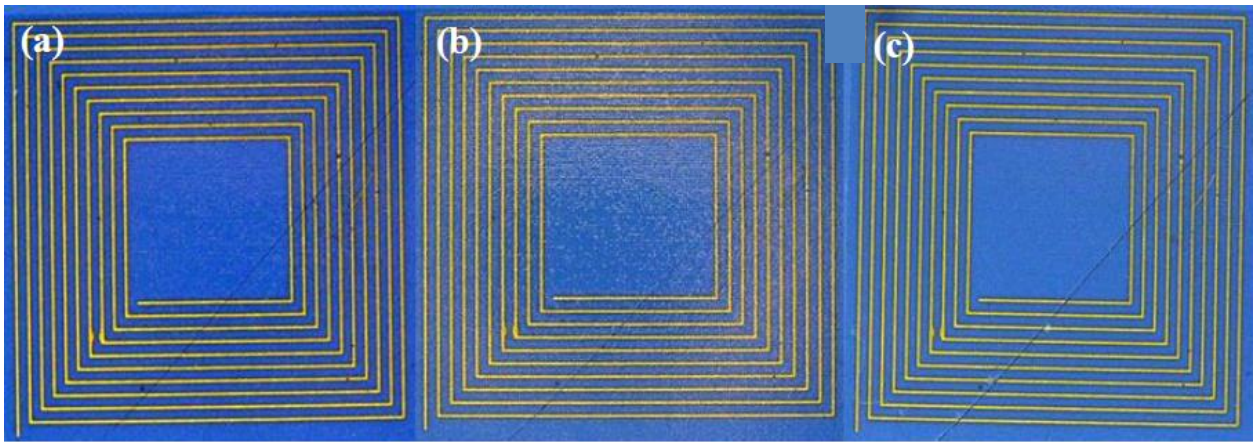

Figure 49: Encapsulated at 10 (a), 50 (b), 100 (c) Cycles, Good Even with Crack

On all subsequent functional electronics boards with glass-encapsulated inductors, no delamination was seen during temperature cycles or g-load tests.

Procurement and Validation of New and Improved Silicon Carbide Transistors

At the midpoint of this project, the supplier of our specialized signal-level silicon carbide (SiC) transistors, Semisouth, closed their doors and informed us they would no longer be able to supply these parts. These transistors were key functional components for our wireless telemetry boards. Twelve to fifteen transistors are used on each board (this number varies between thermocouple and strain boards).

APEI Inc. worked with Microsemi Power Products Group to acquire a SiC transistor to replace Semisouth components. Testing has been performed at APEI Inc. laboratories with good results. Microsemi sampled multiple SiC Static Induction Transistors (SITs) for characterization. APEI Inc. engineers characterized these devices from room temperature to 450°C. Initial analysis indicated that these devices were a superior candidate for replacing the Semisouth transistors. A test was performed to measure the current vs. voltage (transconductance) of these transistors at 300ºC and 450ºC, at source-to-drain voltage (V_{DS}) of 25V and 40V. Results are shown in Figures 50 and 51.

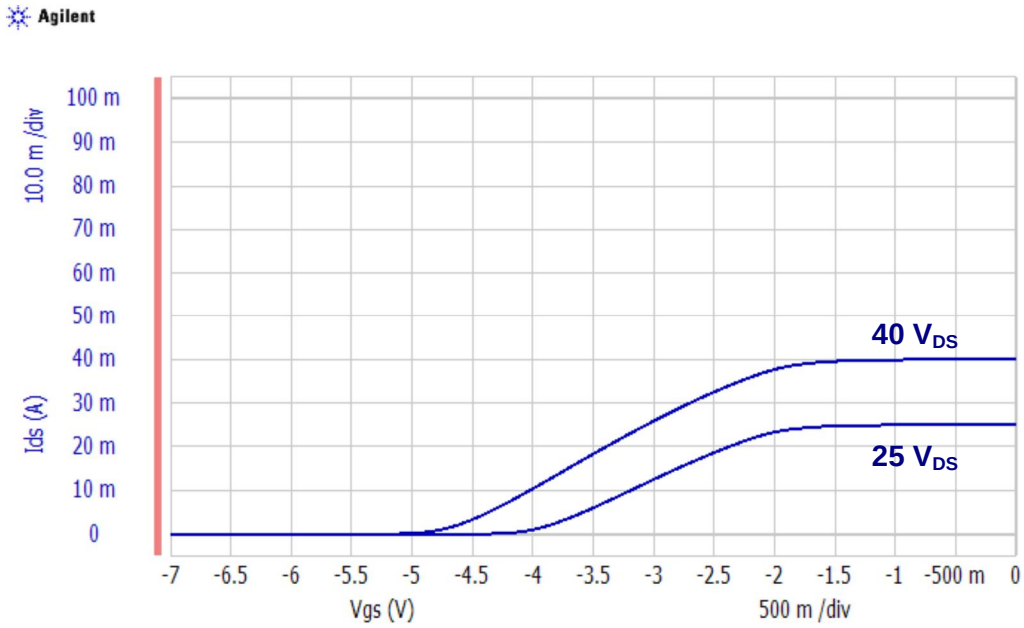

Figure 50: Transistor Transconductance at Room Temperature

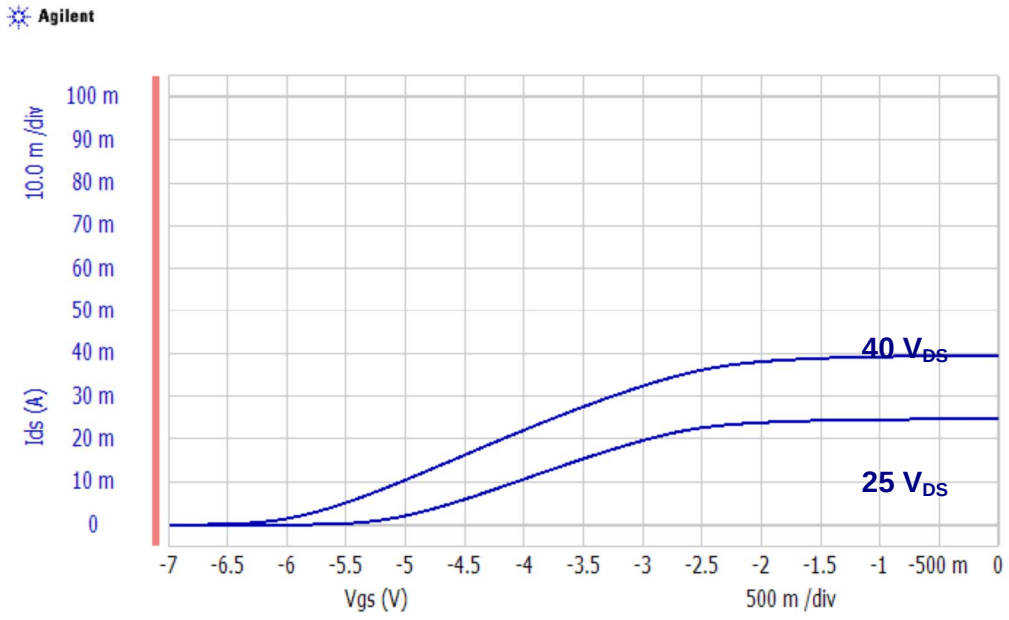

Figure 51: Transistor Transconductance at 450ºC

The curves in Figures 50 and 51 are very similar, with only a slightly lower slope and more negative V_{DS} occurring at 450°C. Thus these devices show very good temperature stability and, therefore, they can be considered a suitable candidate for replacement of the Semisouth transistors.

An order of approximately 100 transistors was placed with the new vendor. Upon receiving the devices, all of the devices underwent characterization (called the first round of characterization) over temperature to determine the best matched pairs for future circuit design. Overall, there were a total of 25 best matched pairs, with no failed devices – demonstrating the potential of these candidate devices. Figure 52 shows a graph of three matched pairs from the current inventory. Almost perfect overlap is observed in the three pairs of devices. This matching is important because it allows for more exact differential amplifier configurations, a key circuit in instrumentation amplifiers.

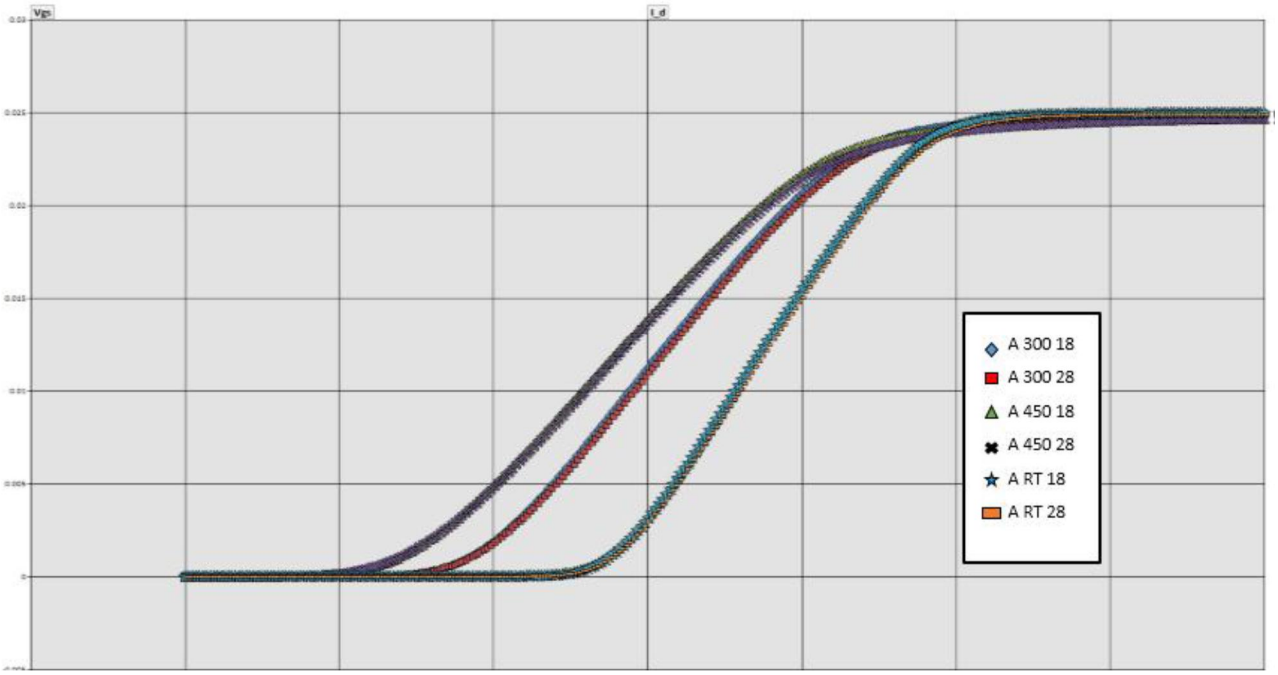

Figure 52: Three Matched Transistor Pairs, with Overlapping Transconductance Curves

APEI ordered 1000 more devices from the vendor, and they were delivered in June 2013. They were characterized over temperature and then optimally matched for later circuit design. In order to facilitate the larger sample size, a fixture was created that enabled a larger number of transistors to be characterized at one time. These transistors were then incorporated into all future boards, including those to be used in the next spin test. All these devices were later consumed in subsequent furnace testing.

The performance of the boards as a system over temperature is further discussed below. The improvements in transistor functionality gained by the switch to the Microsemi transistors were evidenced in the stability of function at temperatures above 350ºC.

Procurement and Validation of High Temperature Capacitors

Capacitors are a key component of the wireless telemetry board. They are used in power rectification, signal shaping, and transistor matching. Because of the high temperature environment to which the wireless electronics board is exposed, Arkansas Power Electronics International, Inc. (APEI) chose to primarily use dielectric on glass devices. These devices are far more temperature tolerant than typical capacitors, yet many have significant variation in their values over temperature, varying in value by as much as 80%. Long exposure to high temperatures leads to the even more detrimental effect of high leakage current. When exposed to high temperatures and AC power, the insulation between the parallel plates within the capacitors breaks down, effectively shorting the capacitor and making it non-functional. Capacitor degradation was observed in long-term high temperature testing of the boards, with significant degradation occurring between ten and twenty hours. Slow changes in these components' capacitances affect the electronic filtering, signal generation, and sensor interface functionality of the boards, reducing measurement accuracy and increasing power losses. In 2012, a number of new capacitor vendors have indicated that their products may have the capability to survive longer at higher temperatures. While none of their in-house tests matched the temperature and duration of our environmental needs, Siemens and APEI came to believe that a significant improvement in capacitor duration may be realized.

In order to characterize and solve this issue, Siemens directed APEI to perform a capacitor substrate test. The methodology of testing is to expose capacitor samples from different vendors to AC power at high temperature for extended periods, and then to evaluate the leakage current of each sample at certain times during this oven testing. Two custom LTCC substrates were constructed. These substrates were populated with multiple capacitors from four different vendors, referred to as Vendors A-D. The capacitors all have individual connections for the bias voltage and share a common ground. The individual power connections allow current measurements for each capacitor during temperature exposure. The capacitor testing methodology is discussed in Section 1.3 above.

One of the capacitance test boards was thermally aged at 350ºC, while the other was aged at 450ºC – each for 500 hours or until capacitor failure, under a bias voltage. Throughout the aging process, the leakage current of the different capacitors was recorded.

The time to failure (TTF) was determined from the leakage current measurements. A capacitor was defined as failed once its leakage current exceeds 0.5 mA. At 30 V, the power consumed at 0.5 mA is 15 mW. For the final application, only 500 mW are being delivered to the circuitry, so this single capacitor would be using 3% of the entire power budget.

At 450°C, only 7 of the 32 capacitors survived: none from Vendor A, two from Vendor B, one from Vendor C, and all four from Vendor D. Vendor B and Vendor C components still have relatively high leakage current, greater than 10 µA. None of the Vendor D capacitors exhibited leakage beyond 8µA. An identical component to the lone surviving

Vendor C component failed after 56 hours, illuminating the component variance that occurs in just two samples.

The results at 350°C were slightly better, but still illustrate the trouble most capacitors have at elevated temperatures. Many capacitors lasted considerably longer, but most still did not last beyond 25 hours of temperature exposure. There were a total of 10 surviving capacitors at 350°C: none from Vendor A, four from Vendor B, two from Vendor C, and all four from Vendor D. The final leakage currents of all but one of the surviving capacitors were below 100µA, and the Vendor D capacitors had final leakage currents less than 1µA. Table 9 shows the results of the capacitor tests. Orange indicates partial to moderate failure and green indicates positive results. Vendor D was a clear standout. Use of these capacitors will allow longer board lifetimes and better accuracy over temperature. Future spin boards will incorporate these devices.

Advanced Thermocouple and Strain Gage Board Manufacture and Test Results

After finding solutions to the problems of wire bond delamination and sagging, inductor delamination, transistor sourcing, and capacitor failures at temperature, APEI embarked on the final design and manufacture of fully functional wireless telemetry boards. Completed in January 2014, these boards contain all the improvements achieved and tested since the summer of 2012, including improved silicon carbide transistors, glass encapsulated planar inductors, dramatically strengthened wire bonds, and robust high temperature capacitors.

Initial testing results of the strain gage board (without the final capacitors) are shown in Figures 53 to 56. In this test, three different 10mV tones were sent into the boards, simulating dynamic strain gage responses at 100Hz, 500Hz, and 1000Hz. The RF output of the board was then amplified, measured, and demodulated to recover these simulated strain gage signals. This was done at room temperature, 200°C, 325°C, and 400°C.

Board Port #	Vendor	Nominal Value	450 °C TTF (Hours)	450 °C Final Leakage (Amps)	350 °C TTF (Hours)	350 °C Final Leakage (Amps)
1	A	80nF	0.82	(failed)	31.05	(failed)
2	A	80nF	0.82	(failed)	33.75	(failed)
3	A	10nF	1.36	(failed)	2.70	(failed)
4	A	10nF	1.36	(failed)	1.44	(failed)
5	A	1nF	1.18	(failed)	2.52	(failed)
6	A	1nF	5.14	(failed)	20.98	(failed)
7	A	100pF	12.15	(failed)	10.43	(failed)
8	A	100pF	0.82	(failed)	1.44	(failed)
9	A	10pF	25.01	(failed)	1.80	(failed)
10	A	10pF	10.17	(failed)	12.59	(failed)
11	B	47nF	0.64	(failed)	1.44	(failed)
12	B	47nF	0.64	(failed)	1.62	(failed)
13	B	10nF	0.82	(failed)	22.24	(failed)
14	B	10nF	1.00	(failed)	26.74	(failed)
15	Board ref.	Open				
16	Board ref.	Short				
17	B	100pF	20.05	(failed)	>500	4.5E-6
18	B	100pF	23.94	(failed)	>500	62.4E-6
19	B	10pF	>500	123.4E-6	>500	21.4E-6
20	B	10pF	>500	193.3E-6	>500	156.6E-6
21	C	10nF	1.00	(failed)	5.04	(failed)
22	C	10nF	1.00	(failed)	4.69	(failed)
23	C	1nF	2.99	(failed)	24.94	(failed)
24	C	1nF	2.62	(failed)	9.72	(failed)
25	C	100pF	2.45	(failed)	19.36	(failed)
26	C	100pF	2.09	(failed)	5.59	(failed)
27	C	10pF	0.65	(failed)	1	(failed)
28	C	10pF	0.65	(failed)	1	(failed)
29	C	1pF	>500	180.2E-6	>500	11.5E-6
30	C	1pF	56	(failed)	>500	202.0E-9
31	D	6.8nF	>500	7.7E-6	>500	356.0E-9
32	D	6.8nF	>500	5.8E-6	>500	458.0E-9
33	D	8nF	>500	6.1E-6	>500	2.0E-9
34	D	8nF	>500	6.1E-6	>500	255.0E-9

Table 9: 500 Hour Heated Capacitor Test Results (TTF = Time to Failure)

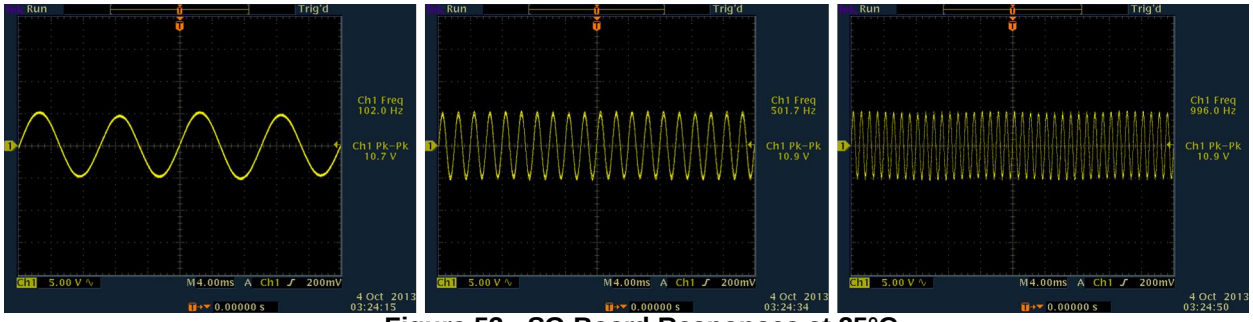

Figure 53: SG Board Responses at 25°C

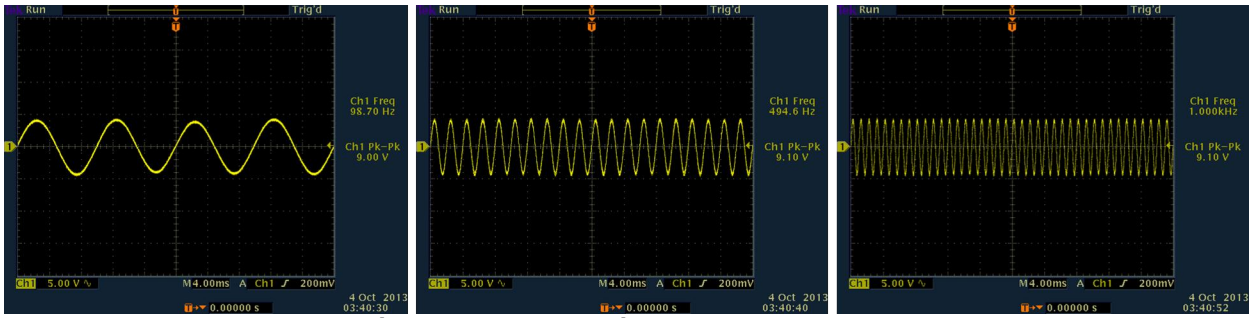

Figure 54: SG Board Responses at 200°C

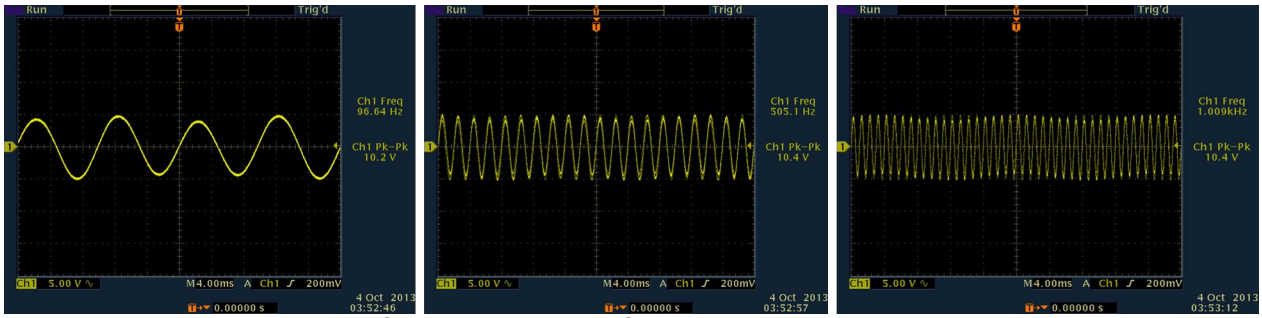

Figure 55: SG Board Responses at 325°C

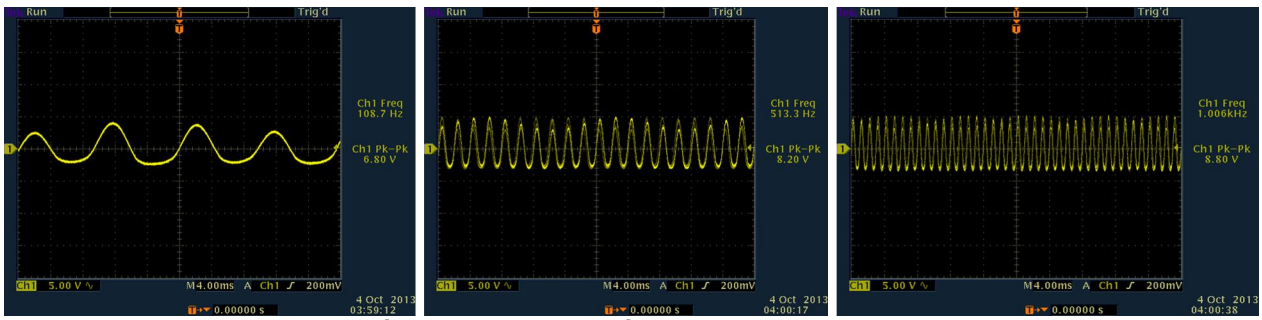

Figure 56: SG Board Responses at 400°C

These results indicate that the strain gage board is functioning over the full temperature range with minimal frequency error and moderate amplitude error. Table 10 summarizes the frequency and amplitude errors as a function of temperature and simulated sensor frequency.

Temperature (°C)	Input Frequency (Hz)	Frequency Error (Hz)	% Frequency Error	Amplitude Error (V)	% Amplitude Error
25	100	2	2.0	N/A	0
25	500	1.7	0.3	.2	1.9
25	1000	-4	-0.4	.2	1.9
200	100	-1.3	-1.3	-1.7	-15.9
200	500	-5.4	-1.1	-1.6	-15.0
200	1000	0	0.0	-1.6	-15.0
325	100	-3.4	-3.4	-0.5	-4.7
325	500	5.1	-1.0	-0.3	-2.8
325	1000	9	-0.9	-0.3	-2.8
400	100	8.7	8.7	-3.9	-36.4
400	500	13.3	2.7	-2.5	-23.3
400	1000	6	0.6	-1.9	-17.8

Table 10: Strain Gage Board Errors over Frequency and Temperature

The frequency error of the strain gage telemetry boards is fairly low, especially at higher frequencies. The amplitude error is somewhat higher. Typically, dynamic strain gage signals have superior frequency accuracy and moderate amplitude accuracy. For wired systems, 30% amplitude error is typical. This error is in the range of that obtained with these un-calibrated strain sensor telemetry boards. After temperature calibration of the boards, it is expected that the frequency and amplitude accuracy will be significantly improved.

In the fall of 2013, boards were rebuilt to incorporate newly available high temperature capacitors on the power input portion of the board. The previous capacitors were estimated to have lifetimes of 4-10 hours at target temperatures of 350ºC and 400ºC. These new capacitors are expected to last 20-500 hours at 400ºC. The addition of these new, more robust capacitors increases the likelihood of a successful spin test. The capacitors were delivered by the vendor four weeks later than initially promised, and that pushed out the delivery of the wireless telemetry boards accordingly. Also, there were a few larger capacitor values which were not available from these new vendors.

Arkansas Power Electronics International experienced technical difficulties in tuning the wireless telemetry boards. The tuning process balances the internal signals on the boards so that there is a flat amplification response over the desired temperature range. This proved to be more difficult than expected for the thermocouple board due to limitations in the available types of high temperature silicon carbide transistors. While

ultimately successful, the tuning of these boards caused significant additional delays in board delivery, with delays stretching to February of 2014.

Final Integrated Heated Spin Test Preparation and Results

Once completed, the boards were then coupled to an inductive power system and their functionality was confirmed in that configuration, with nominal results. These boards were then shipped to Aerodyn to be mounted into a high speed spin rig. Figure 57 shows one of the APEI electronics boards installed on the rotating spin rig disk. Figure 58 shows the electrical connections after the test, cemented in place. The gold box is the packaging of the APEI electronics board. It is connected to the rotating antenna (white box), from which it receives power. The APEI board is also connected to the slip ring in order to allow certain outputs to be viewed from the control room, and to introduce simulated sensor data signals for the board to modulate.

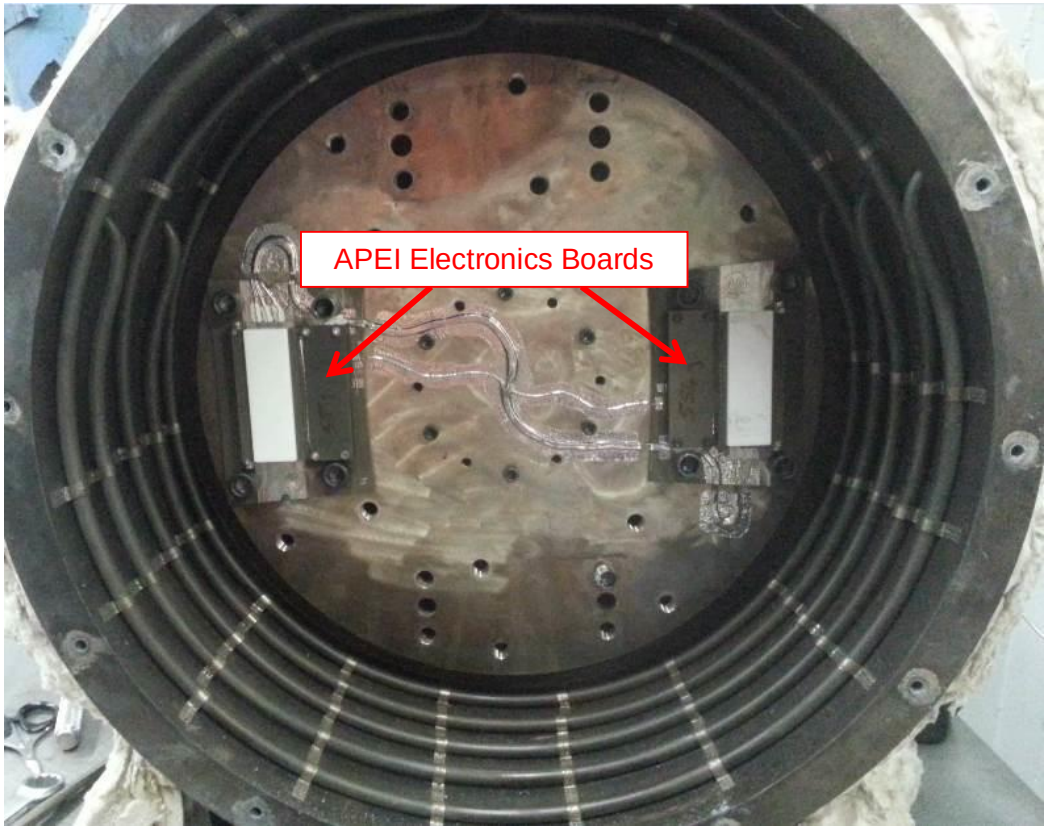

Figure 57: Aerodyn Spin Disk Mounted in Spin Rig

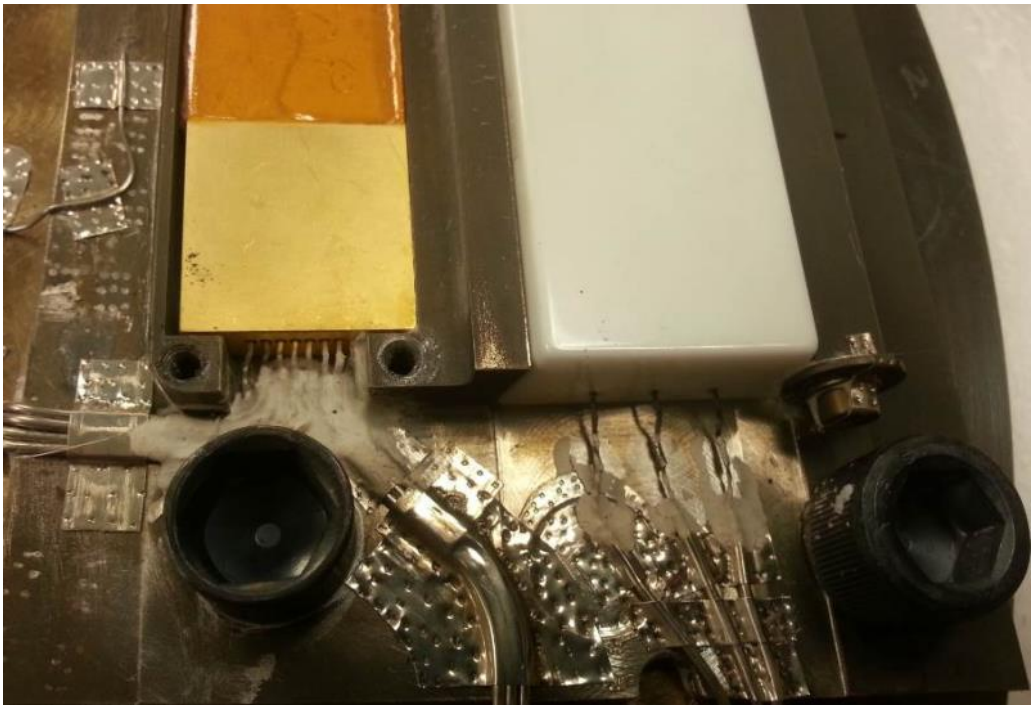

Figure 58: Electrical Connections on Rotating Components After the Test

During this spin test, the strain gage board functioned nominally up to 350ºC with no g-load. The board was powered wirelessly via inductive power. A 500Hz millivolt electrical signal was introduced to the electronic board via a slip ring in order to simulate a strain gage signal. This sensor signal was correctly modulated by the electronic board onto an RF carrier. The RF carrier was transmitted wirelessly. The received RF signal was demodulated, and the simulated sensor data was recovered successfully. While the temperature remained at 350ºC, the spin rig was spun at progressively higher speeds. The strain gage continued to function properly up to a speed of 3000rpm, which corresponds to 1500g. At this speed, it is believed that the power rectifier circuitry in the board failed.

The electronics boards receive alternating current (AC) power from the inductive power supply. In order to be utilized by the chips on the board, this power must be rectified, or converted, from alternating current to direct current (DC) power. At this point in the circuitry, this DC power is sampled to external pins on the board. These external pins allow the user to check the DC voltage levels being made available to the remainder of the board. In the spin rig test, these DC voltage pins are relayed out of the spin rig via a slip ring to the control room, where they are monitored (see Figure 59). When the spin rig was at 350ºC and 1500g, this voltage went from >15VDC to less than 0.5VDC. At the same time, the RF carrier signal from the strain gage board was lost. It is, therefore, assumed that the rectifier circuit malfunctioned.

Figure 59: Monitoring of Rectified Voltage on Spinning Electronics Board

The existence of these external pins, however, provided further test opportunities with the strain gage board. Because they are a power connection to the spinning board, it is possible to deliver DC power to the board via these pins to replace the power no longer available from the inductive power system. When this was done, the strain gage board produced an RF signal, and the simulated sensor signal was again recovered wirelessly. See Figures 60 and 61, which show the RF carrier signal and the demodulated simulated sensor signal, respectively.

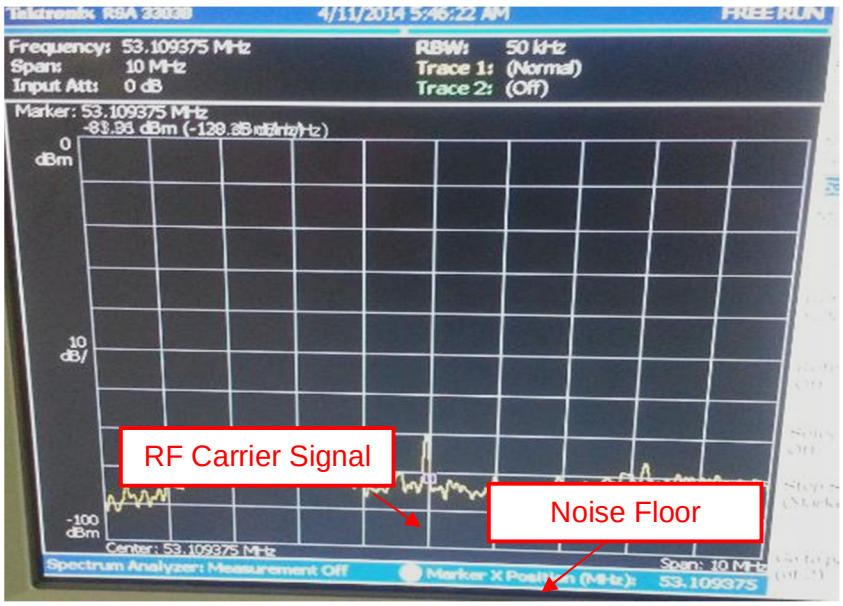

Figure 60: RF Carrier Generated by Strain Gage Board during Spin Test

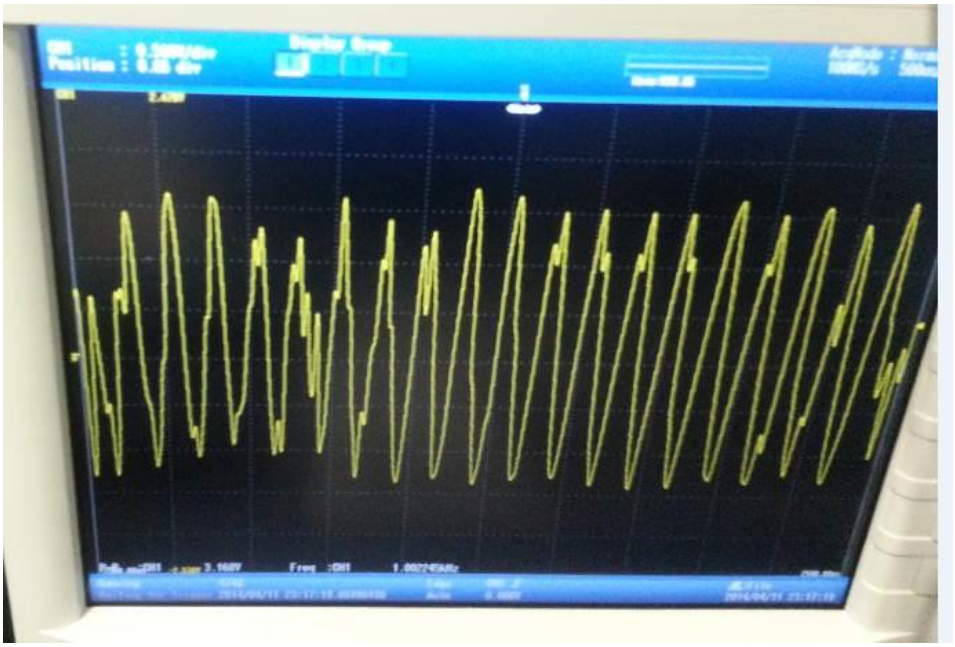

Figure 61: Demodulated Strain Gage Signal during Spin Test

On a subsequent day of testing, the strain gage board again functioned at high temperatures approaching 300ºC and g-loads up to 1,500g. During this portion of the test, the strain gage rectifier was not working, and no carrier could be found on the RF output. The board, therefore, was powered via the slip ring power circuit, and the RF signal was measured on those same slip ring pins. The board stopped producing an output after the g-load surpassed 1,500g.

The strain gage board's operation suffered failures in two different ways. First, the rectifier circuit failed. Second, the transmitter circuitry failed. Post-test inspection of the strain gage board revealed the likely causes of these failures. In the rectifier circuit, a capacitor failed (short circuit). This caused complete failure of the resonant rectifier circuit. In the section of the board which amplifies and modulates the RF signal, one end of a wire bond became disconnected. This wire bond appears to have come in contact with the grounded package. This shorted the RF signal path to ground. This explains why the RF signal was lost at certain g-loads (above 1,500g on two different days), and the signal was then recovered at lower g-loads. The wire bond was likely pulled into contacting the grounding package only while the g-load was relatively high, making the failure intermittent and recoverable.

The thermocouple (TC) board proved to be somewhat more robust than the strain gage board. It survived the initial 350ºC test, being powered wirelessly, and transmitting an RF carrier wirelessly. Over temperature, the TC board exhibited poor modulation. See the demodulated signal waveform in Figure 62, taken when the board was at 14,500g and 300ºC. Neither AC nor DC signals fed into the board were modulated properly. Distortions in the recovered waveform were present. Due to the nature of the design, a careful balance was struck in the resistances and capacitances attached to each amplifier

pair in the sensor signal processing chain. This design weakness is due to the lack of complementary types of silicon carbide transistors. Transistors of the MOSFET type generally come in two different internal configurations: N-type and P-type. Amplifier and circuit conditioning circuits generally require both N- and P-type transistors working in tandem for proper functioning. Because very high temperature, high frequency silicon carbide transistors are only available in the P-type form, certain design compromises were necessitated. Tuning these P-type only circuits was very difficult and time consuming. This process was responsible for a large portion of the delays in board delivery. It also resulted in boards whose modulation properties were existent, but poor.

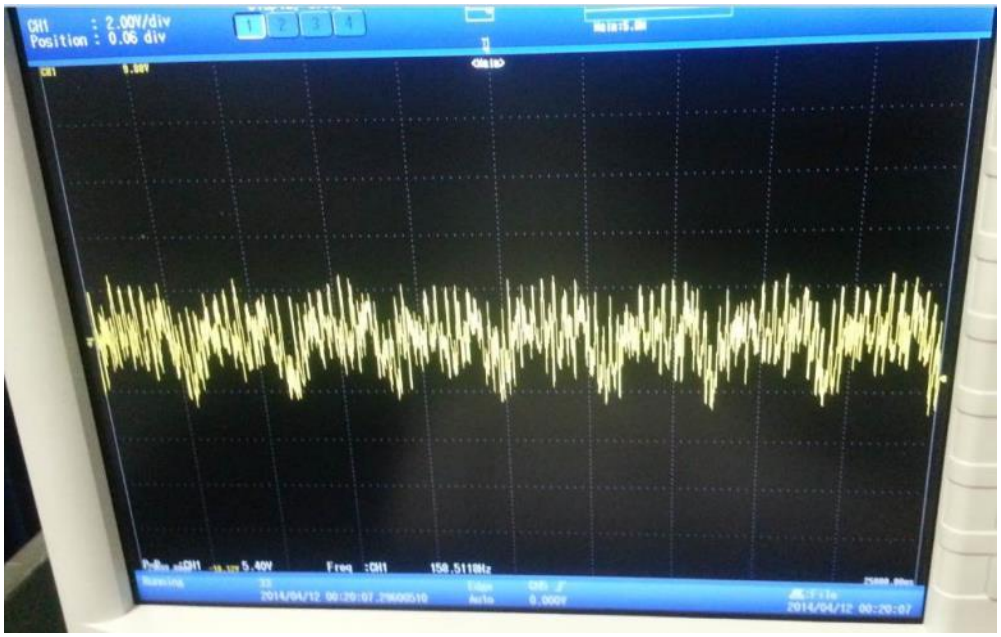

Figure 62: Demodulated Thermocouple Signal During Spin Test

Though the modulation of the sensor signal was poor, the board performed very well in other ways. The rectification circuit, as measured by the board DC output via the slip ring, performed very well throughout the full spin test, up to 350ºC and 14,500g for hours. The RF carrier output was strong, and it was conveyed properly via the inductive power system to the equipment outside the engine (see the RF carrier signal in Figure 63).

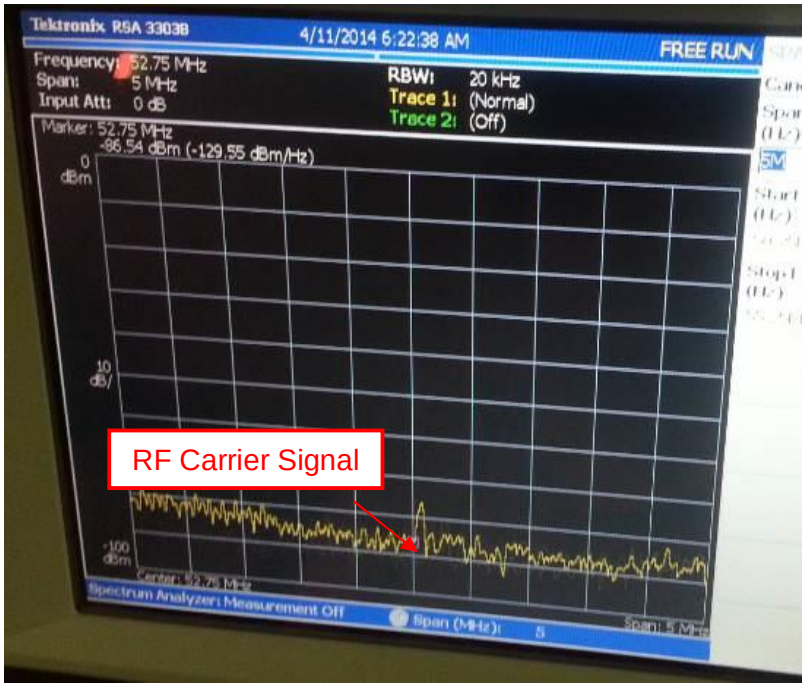

Figure 63: Thermocouple Board RF Carrier During Spin Test

Except for the poor sensor signal modulation, the TC board performed nominally up to 350ºC and low g-load. As the g-load increased above 1,500g, the RF carrier signal was lost during one spin campaign, though the rectifier continued to operate properly. When the g-load was increased to 10,000g, the TC board RF carrier reappeared with a strong signal. This signal was maintained up to the target g-load of 14,500g, where it remained steady for over an hour. At that time, the inductive power supply failed due to a power short circuit (see Section 2.4). Inspection and investigation of the TC board after the spin test revealed that the board was still functioning properly.

Another concern with these boards has been the robustness of the external pins. In some previous spin tests, these external pins had become damaged due to the high g-load. Post spin test inspection revealed no failures, and electrical tests confirmed proper continuity on each pin. Some minor bending is seen at the pins, and the white cement shows possible minor fractures. The assembly appears to have survived quite well. Figures 64 and 65 show the integrity of the pins at each of the electronics boards after the heated spin test.

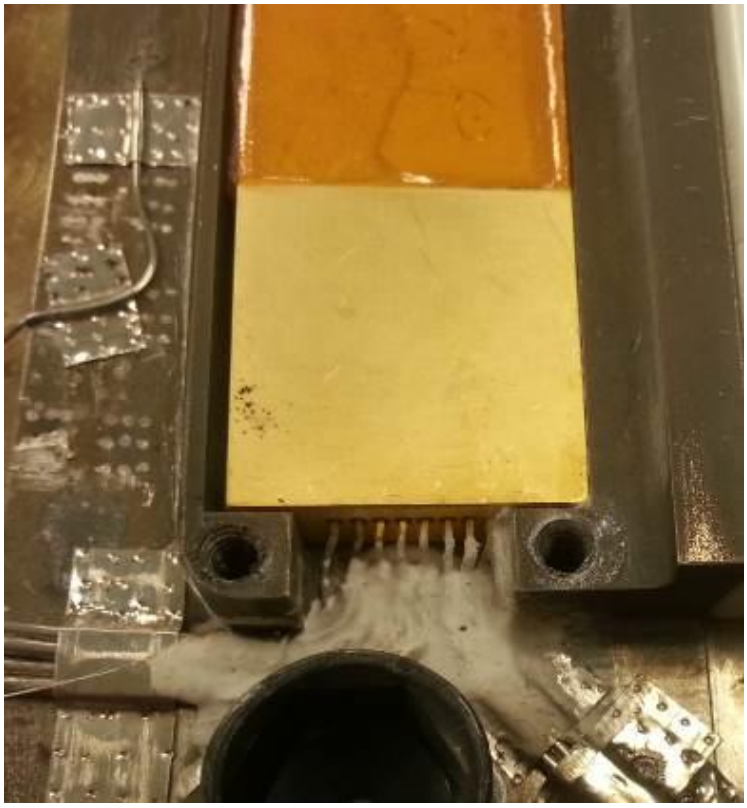

Figure 64: Strain Gage Board External Pins after Test

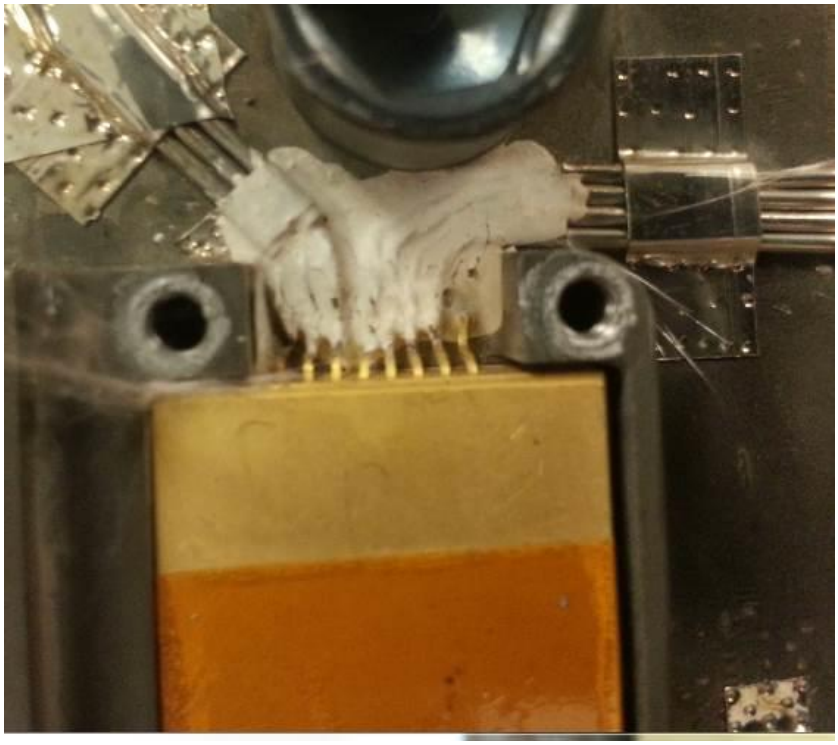

Figure 65: Thermocouple Board External Pins after Test

This spin test was, by far, the most successful spin test to date in terms of these electronic boards. No board had ever successfully operated while being powered wirelessly and transmitting wirelessly at any g-load above 500g during the previous 15 spin tests. No board had operated wirelessly at full temperature and any g-load. In this test, the strain gage board functioned properly at 350ºC and up to 1,500g. The TC board functioned completely wirelessly up to 300ºC (the rig cools at higher speeds) and 14,500g for a full hour. The design improvements made to the circuit boards over the project's last 18 months show significant improvement in the boards' ability to function in these harsh conditions. While the boards are not yet robust enough for an engine installation, this testing shows that the technology path chosen is feasible.

2.4 - TASK 4: ROBUST 450^{O}C WIRELESS TELEMETRY SYSTEM RESULTS

The wireless telemetry system discussed in this section involves two functionally different systems, the wireless power induction system and the RF telemetry antenna system. Task 4 develops and fabricates high temperature, high g-load wireless telemetry system induced power coils and data transmission antennae for engine testing, and miniaturized or long range induced power concepts for spin tests at 450 °C and 14,500g. The wireless power induction system is comprised of four main parts: the external power supply high-temperature cables, stationary power inducing stators inside the engine, and the rotating power receiving antenna, which resides in the engine on the base of a blade. The custom-designed external power supply produces a very high voltage, high current AC waveform. This power signal is conveyed to the power inducing stators via high temperature cables, which must be able to survive temperatures in excess of 600^{o}C, while also providing impedance performance at the high frequencies used in the power induction system.

First Generation Stator Power Coils

The "first generation" power induction transmission and receiving hardware were developed before this DOE project commenced. They are described in order to give a baseline of the power induction system functionality issues that existed when the project began.

For the first generation system, the power inducing stators are comprised of a row of magnetic cores wound together with high-temperature insulated wire shown in Figure 66. These wound magnetic cores are then cemented to the steel stator segments. The rotating power receiving antenna is housed inside a magnetically transparent ceramic box in order to survive the very high g-loads. Inside the box are smaller magnetic cores wound with high temperature wire. These are all held in place inside the box with high temperature ceramic potting, and the wires are fed through holes in the box. These wires provide AC power to the wireless telemetry board. In addition, the rotating power receiving antenna has an RF antenna embedded inside itself. This RF antenna is connected to the wireless transmitter board, and is used to transmit the RF telemetry signal to an RF antenna embedded in the power inducing stators. More high temperature

cabling is used to connect the stators' RF antenna to the outside the engine, where the RF telemetry signal is demodulated, and the sensor signals are recovered.

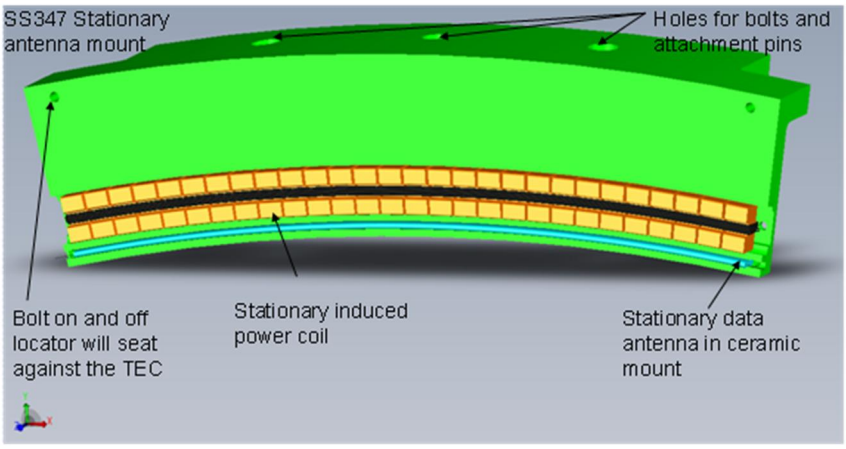

Figure 66: Illustration of First Generation Power Inducing Stator

The stationary parts of this system (power inducting stators) were built and installed in an H-class engine. However, bench tests on uninstalled stators in late 2011 indicated that their performance dropped off significantly above 200°C, and above 375°C, as shown in Figure 67. The first generation stators were incapable of inducing enough power to maintain system functionality at high temperatures.

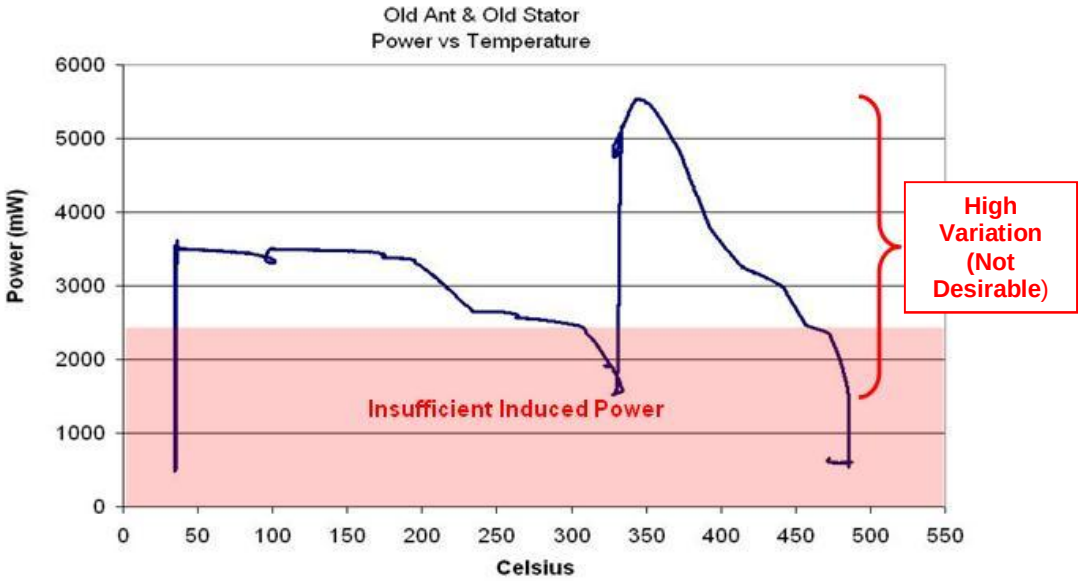

Figure 67: First Generation Stator Power Transfer Characteristics

Later tests showed that the high temperature wire used in the engine installation was not vibration-resistant. An effort to redesign the stators began in late 2011, but it was too late to replace the stators already installed on the H-class engine since the engine had been assembled. Another problem was found with the first generation design. Tests on the rotating power receiving antenna showed that as of October 2011, this component was

not able to survive spin testing due to cracks in its ceramic potting which exposed the windings and caused complete loss of functionality.

While the redesign of the rotating antenna and external power supply brought the inductive power system power transfer rate up significantly, the power inducing stators were only marginally powerful enough to power the transmitter boards. H-class engine testing showed that the original stator design was also too fragile for use in engines. Section 2.6 provides the details of this test. A complete redesign of the power inducing stators was, therefore, initiated in February 2012.

In order to better understand the progress made in the inductive power system and the data antenna, it is necessary to describe these systems and their components in more detail. Improvements made in this project period will then be discussed on a component-by-component basis, with analysis of how these changes impact system performance.

The stationary power inducing stators form a continuous ring around the rotor at the same radius as the rotating power receiving antenna in order that the power receiving antenna sees a continuous and consistent magnetic field. They are installed below the hot gas path on a stationary disc in the turbine section of the gas turbine, next to and facing the rotating ring which holds the blades to be measured (Figure 68). The stator ring is comprised of 16 stator segments, connected electrically into 8 pairs of stators. Each stator pair is powered by a separate external power supply. These 8 power supplies have synchronized phases so that the entire ring has one phase, all the segments being in sync with each other. These power supplies provide power to the stators. Because a large percentage of the electrical load of these stators is inductive, the majority of this energy is converted into the oscillating magnetic field. These stators must function at temperatures up to 450^{o}C, and they must survive in a high-vibration environment.

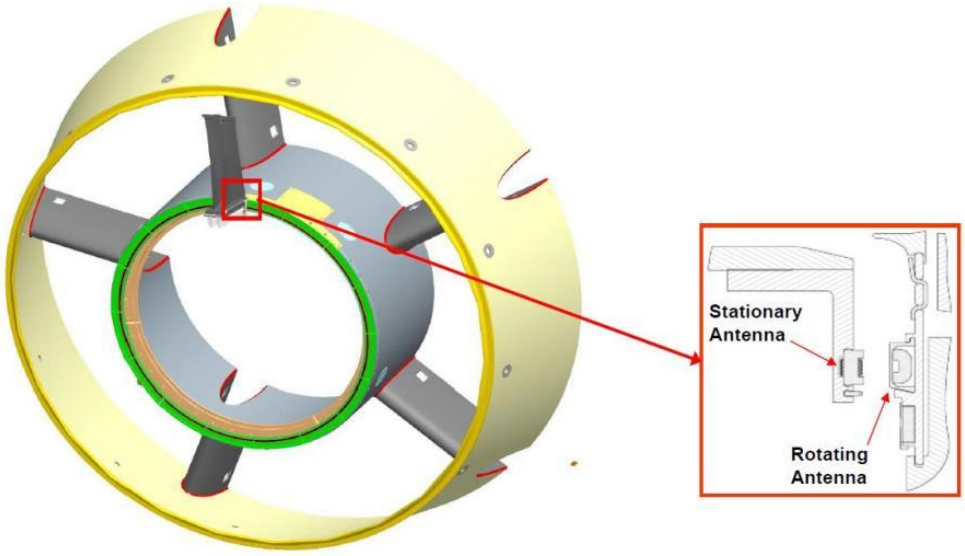

Figure 68: Wireless Telemetry System Component Locations

Figure 68 shows the implementation of the core parts of this system. The large circular turbine component shown above does not rotate. The outer part, the yellow turbine exhaust casing, is connected to vanes, which are in the hot gas flow. These vanes help direct and stabilize the air flow between different rings, or stages, of turbine blades. At the bottom, or inner, part of the vanes, there is a cylindrical piece of metal called the stator. In order to get wireless power to the engine blades, we have targeted the edge of the stator that is next to the ring of rotating blades. This edge, highlighted in light green in Figure 68, is where we affix our power inducing stator segments in a complete ring around the edge of the stator. A single, free-floating turbine blade is shown above, in the 12 o'clock position. This blade is representative of an entire ring of turbine blades which rotate in a circle less than 2cm from the green stator ring edge. This small, stable gap is where we have chosen as our wireless power induction area (see inset on right of Figure 68).

The power inducing stators are powered by an external power supply which sits outside the engine. Through wires connecting it to the stators, the external power supply sends alternating current (AC) electrical power to segments of the power inducing stators. A varying magnetic field is produced along the entire ring of stators. Figure 69 shows the scale of the stator ring in the H-class engine, and the Figure 70 shows a section of the stator ring (showing three of the sixteen segments) installed in the H-class engine.

Figure 69: Stator Ring Installation in H-Class Engine

Figure 70: Stator Segments Installed in H-Class Engine

Less than 3cm away, on the seal plate at the root of a selected rotating blade, there resides a ceramic box filled with wound magnetic cores which we call the rotating power receiving antenna. In the presence of the varying magnetic field, those wound cores of the rotating power receiving antenna produce electrical power in the form of an alternating current. This power is then fed into a transmitter board which sits next to the rotating antenna on the blade's seal plate.

This transmitter board receives the AC power and conditions it into direct current (DC) power which can be used by the electronics on the board. These electronics read the data from the sensor on the blade (we have implemented different versions of these boards for use with thermocouples or strain gauges). This sensor data is then modulated by the transmitter board onto a radio frequency (RF) signal. A wire carries this signal from the transmitter board back to a small antenna embedded within the rotating antenna. This small antenna transmits the RF data signal into the space between the rotating turbine blades and stator.

There is another RF antenna embedded in the ring of power inducing stator segments on the stator. This RF antenna receives the RF data signal. A wire carries this received signal back outside the gas turbine, where electronics decode the signal and recover the data. Thus, the sensor data from the rotating blade is readable outside the engine on a continuous basis.

One of the major concerns with this stator design was that in the highly thermally variable engine environment, these stators, which are bolted to the engine structure, may liberate.

Figure 71 shows the face of the power inducing stator segment that is bolted to the engine.

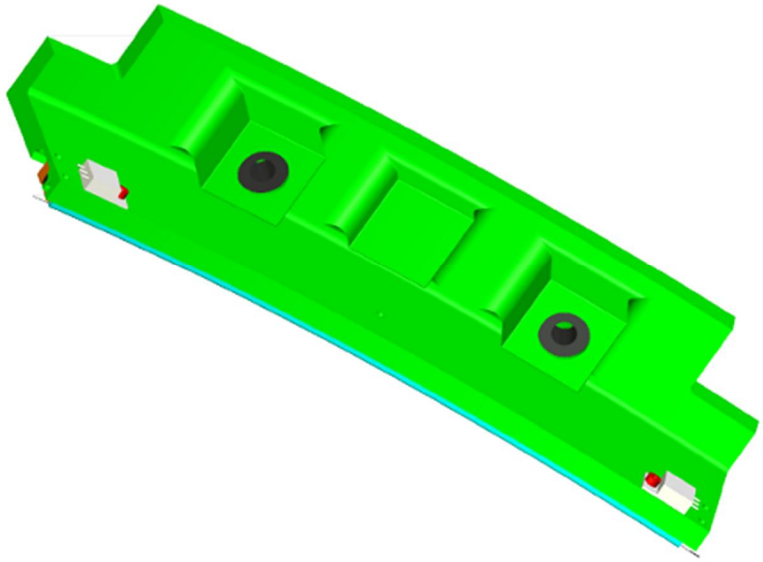

Figure 71: Model of the Back Side of the Stator

Therefore, extensive calculations, simulations, and tests were done to ensure the bolts would stay in place. A Junker bolt shaker test (See Figure 72) was performed, and the bolts held in place. Four different bolt retention methods were tested, and one was chosen. Bolt tension analysis led to a recommended torque, which was implemented.

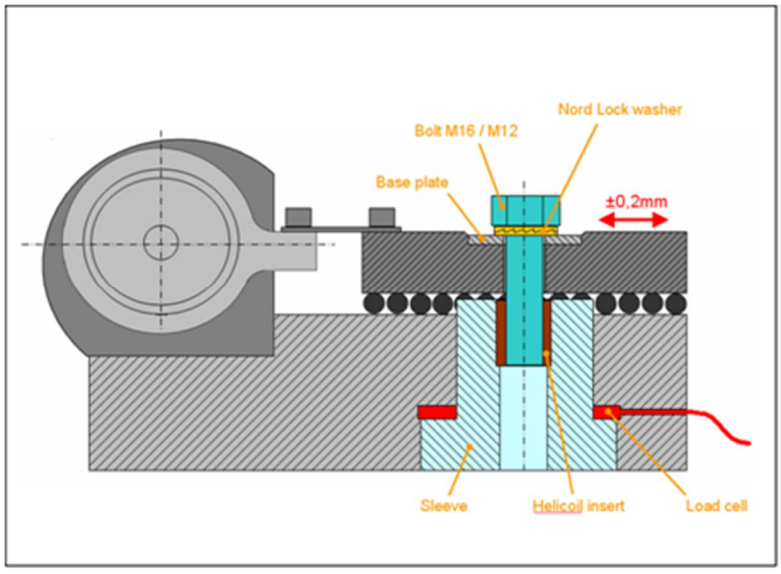

Figure 72: Junker Bolt Test Configuration

The power inducing stators have experienced engine operations over test cycles spanning from September 2011 to present day. No indications of bolt loosening or stator liberation have been observed. The stators will be removed from the engine in the fall of 2012, and any noteworthy observations regarding mechanical aspects of stator attachment will be submitted in subsequent reports.

Stator performance over temperature has been a significant challenge. As the H-class engine warms up and experiences different loads, the air gap between the stators and the rotating power receiving antenna changes. At the maximum gap, sufficient power can be induced only up to a temperature of 420°C. Because of how the air gap changes with load and temperature, this is likely sufficient for the great majority of engine operations, but it leaves very little operational margin.

Failure of the First Generation Inductive Power Coils

In late 2011and early 2012, inspections and measurements of the power inducing stators installed on the H-class engine revealed several instances of damage to the wire connections, windings, and RF antenna of these stators. These failures are detailed in Section 2.6. This damage was significant enough to preclude full wireless system testing on that engine, because access could not be gained to repair these issues, and a more limited wireless system test regime was adopted. Other shortcomings of the system, such as high variability of power transfer over temperature, difficulty of manufacture, and electrical insulation failures, led to the abandonment of the first generation inductive power system.

Second Generation Wireless Power Induction System

Because of the first generation stator high-temperature power transfer issue and wire robustness issue, a major re-design of the stator was initiated in late 2011. The overall architecture of the system is very similar to the first generation design. However, each component of the system is completely replaced or redesigned. The new design delivers superior functionality over temperature, vibration resistance, and simplicity of construction.

Second Generation Stator Power Coils

Prototypes of the new stator were first realized in printed circuit board form and tested at room temperature over the summer of 2012. In the fall of 2012, the finalized design of the high temperature planar stators was implemented in low temperature co-fired ceramic (LTCC). This material is stable to above 800ºC.

Siemens' new design of the power inducing coils is a novel approach to wireless power transfer. Because of this novelty and the high temperature and high vibration environment, mechanical concerns were addressed early in the design phase. Siemens

developed a full 3D model of this design and simulated expansions and stresses for temperatures up to 450^{o}C. From these simulations, we were able to determine how much the device would grow or shrink relative to the stationary ring metal below it, which allows us to make informed choices in bolt hole sizes. Stress analysis indicated weak points to improve deign aspects. Figures 73 and 74 show stress diagrams for the stator design and the bolts used in the design.

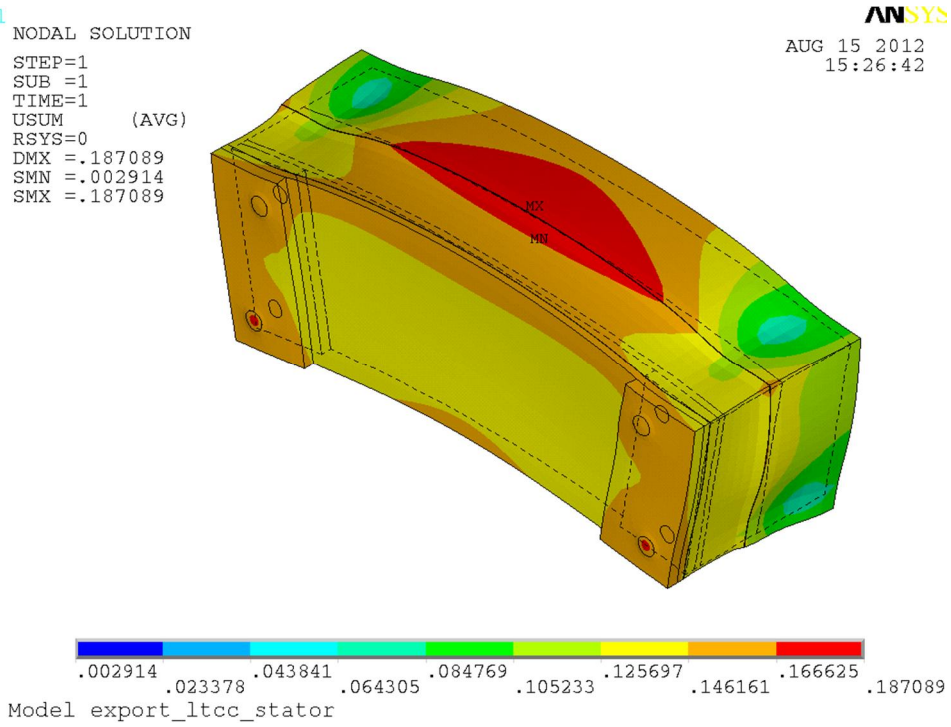

Figure 73: Thermal Stress Analysis of Power Coil Assembly

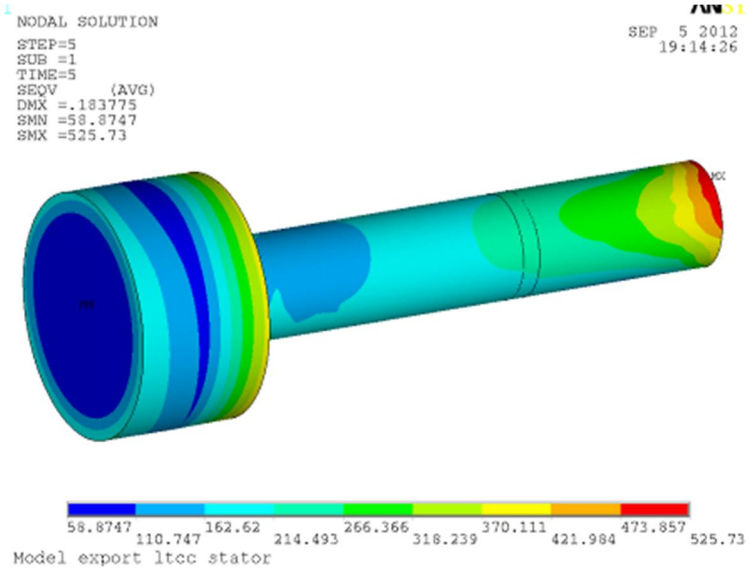

Figure 74: Stress Analysis of Attachment Bolt

This new design is composed of several layers of high temperature material. It is constructed on a plane of metal to simulate the installation of such a system in a gas turbine engine. Figure 75 shows the cross-section of the construction. A thin layer of alumina fiber is placed on the metal for mechanical isolation. This fiber maintains its softness and pliability to temperatures above to 1000 C. The softness helps protect the construction from excessive vibration. The pliability allows the metal and the ceramic above the fiber to grow at different rates laterally (parallel to the surface of the metal) due to their differing coefficients of thermal expansion. Next, an arced piece of ceramic is placed upon this fiber. This ceramic exists to separate the magnetic coils from the grounded plane of the metal. The further the coils are from this grounded plane, the better the performance of the inductive power system. Above this ceramic is placed another layer of alumina fiber, which again provides protection against vibration and thermal mismatch expansion deltas. Upon this is placed the LTCC-embedded magnetic coils depicted in Figure 76. On these magnetic coils is placed another ceramic plate which distributes the force of the stack fastening system. This electrically active device induces an oscillating magnetic field in the direction normal to the metal plate. Connected to an outside power source, it magnetically drives a voltage in the rotating receiving antenna (not shown), from which it is separated by 20mm of free space.

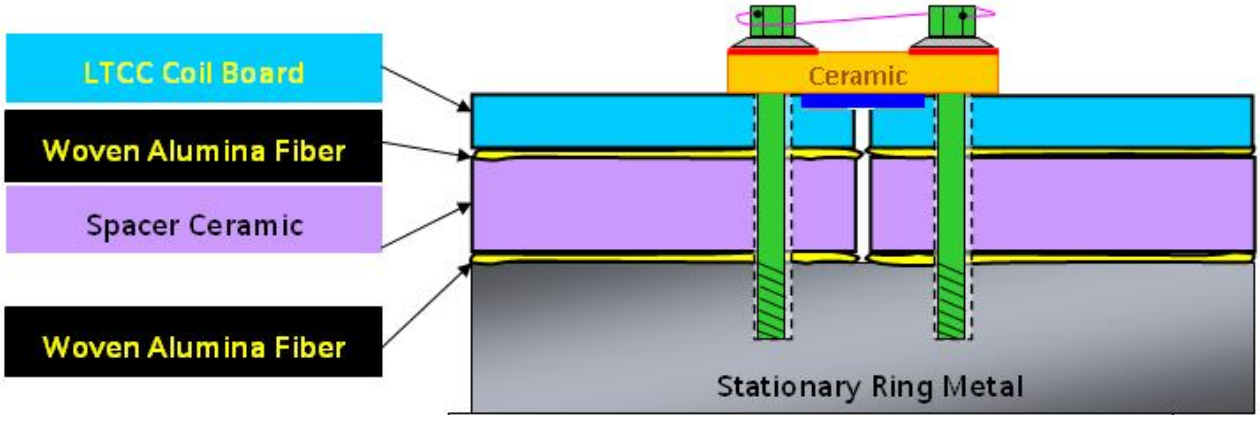

Figure 75: Cross-Section Diagram of Power Inducing Stators

Figure 76: Internal Diagram and Photo of LTCC Magnetic Coil Arc

The stack is compressed together and held in place by bolts threaded through four different holes in each of the arc pieces. These holes go through all layers and into threaded holes in the metal plate. Spring washers are compressed under the bolt head to maintain compression on the stack over temperature, because the bolt grows with temperature more than the stack does.

At temperatures above 300^{o}C, typical solder melts. The application of higher temperature solder creates extreme temperature gradients which damage the LTCC magnetic coil pads. Additionally, solder connections have poor performance in high vibration environments. Therefore, utilizing Siemens proprietary technology, electrical connections are accomplished by holding thin pieces of metal in place via compression over pads on the top of the LTCC magnetic coil pieces. These thin metal strips bridge one magnetic coil arc to the next, forming an entire ring or circuit for the current. External wire connections are made by threading the wires up through the metal plate and the ceramic stack, and laying the wire conductors under the metal strips. These strips are then compressed via the bolts pressing on the top ceramic plate.

Vibration testing of this design was performed based on actual engine acceleration data. We constructed a test article of two arc pieces, containing six separate electrical connections shown in Figure 77. A vibration test was performed at 1.5g at 60Hz along with a sweep of 0.3g over a range of 20 to 250Hz in the direction normal to the metal plate as shown in Figure 78. This simulated our measured engine environment. This test lasted 10 hours, during which continuous circuit integrity data was gathered. No failures or degradations of the electrical connections were observed.

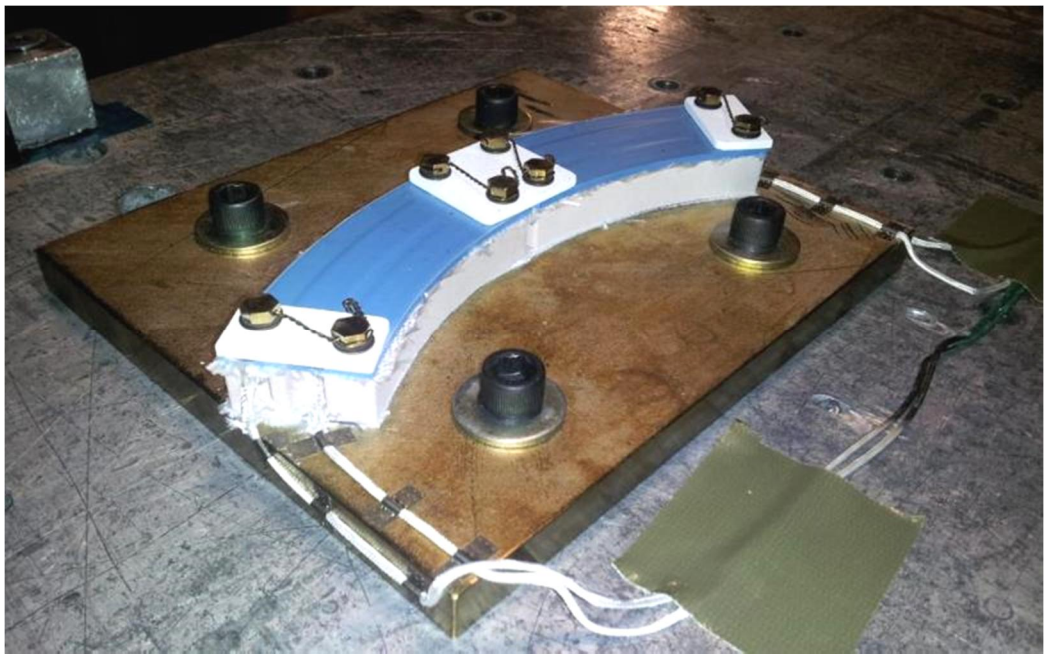

Figure 77: Stator Vibration Test Article

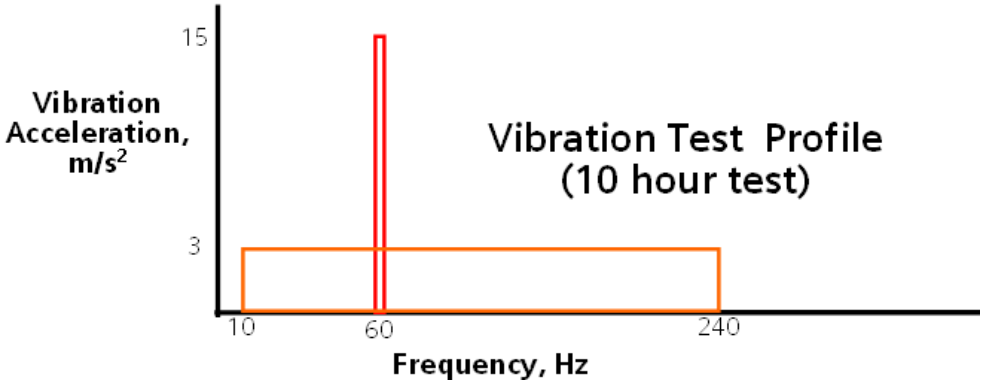

Figure 78: Stator Vibration Test Profile

The electrical performance of this stator system is best captured in terms of an integrated system with the power supply, matching circuit, and power receiving antenna. The detailed results of the electrical performance of this new planar stator system will be described below after the descriptions of the development of these individual components.

First Generation Rotating Power Receiving Antenna

The rotating power receiving antenna resides on the blade bracket (seal plate) at the bottom of the rotating blade. It transduces the magnetic energy from the stators into electrical power. This electrical power from this rotating antenna is sent by wire to the

wireless telemetry board, which resides on the same rotating blade bracket. The rotating power receiving antenna must produce at least $30V_{RMS}$ at 500mW in order to sufficiently power the wireless transmitter board.

The initial design of the rotating antenna was developed by Rove technology. The rotating antenna is composed of seven custom-designed magnetic cores wound with small diameter ceramic insulated high temperature wire (the red lines in Figure 79). This wire is wrapped in a bifilar method, meaning that pairs of the wire are wound simultaneously. There are two layers of 8 wire pair windings each, for a total of 32 windings. This core assembly is then placed inside a custom-designed ceramic box, and potted into place using specialized ceramic cement shown in Figure 80. During this potting process, a length of wire is also laid in the box, not touching the core assembly. This length of wire extends out of the ceramic box and serves as the RF telemetry antenna, which allows the wireless telemetry board to communicate the RF modulated sensor data across the air gap to the RF antenna embedded in the stators.

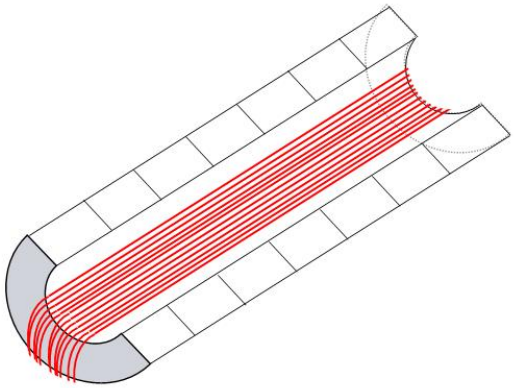

Figure 79: Diagram of Magnetic Cores in the Power Receiving Antenna

Figure 80: Wound Core Assembly Potted into the Ceramic Box

Several issues with this initial design were revealed during oven tests and spin tests. At temperatures above 300ºC, significant changes in transduced power were observed, and above 375ºC, transduced power was reduced below the useable level of 500mW. The initial design of the rotating power receiving antennae also failed in all mechanical spin tests up through the fourth quarter of FY2011. Vibration of spin testing caused the ceramic cement to crack, which damaged the core windings and exposed them to the metal of the blade bracket. This vibration damage caused the rotating power receiving antenna to become completely non-functional. Another issue encountered was caused by the small diameter wire used to wind the core assembly in the rotating power receiving antenna. This wire was very fragile and susceptible to breaking at the point where it exits the ceramic box. Multiple wire breaks were observed during spin testing.

Generation 1.5 Rotating Power Receiving Antenna

Because of these issues, Siemens redesigned the rotating power receiving antenna as shown in Figure 81. This redesign will be referred to as Generation 1.5. Design improvements included:

- Providing a method for strain relief and insulation within the wire windings
- Changes in the potting material to increase electrical isolation
- Magnetic core geometry changes to increase mechanical stability
- Improved manufacturing process for mechanical stability
- Improvements pin design to improve mechanical stability
- Improvements in winding coating to increase high temperature electrical isolation

Adhesion of cements was tested extensively, as this can have a major impact on mechanical integration. The coefficient of thermal expansion differences in materials often cause cements to simply drop off their adhering surfaces, ruining their functionality. Drops of different cements were placed on substrates of interest, and temperature shock tests were performed after curing. Lateral loads were applied to these drops in order to test their adhesion. Optimal cements were chosen based on these tests.

Figure 81: Redesigned Power Receiving Antenna

When these improvements were implemented, the results were dramatic. The rotating antenna now transduces power with little variation at temperatures above 500°C (see Figure 82). The variation in power induced improved to approximately 20%, instead of the 50-100% seen with previous antennas.

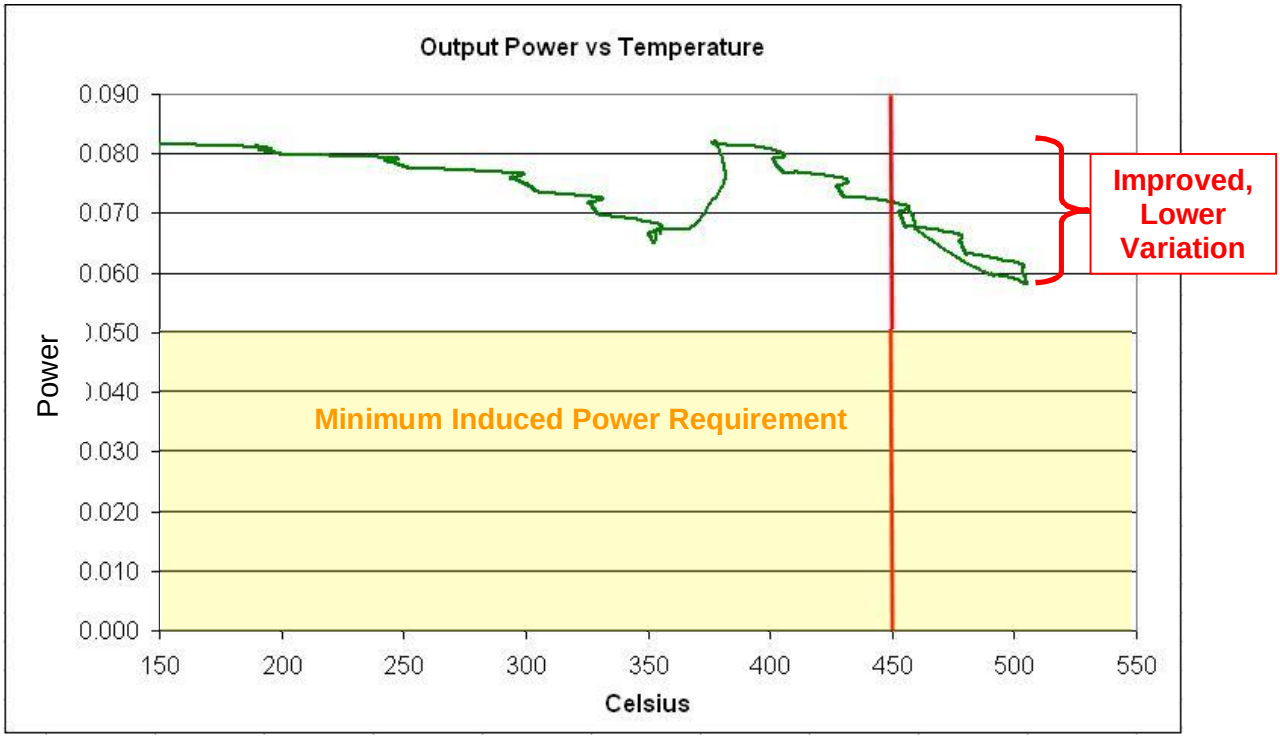

Figure 82: Second Generation Rotating Power Receiving Antenna Output

After the redesign of October 2011, a 5-hour mechanical spin test at 450°C and 14,500g was performed on two rotating antennae. These articles were tested before and after the spin test, and no degradation was seen in the rotating antennae. Additionally, further mechanical spin testing in early 2012 of four rotating antennae for 5 hours at similar conditions resulted in no functional degradation. In total, six rotating antennae have experienced full g-load and temperature in spin tests since the redesign, and every one of them have survived the tests with complete functionality. No cracks were observed in the potting, and no wire damage is evident in electrical tests. The addition of steel pin wire extensions has also proven effective, with no pin breaks observed in all spin tests which incorporated this improvement. This version of the antenna, which contains magnetic cores, is considered Generation1.5 technology in this project. It was meant to work with the magnetic stator power coils. This rotating power receiving antenna was validated to work at 14,500g and 450°C.

Construction of the Rove magnetic antenna and the Generation 1.5 magnetic antenna involved meticulous winding of magnetic cores and cementing these wound cores very carefully in a ceramic box. The construction took 20 man hours, and there were approximately 50 steps in the manual construction process, involving nine different

materials. The complex three-dimensional shape resulted in a number of failure modes and structural weaknesses.

When the new planar stator design was conceived and prototyped, it was quickly realized that the magnetic field receiving geometry of the existing rotating antenna was not compatible with the geometry of the new planar stators. This is the primary reason that a new planar version of the receiving antenna was designed.

Second Generation Power Receiving Rotating Antenna

Siemens developed a new planar LTCC antenna design that is capable of transducing sufficient power (500mW) across a maximum expected gap. We refer to this planar design as the second generation power receiving and rotating antenna. This is the final design tested through the completion of the program. There are many benefits to the new design. Because the device is fabricated using automated processes, all tolerances are vastly superior to the manually fabricated version, reducing errors and improving robustness. The time it takes to assemble the antenna is now minutes instead of days. The new design will also allow operation at temperatures higher than the Curie temperature of the magnetic material (Vitroperm 800). Thus, the maximum operating temperature was raised from ~515ºC to ~600ºC. This device is 20% lighter than previous antennae, which improves the robustness of this device which must function at continuous g-loads of 14,000g to 17,200g.

The functionality of the new planar rotating antenna was measured as part of a full inductive power system testing. This performance will be described below after the description of the other inductive power system components.

Power Supply

As stated above, the power inducing stators are energized by an external power supply. This external power supply was originally comprised of two devices (see Figure 83 below). The first is an off-the-shelf DC power supply which can be plugged into facility power, and will output voltage-regulated DC power. The second is a 30-50W, 250 kHz DC-to-AC converter which was custom designed and built for this wireless system. This device was designed and built before the current project period by Rove Technical Services; however, beginning in late 2011, a significant redesign commenced. This AC-to-DC converter redesign provides significant external power supply improvements. These improvements included a lower-resistance transformer, the flexibility to change the AC frequency, and the ability to induce a variety of different waveform shapes.

Figure 83: External Power Supply

Partial implementation of these improvements allowed the maximum operating temperature of the First Generation power induction system to extend its maximum functional temperature from 355^{o}C up to 420^{o}C (by allowing more power to be coupled into the stator-induced magnetic field).

Even with these improvements, however, the fall of 2012, power supply failures prevented characterization of the high temperature version of the planar power supply. The very nature of this power supply (being dependent on finely tuned resonances and being a zero ohm power source), precluded the use of this type of power supply from being used with the power inducing stators. Because the planar system does not contain magnetic materials (for reliability and manufacturability reasons), it has a wide resonant peak. Also, a significant current is needed to induce sufficient wireless power across a large 20mm gap.

A significant research program was initiated to find a sufficient off the shelf power supply to replace the previous system. By moving to a commercial off-the-shelf supplier, gains in reliability and cost effectiveness can be realized. In the spring of 2013, an off the shelf power supply was obtained which is capable of driving the inductive power system. This E&I 1140 LA RF amplifier was integrated with the power inducing stator ring, and characterization of the inductive power supply proceeded. Relationships with power input, output power, and electrical ring parameters were obtained. Full ring characterization was performed (described below).

High Temperature Power Cables

In order to transfer the electrical power from the external power supply outside the engine to the power inducing stators inside the engine, high temperature wire must be used. Prior to the commencement of this DOE project, twisted pairs wrapped in alumina fiber were selected to connect the external power supply to the power inducing stators in the H-class engine. Bench tests showed this cable was able to survive. During H-class engine operation, it was revealed that the environment to which the cable was exposed was more extreme than was originally known. Sections of the cable were subjected to very high temperatures and significant vibrations. These higher temperatures, coupled with the vibration environment, caused severe degradation of the cable.

This left several stator pairs completely unpowered, crippling the wireless system. In January of 2012, the damaged sections of the cable were replaced with a much more robust mineral insulated cable. This cable contains insulation which is rated to 700^{o}C. However, due to its high capacitance, it can be used only for short (<2m) cable runs. Appropriate lengths and cable types are chosen to accommodate the turbine environment. Typical lengths are 3 to 4 meters. Therefore, intense investigation of multiple cable types was commenced. The cables settled upon were mica polymer-based cables wrapped in alumina fibers which are mechanically and electrically stable up to 400ºC. The stranded nickel center conductor of these cables is oxidation resistant at high temperature. These cables have insulation resistance specified to above 25kV across the temperature and frequency ranges in question. This cable is also used for the RF transmission line.

Power Matching System

Because the power inducing stator ring is inductive, and the power supply is at 50 ohms (not inductive), a power matching system is needed to maximize power transfer. Additionally, it was discovered that optimal performance and safety is realized through the use of an impedance-matching isolation transformer. Thus series capacitors and a transformer are needed for power conditioning between the power supply and the power inducting coils. In order to accomplish this, a standalone power conditioner was designed and implemented.

The power conditioner electrically matches the inductive coil circuit to the AC power source. It is comprised of a transformer, series capacitor matching, and a cooling fan. These have all been integrated into a small enclosure for safety and ease of use. Figure 84 shows the interior of the power conditioner. The black cooling fan, yellow transformer, and blue matching capacitors can be clearly seen.

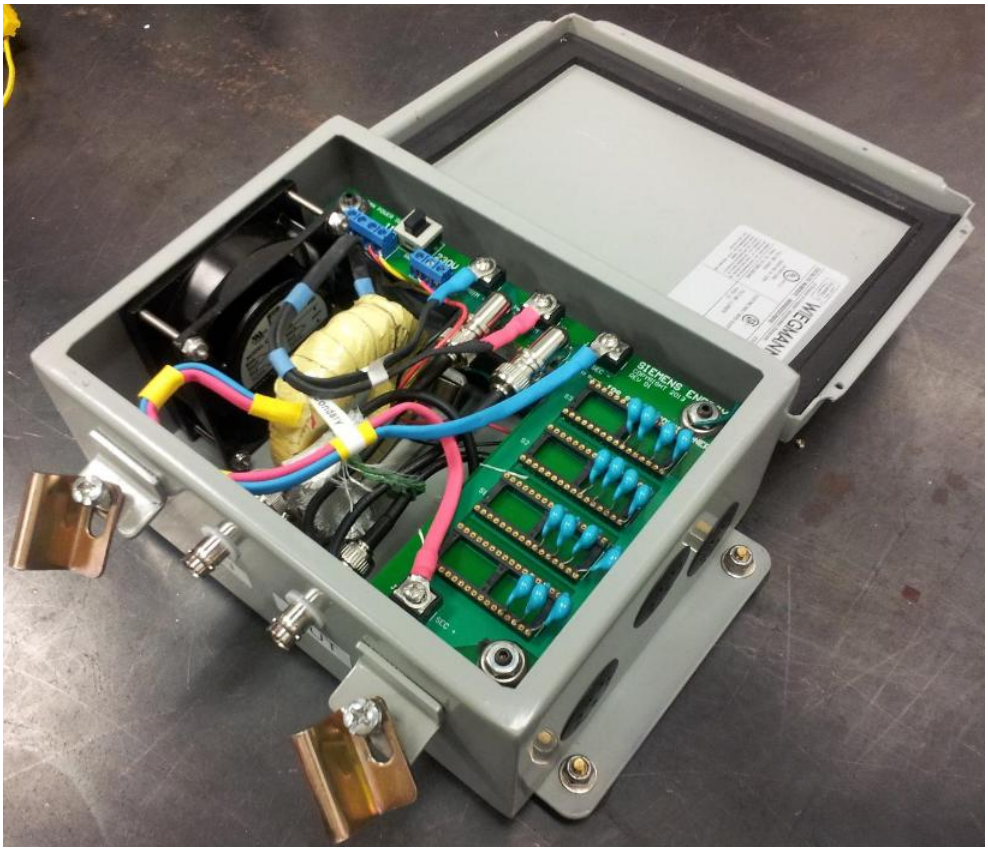

Figure 84: Inductive Power Supply Diagram

Blade Brackets (Seal Plates)

The blade brackets (also known as seal plates) were custom designed to hold the rotating power receiving antenna and the wireless transmitter board in the H-class engine environment. Vibration, differing coefficients of thermal expansion, and extreme g-loads presented significant design challenges. However, this design (see Figure 85) has been validated in multiple spin rig tests at 450^{o}C and 14,500 g. It is our assessment that this design is robust and complete, and only minor adjustments will have to be made for installations into other types of engines. Six blade brackets were machined for use in the H-class engine test, and two are being installed in July 2012.

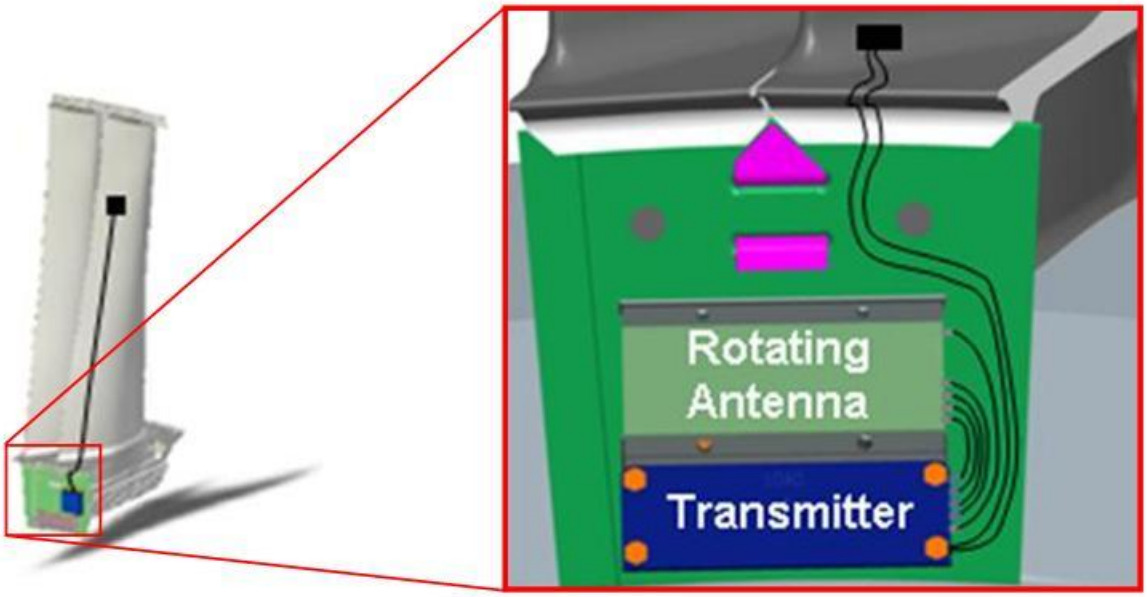

Figure 85: Location of Seal Plate (Green) on Instrumented H-Class Turbine Blade

Extensive modal, thermo-mechanical loading, stress, buckling, low cycle fatigue, and strength analyses were performed on the modified seal plate to ensure it could survive the engine environment while holding the rotating antenna and the wireless telemetry board. An extensive internal design review was held and November of 2011, and this seal plate design was approved for installation into the H-class engine. This installation was due to be performed in early 2012, but failure of the first generation stator in the H-class engine before system testing could commence caused test cancellation (see Section 2.6). In all integration testing, a seal plate extremely similar to the engine seal plate is used to hold the power receiving antenna in proximity to the power inducing coils.

Fully Integrated Wireless Power Induction System (2nd Generation)

By late spring 2013, the new planar power inducing stators, the new planar power receiving antenna, the new power supply system, the new cables, and the new matching system were all obtained and individually tested. A final integration effort then commenced. The ring is mostly inductive, with the ratio (Q) of inductive impedance to resistance being about five. In order for this ring to resonate properly, series capacitors must be added to the circuit to match the ring's series inductance. When this is done properly, the ring impedance becomes much lower, and more power and current can be coupled to the ring. After this matching, the circuit's resistance is about 25 ohms. This needs to be matched to the 50 ohm output impedance of the power supply to further maximize power transfer. A transformer is used to accomplish this second stage of matching. For low power testing, hand-wound transformers were used. Once an optimal transformer winding ratio was determined, a commercial transformer was purchased and integrated into the system. Figure 86 is a circuit diagram of the inductive power supply.

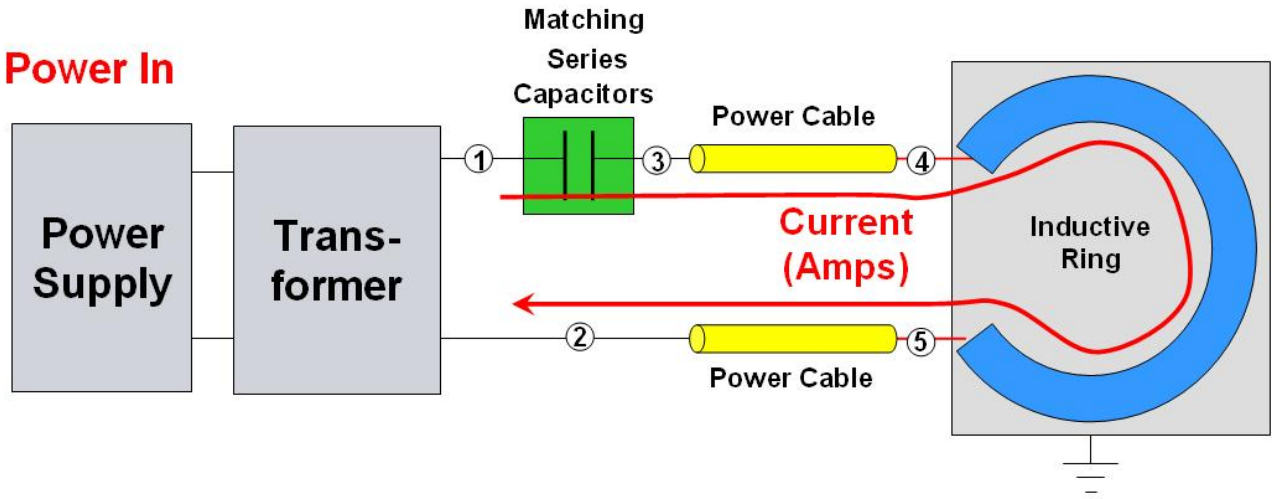

Figure 86: Inductive Power Supply Diagram

The yellow power cables depicted in the diagram above connect the inductive ring inside the turbine to the power supply and matching capacitors located outside the turbine. Appropriate lengths and cable types are chosen to accommodate the turbine environment. Typical lengths are 3 to 4 meters. Note that the inductive ring resides on a large plate of metal. This plate is grounded to match the grounded metal on which the ring will reside in a gas turbine.

A larger ten arc-piece stator test article, shown in Figure 87, was constructed. The seal plate containing the power receiving antenna can be seen suspended above the power coils, held in place by three metallic standoffs.

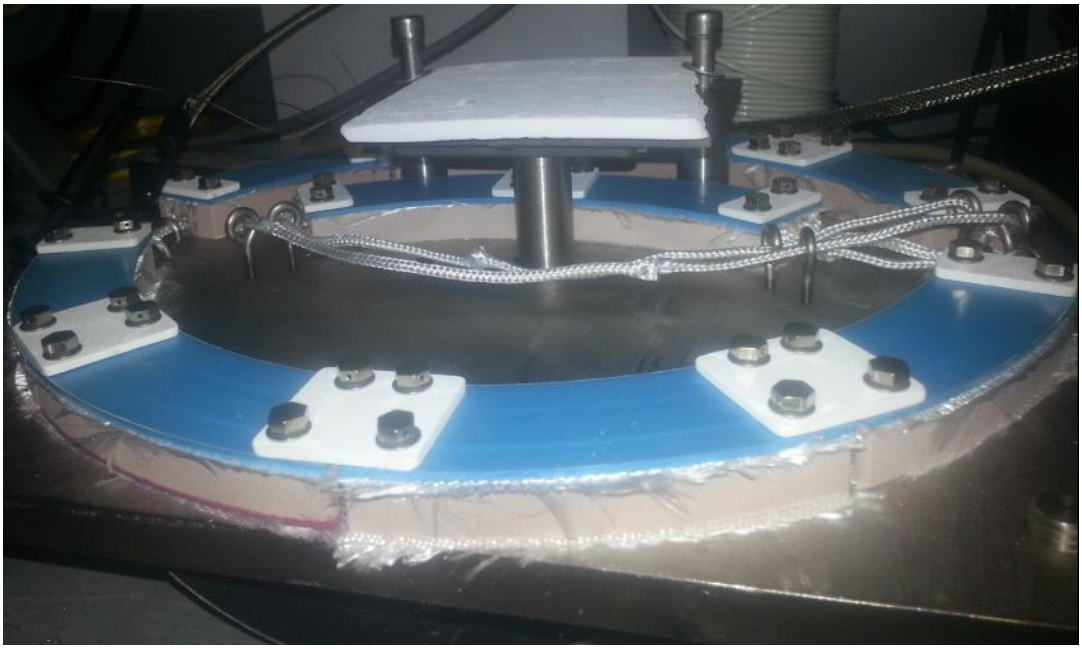

Figure 87: Stator Oven Test Article

As integration and testing proceeded, a number of test issues occurred. The most troublesome were instrumentation ground loops that resulted in spurious output power readings. An oscilloscope was used to measure the received magnetic power as a voltage. This oscilloscope shared a ground with the RF amplifier driving the ring, and this ground contamination caused the oscilloscope to report a power output several times higher than the actual power output. This was remedied by switching to the use of a passive rectifier board and a battery operated digital multi-meter for reading the output of the circuit. Additionally, a high frequency current probe was obtained to measure the current at various points in the circuit. With these test issues resolved, ring characterization proceeded. The final circuit is represented in Figure 88.

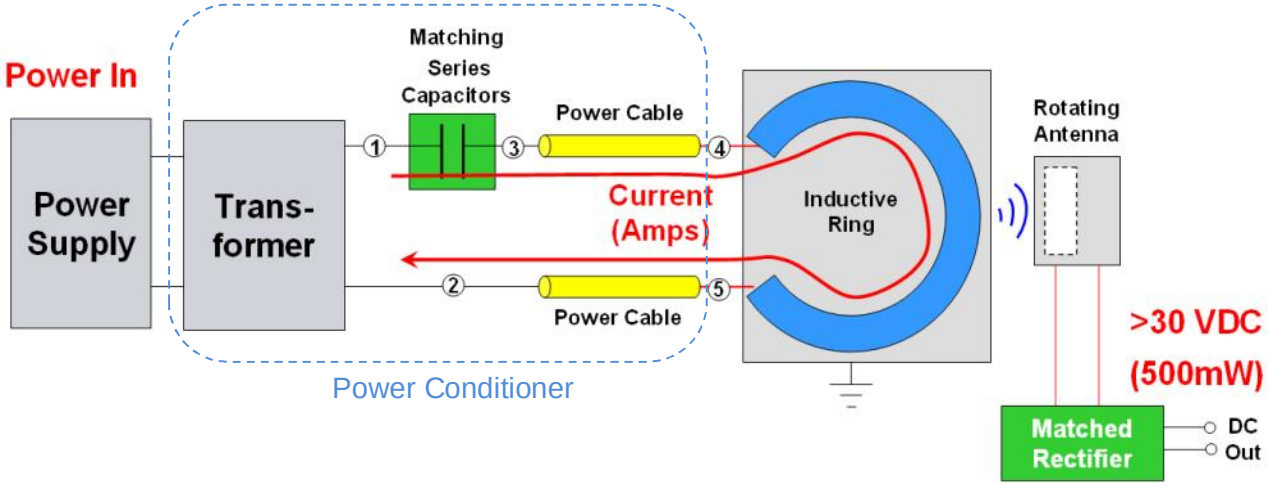

Figure 88: Inductive Power Supply Test Configuration

Wireless Power Induction System Electrical Results (Initial)

The goal of this inductive power supply is to get 500mW out of the rotating antenna to power the wireless telemetry board. A relationship was established between current in the ring and volts seen across a loaded rotating antenna. For our testing purposes, we used a load on the rotating antenna which matches the load of the wireless telemetry board, 1780Ω. With this load, a power transfer of 500mW results in a voltage of 30 VDC. All measurements were made with a 20mm gap as would be seen in a gas turbine installation. This relationship at 800kHz with this 20mm gap is shown in Table 11.

Input Current (mA)	Rotating Antenna Output Volts
200	2.2
400	4.5
500	6.1
1000	12.3
1500	19.1

Table 11: Input Current vs. Output Voltage at 800kHz

Clearly, there is a linear relationship between current in and voltage out. We found this to be true in all configurations and at all frequencies. If the current is doubled, the output voltage doubles. Because 1 Amp (1000mA) is needed to induce 12.3 volts at this frequency, we can project that 2.44 Amps is needed to induce 30 volts. Generally, we established:

$$V_{OUT} = \alpha * I_{IN} \qquad \textbf{(Eq. 1)}$$

Where V_{OUT} is the voltage output of a loaded rotating antenna, α is a proportionality constant (for a single frequency), and I_{IN} is the current in the inductive ring. For 800kHz, α = 12.3Volts/Amp.

Due to the nature of magnetic induction, induced voltage will increase in magnitude with frequency. Figure 89 shows how α increases with frequency for this system. The fitted slope of this graph shows that for every increase of frequency of 100kHz, the output voltage increases about 0.67 volts. Increasing the frequency by 100% increases the power transfer by about 34%.

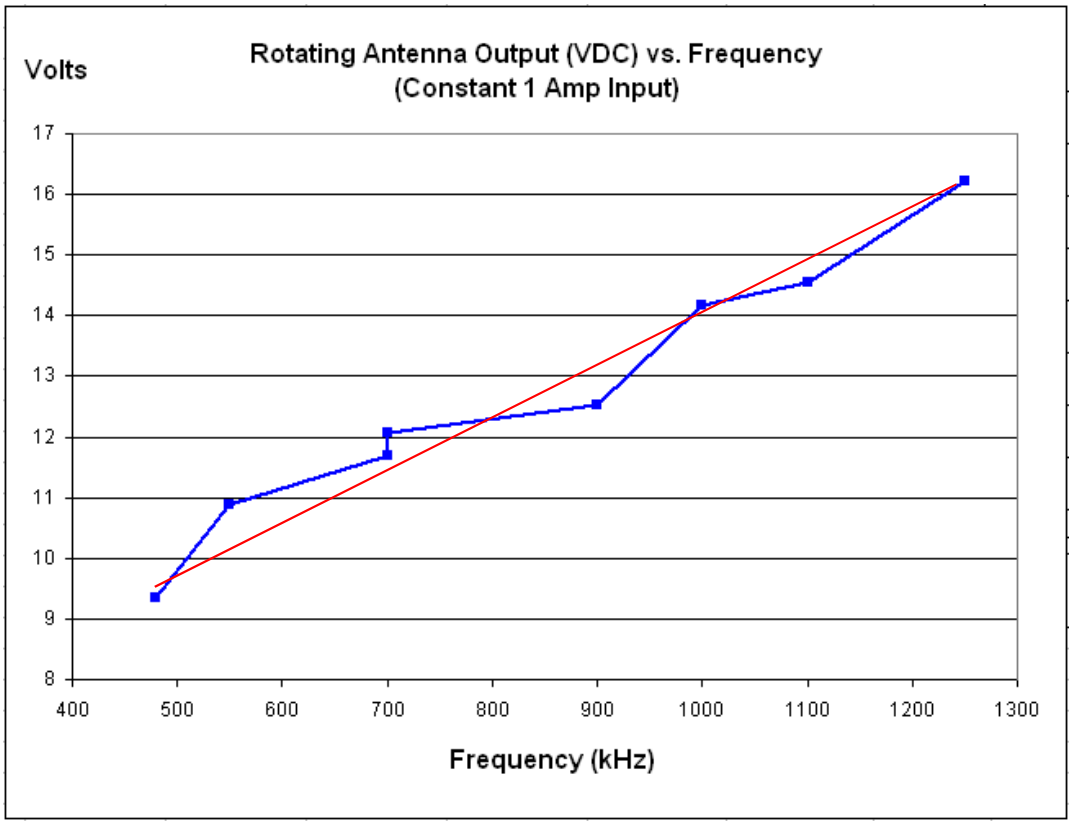

Figure 89: Change in Voltage Out vs Amps In Over Frequency

Based on this graph, the system appears more efficient at higher frequencies. Because power scales with the square of the voltage, the power transferred actually goes up with twice the slope of the voltage.

The ring's resistance to current, however, also increases with frequency. More power is needed to get each amp of current to flow into the ring. As can be seen in Figure 90, matched ring impedance goes up dramatically with frequency:

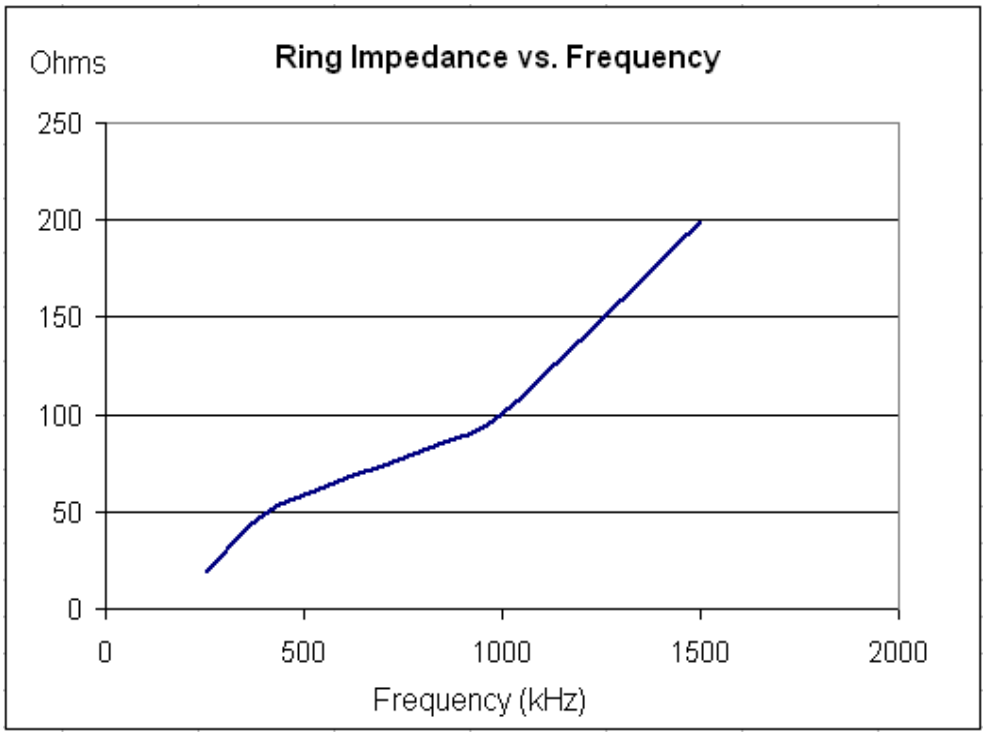

Figure 90: Ring Impedance vs. Frequency

The power it takes to excite 1 amp in the ring is linearly proportional to the resistance:

$$P = I^2 * R \qquad \text{(Eq. 2)}$$

If the resistance doubles (as it does between 600 kHz and 1200 kHz), then the power it takes to excite 1 amp in the ring also doubles. Figure 91 shows the input power necessary to excite 1 amp in the system vs. frequency.

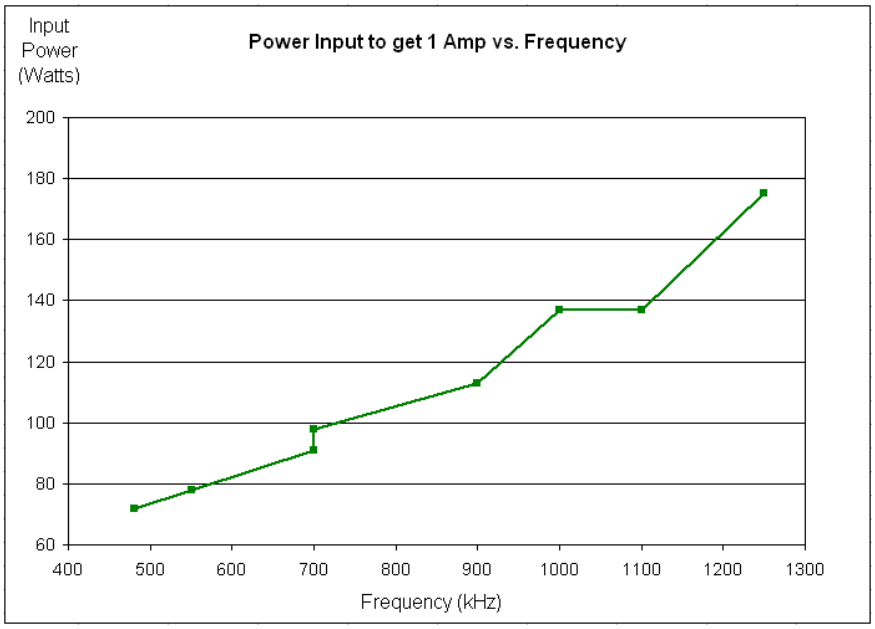

Figure 91: Input Power to Get 1 Amp vs. Frequency

Because the ring resistance doubles between 550 kHz and 1100 kHz, the power it takes to excite 1 amp also doubles (from 70 Watts to 140 Watts).

As frequency increases, therefore, the total system efficiency does not increase, but stays relatively flat. Figure 92 shows the amount of input power it takes to get the critical value of 30VDC out of the power induction system.

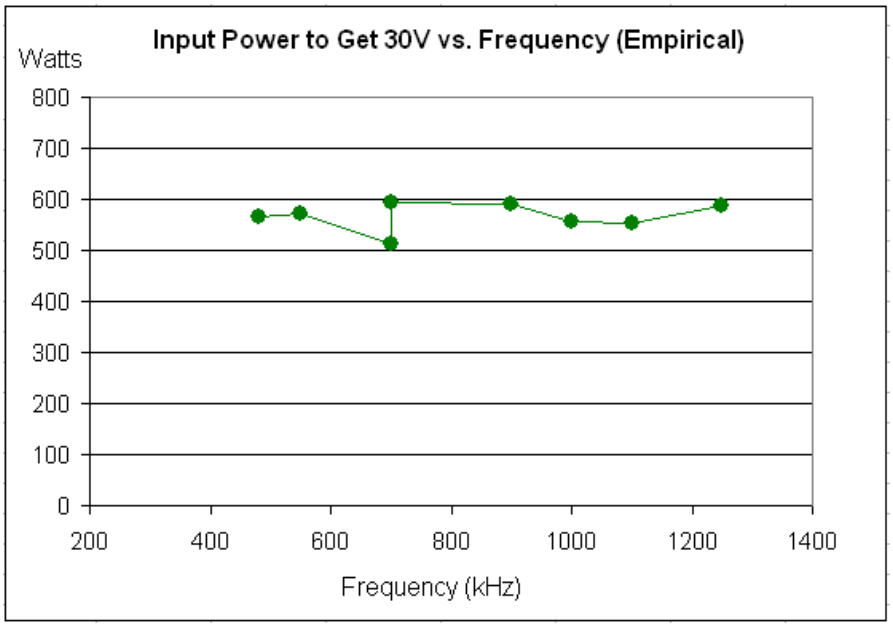

Figure 92: Input Power to Get 30VDC Out vs. Frequency

The two points at 700 MHz exist because two tests with two different transformer types were used. The above data indicate that total system efficiency is not frequency dependent. This is true because the gains in efficiency per amp are counteracted by the higher ring impedance requiring more power to excite each amp.

Based on this data, 700 kHz was chosen as the operating frequency of this system for the oven testing. This was chosen because of the slightly better efficiency at this frequency (for one of the transformers), and because our most robust transformer functions well at that frequency. Also, at higher frequencies there is more parasitic capacitive loss to grounded elements in the turbine and test apparatus.

It is clear from this analysis that one of the key parameters which strongly affect system efficiency is the resistance of the power inducing ring. If this could be reduced by half, the power required to drive the ring is also reduced by half, doubling the efficiency. We held discussions with the inventors of the low temperature co-fired ceramic (LTCC) system used in this project, DuPont. They believe that if a different silver paste was used for our coil traces, a significantly lower resistance at frequency may be realized. A fabrication run is being performed at this time to test whether a metallization change and increases of metallization thickness can reduce the series resistance significantly.

Using the final configuration shown in Figure 88, at 700 kHz, an oven test was performed to evaluate the inductive power system performance over temperature. The key parameter was the input power required to get 30VDC out of the rotating antenna. The voltage needed to run the wireless telemetry board is 28.5VDC. Figure 93 shows a graph of this key parameter vs. temperature.

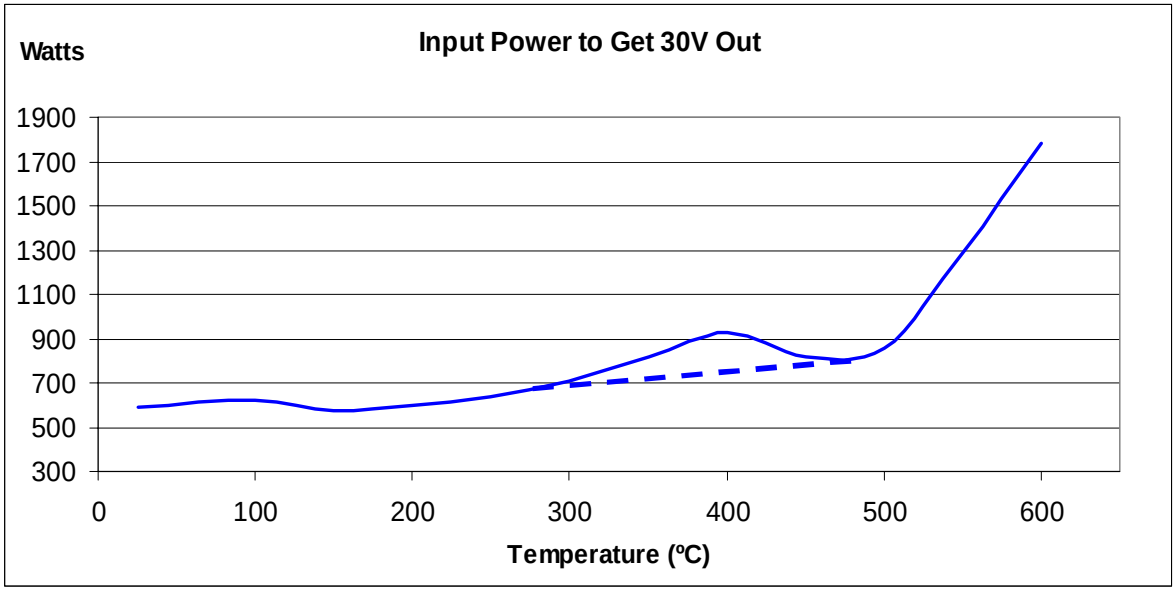

Figure 93: Input Power to Get 30VDC Out vs. Temperature

The graph above shows that the power required to successfully induce the needed 30V output is fairly stable below 300ºC, and it increases somewhat at 400ºC. At this point, the

capacitive matching was adjusted, as the measure inductance of the ring increased with temperature. This is an adjustment that could be done before the turbine is run, to optimize the matching for the small inductance drift seen with temperature. The dotted line indicates the efficiency if the matching is adjusted.

The relative flatness and smoothness of the power requirement over temperature stands in stark contrast to the power transfer seen with the previous inductive power supply, shown in Figure 94. This graph shows a variation in power transfer efficiency that varies by over 300%, with step-wise transitions as internal shorts are created as materials fail over temperature. Figure 8 (the new system) shows only a modest increase in the power required (below 500ºC), and there are no discontinuities do to electrical connection disruptions.

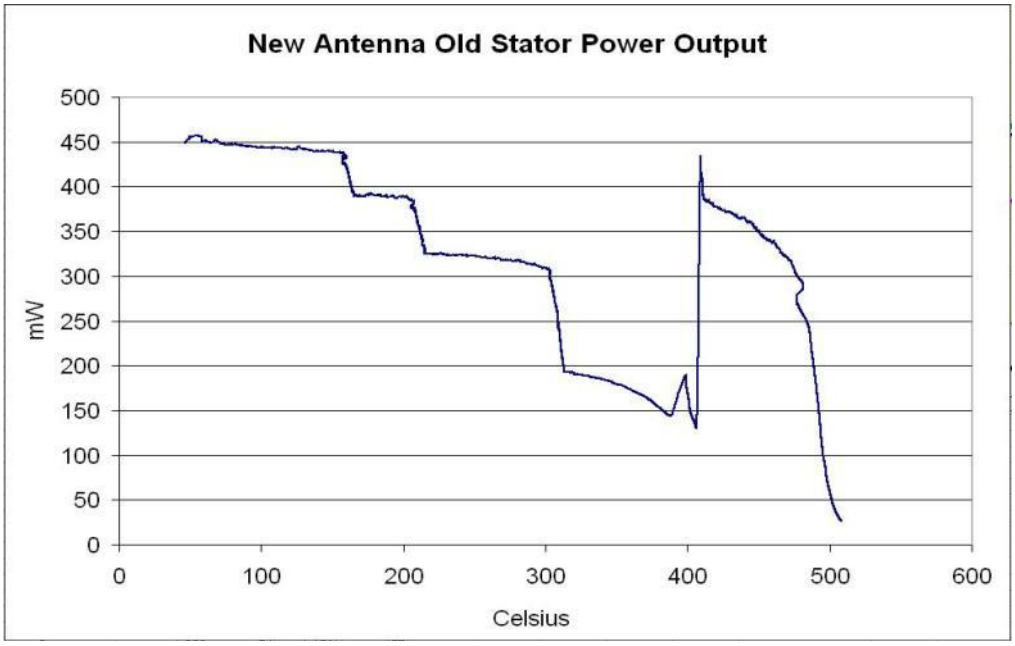

Figure 94: Power Output at Fixed Input – Old System

It should be noted that the inductive power transfer efficiency of the new system is not as good as the previous version. Mechanical robustness, automated manufacture, ease of assembly, and improved temperature performance are very desirable to make this project viable inside a gas turbine. The tradeoff for these improvements is a reduction in efficiency at room temperature from 1% to 0.1%. As discussed above, a minor change to the metallization may increase the efficiency significantly. Additionally, multiple rotating antennas (to support multiple instrumented blades) can be powered by the same ring, with no needed increase in power.

Coil Shape Redesign

Testing in the summer of 2013 revealed a significant drop in the transferred power as the power receiving antenna was swept along the ring circumference. When the receiver

was above the intersection of two coil segments, the power dropped by 50% compared to the power transferred when the receiver was above the middle of a coil segment. In operation, this would result in a 600 Hz, 50% power ripple. Simulations by Arkansas Power Electronics show that this ripple would degrade the operation and accuracy of the wireless telemetry circuit board, which is powered by this wireless power system. Tests showed that this power variation is ultimately caused by the gap between the inner edges of adjacent coils. To compensate, the coils were redesigned to bring the coil inner edges as close to the edge of the segments as possible as shown in Figure 95.

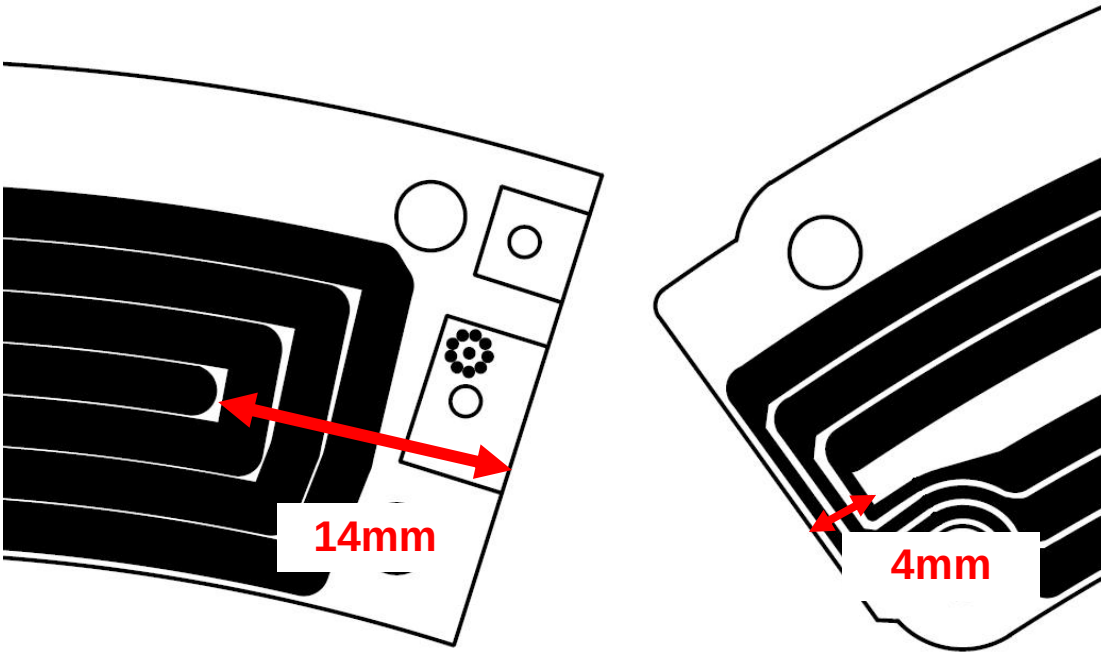

Figure 95: Old Coil Edges (Left) vs. New Coil Edges (Right)

The result is that the power drop between segments is reduced from 50% to 20%. Arkansas Power reports that their simulations indicate this is an acceptable power variation. The coil segments were made twice as long (7.54" max dimension) and more than twice as thick, at 4.6mm as shown in Figure 96. The longer design results in fewer gaps between segments during each rotation. Even if the power drops between segments results in wireless telemetry board data dropouts, therefore, we will still be able to get good data during the time that the rotating segments are adjacent to the much longer middle of the stator coil segments. Vibration testing will confirm the robustness of this new design.

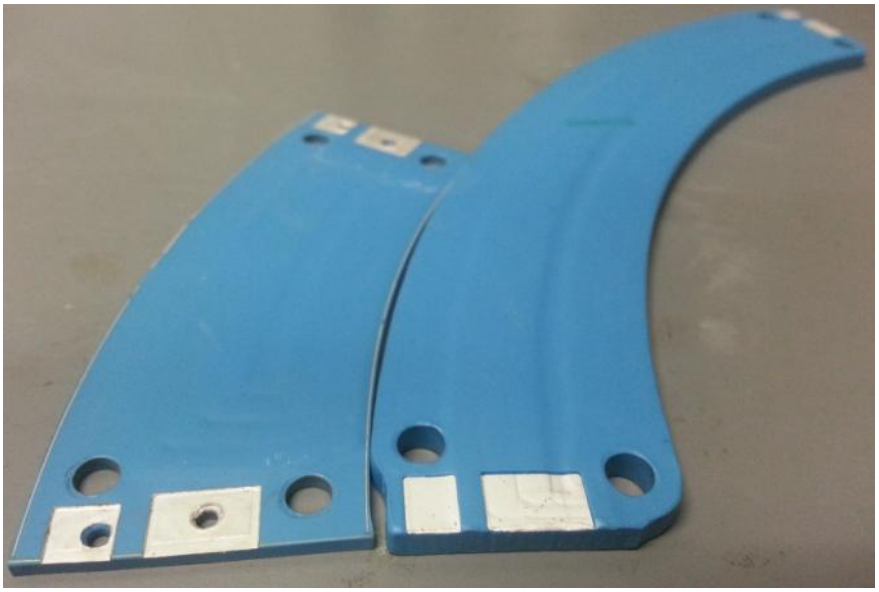

Figure 96: Old Inductive Power Coils (Left) vs. New Design (Right)

Wire Connection Redesign

Progress was also made in the connection system used to connect the inductive power coils to the power source. Bolts with washers are used to compress a ceramic piece, which in turn compresses a wire onto the flat pads of the coil segments as shown in Figure 97.

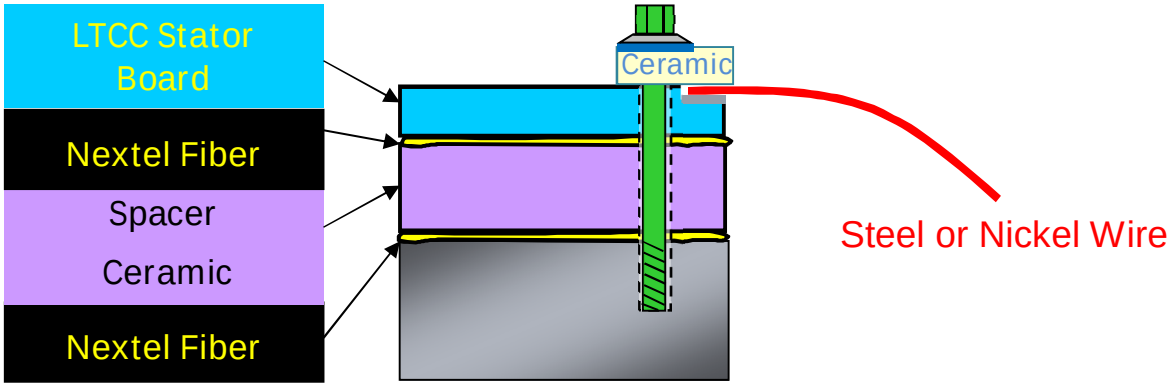

Figure 97: Inductive Ring Wire Connection Scheme

Previously, steel wire test leads were used due to their long fatigue life in the expected high vibration environment. Small diameters of wire (16AWG) were used so that the wires were ductile enough to be bent into useable shapes. The combination of this small diameter and the hardness of steel resulted in small contact area with the flat coil pads that are silver. The compression method worked fairly well below 300ºC. Even with the

small contact area, the higher frequencies used (700 kHz) resulted in a fairly low impedance capacitive connection. Measurements showed higher than desired impedance of 15 ohms (coil ring impedance should be about 7 ohms). This discrepancy at low versus high frequency reflected that fact that the contact resistance is high, but at high frequency, the connection capacitance acts as a very conductive path, even though it blocks DC signals. Fortunately, no DC signals are intended to be sent into the ring during operation. At temperatures above 350ºC, oxidation began to form on the steel wires. The DC resistance went above 50 ohms. The high frequency connections become more intermittent, and ring impedance increased up to 70%.

A new electrical connection was designed and tested. Nickel stranded wires replaced the steel wires. Also, silver foil was wrapped around the ends of the nickel stranded wires at the compression points. This method has the following benefits:

1) Nickel does not form a non-conductive oxidation layer at temperatures of interest (<500ºC).
2) Stranded nickel wire is very robust against vibration fatigue due to its stranded nature.
3) The many strands of the nickel wire provide many times more contact resistance.
4) Nickel is softer than steel, providing better ductility and more contact surface area when compressed.
5) The silver foil further distributes and increases the contact surface area of the nickel wires.
6) The silver foil is very chemically similar to the silver pads of the coils, and even forms a moderate-strength diffusion bond over temperature and time.

This new connection system was tested over temperature to 500ºC for 40 hours. No change in resistance of the electrical connections was seen. Vibration testing of this new scheme is planned for late October.

Ease of installation is an important goal for this product. Whether installed in a test bed or a customer engine site, quick and reliable assembly is an important criterion for successful implementation. With the latest iteration of the inductive power ring and electrical connections, a ring of about 60 cm diameter was constructed in about one hour by one person, and all tests showed good electrical connections. Another hour or two would be required to install the lock wire of the bolts.

Once stable wire connections were realized, long term oven tests and vibration tests were performed to assess the robustness of the entire power induction and RF telemetry systems.

Wireless Power Induction System Electrical Testing (After Refinements)

A 200 hour, 400ºC temperature test was performed on the inductive power ring. Resistance and inductance measurements of the power coils and the RF antenna were

made before, during, and after the test. The circuit measurements were made at DC (zero frequency) and at 700 kHz. This gave more insight into the nature of any possible changes or failures. A DC measurement is more sensitive to minute open or short circuit problems, while the 700 kHz readings show the characteristics of the ring at the frequency of operation. For instance, because the electrical connections are based on thin sheet compression, any open in the circuit at those points may look like a capacitor with a large value. This may not be visible at 700 kHz, but it would be obvious at DC. Conversely, inductive crosstalk to ground resulting in power loss may impact the functioning of the ring. This would be visible at 700 kHz, but invisible in a DC measurement.

There are two electrical lines on the inductive power stator ring: the power coils and the RF antenna. They both use the same type of pads and electrical connections, but the power coils are about 30 times the length of the RF antenna. Any changes in impedance due to electrical connections will, therefore, be more pronounced on the RF antenna due to the shorter internal line length, while the impedance changes due to internal lines will be more pronounced in the power coil paths.

Figures 98 through 101 show the results of this test.

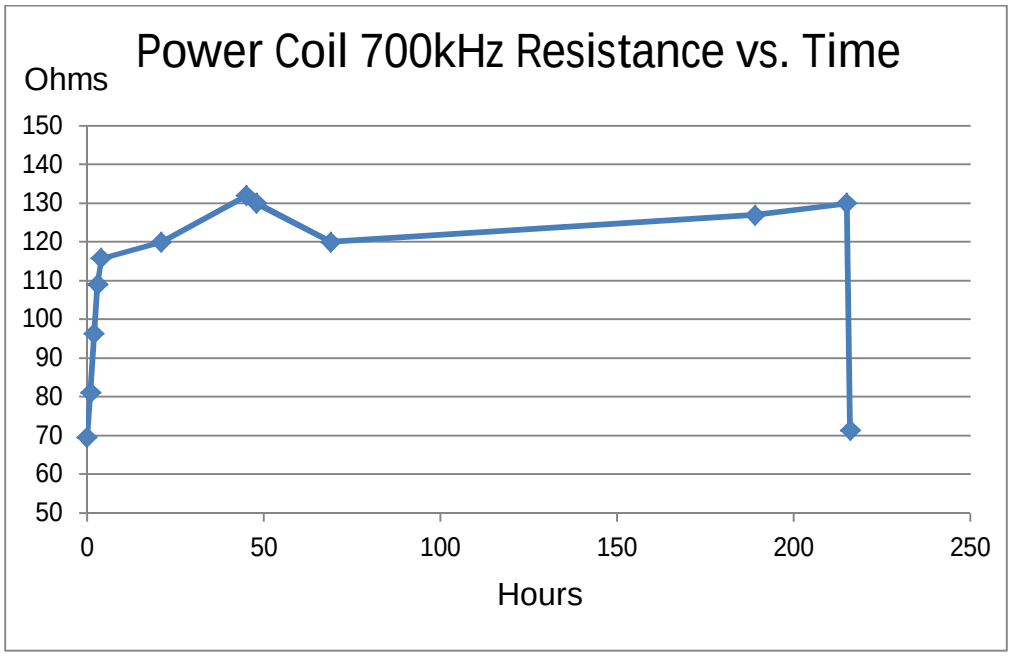

Figure 98: Stator Power Coil 700kHz Resistance During 200 Hour Test

The resistance of the power coils is an important parameter for several reasons. Besides the electrical contact continuity mentioned above, any increases in impedance have a strong effect on the power required to run the circuit. If the resistance doubles, then the power required to produce a given magnetic field intensity also doubles. In Figure 98 there is a quick ramp in resistance as the temperature is increased from 25ºC to 400ºC. This is due to the increased resistivity of the metal traces of the power coil, and it is on the high end of expected resistance increases (i.e., an increase of 80%). Once the

temperature stabilizes in the first few hours, the resistance also stabilizes, with changes of approximately 10% or less. This indicates that the electrical contacts and line traces are stable over the duration of the test, at least at this higher frequency. If there are physically small disruptions in the circuit, they are not affecting the operation of the power coils in an erratic way. It is also important to note that the first and last points, which are both taken at room temperature, have very similar values (69.5Ω and 71.4Ω). This means that the circuit did not appreciably degrade as far as this parameter is concerned.

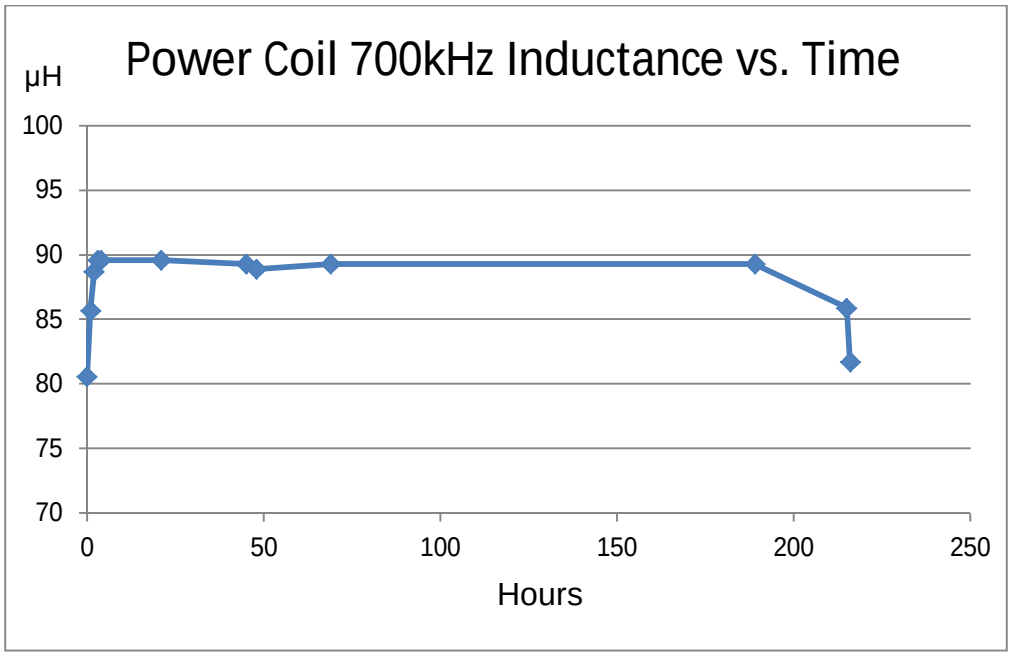

Figure 99: Stator Power Coil 700kHz Inductance During 200 Hour Test

Likewise, Figure 99 shows that the inductance of the power coils did not degrade or change considerably while at the target temperature of 400ºC. The inductance improved (increased) between room temperature and 400ºC, which slightly increases the magnetic field production. The inductance before and after the test (80.6µH and 81.7µH, respectively) are very similar, which implies good circuit stability at the operational frequency.

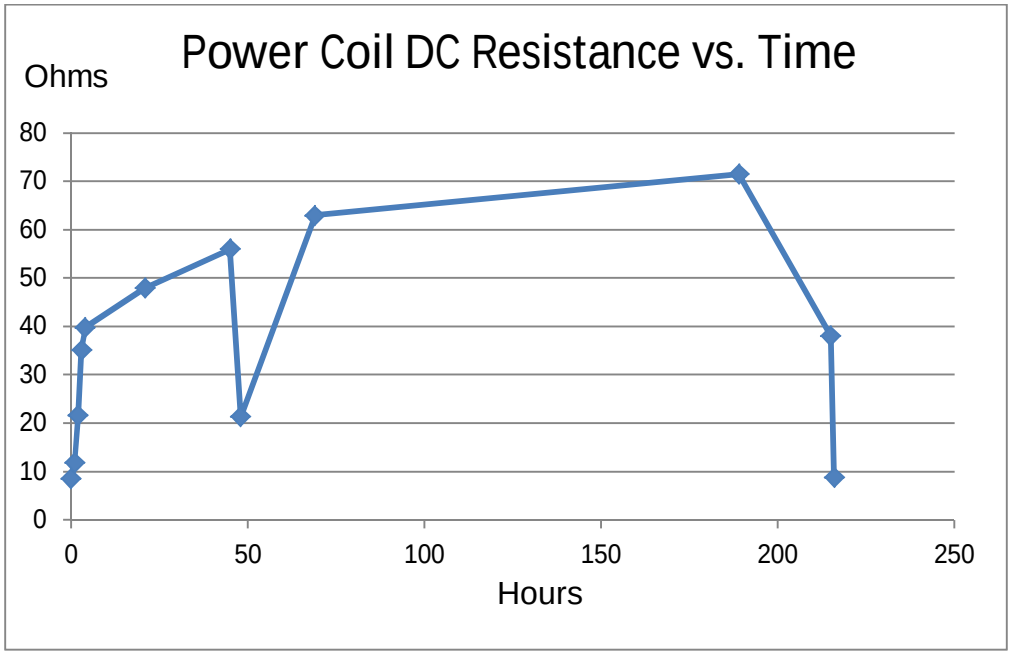

Figure 100: Stator Power Coil DC Resistance During 200 Hour Test

Figure 100 shows a very large jump in DC resistance of the power coils from 9Ω to as high as 71Ω, and the reading was somewhat erratic.

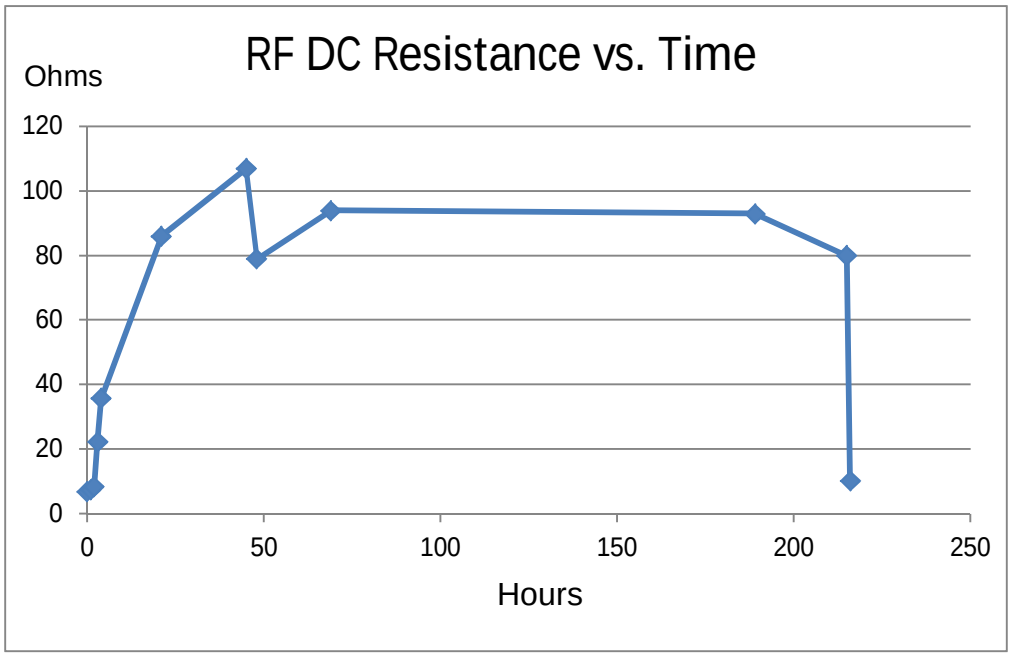

Figure 101: Stator RF Line Resistance during 200 Hour Test

Likewise, the DC resistance measurement of the RF line increased dramatically from 7Ω to as high as 107 ohms s shown in Figure 101. Together with the high frequency measurements, this indicates that the connections between the stator boards or between

the external wire connections and the stator boards are having issues with slightly open connections (likely insufficient contact area and/or oxide buildup on contact surfaces).

It was quickly determined that the cause of the issue is the external connections to the boards. The thin steel wires have minimal contact area; they are held against the stator board pads with silver foil and compressive force. At temperature, a thin oxide layer is observed to form on the surface of the wire, causing a higher DC resistance. This oxide layer acts similarly to a high value capacitor, meaning that it resists DC current significantly, but passes AC current.

These wires were replaced with stranded wires of a non-oxide-forming element, thereby increasing surface area and eliminating the oxide contact issues. Figure 102 shows an example of the new contact.

Figure 102: New External Line Contact

With the new contacts there was a major improvement in the circuit both at high and low temperatures. Table 12 shows the differences in the DC and RF resistances of the power coils and RF antenna.

Type of Electrical Contact	Power Coil DC Resistance (Ω)	Power Coil 700kHz Resistance (Ω)	RF DC Res. (Ω)	RF 700kHz Res. (Ω)
Single Steel Wire	8.6	69.5	6.7	8.8
Stranded New Conductor	5.35	61.9	0.68	1.41

Table 12: Stator Resistances vs. Contact Type

Figures 103-106 show the performance of this new contact over temperature.

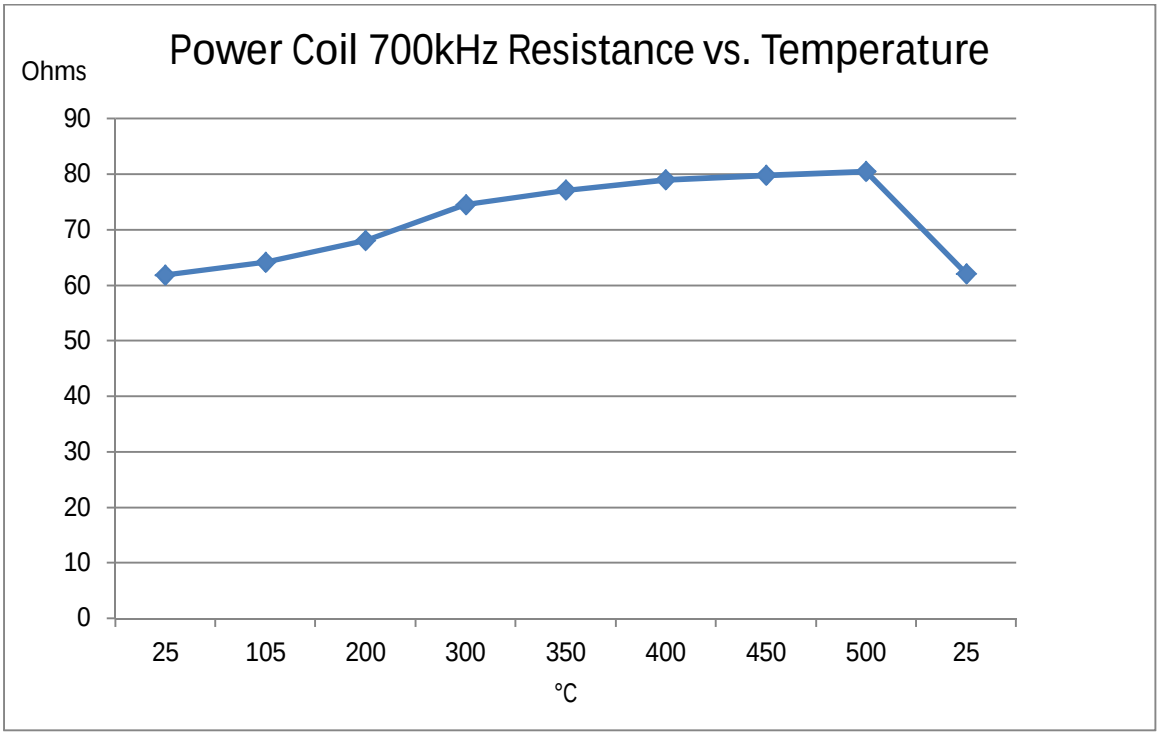

Figure 103: Stator Power Coil 700kHz Resistance vs. Temperature with New Contact

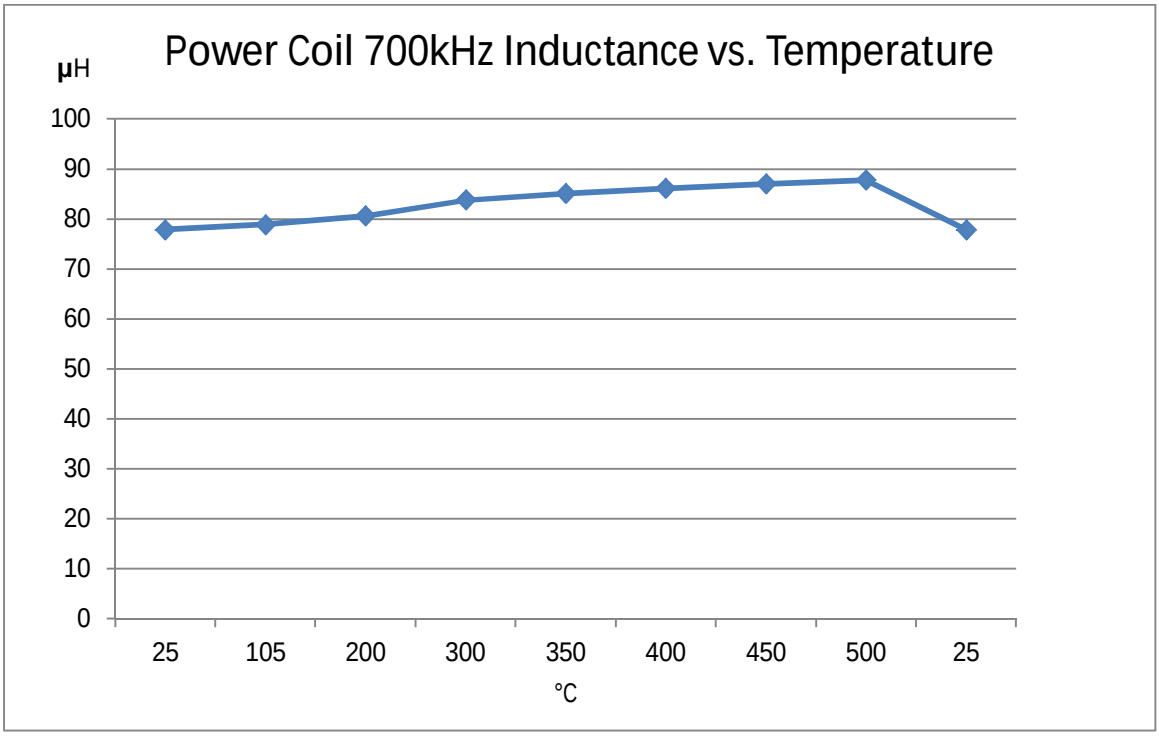

Figure 104: Stator Power Coil 700kHz Inductance vs. Temperature with New Contact

The high frequency inductance of the power coils is not significantly changed by the contact change. However, the resistance at temperature of 400°C is significantly lower.

The average power coil resistance with the old contacts was 123Ω, while the measure resistance with the new contacts is 79Ω. This means that the new contacts increase power efficiency by 34% through lowered resistance. The previous, higher increase in resistance must, therefore, have been partially due to issues with the old contact design.

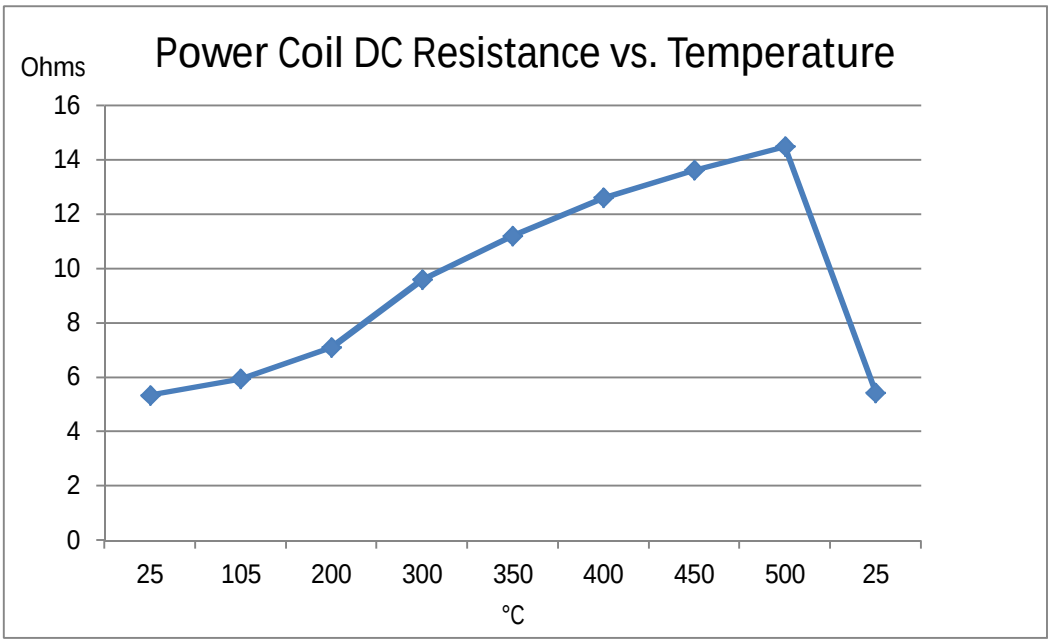

Figure 105: Stator Power Coil DC Resistance vs. Temperature with New Contact

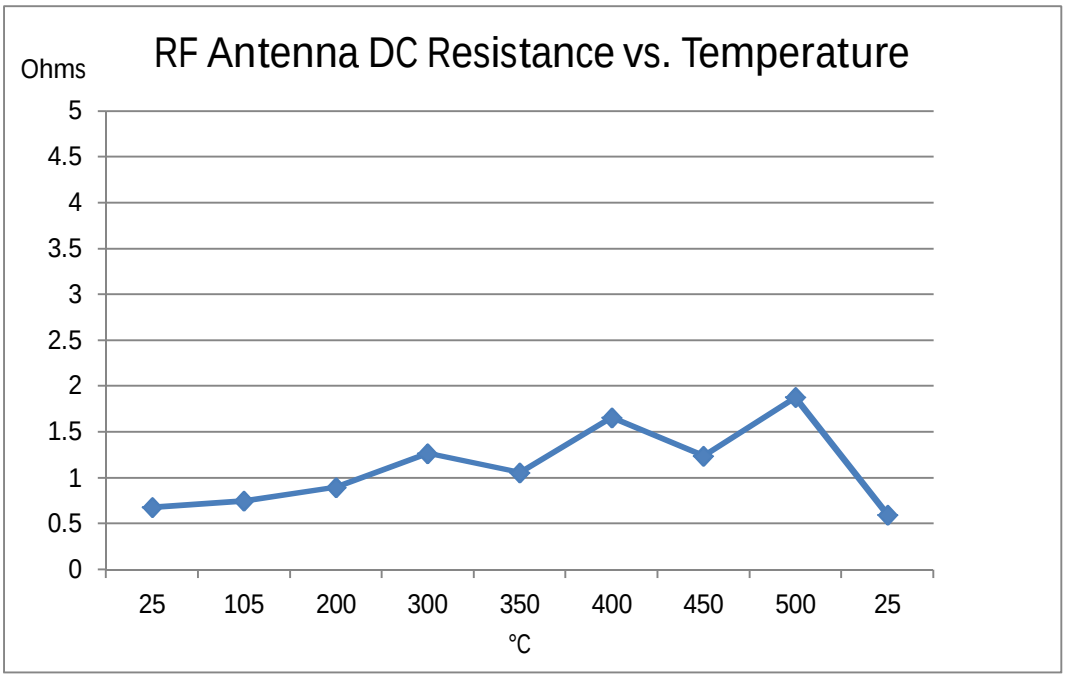

Figure 106: Stator RF Antenna DC Resistance vs. Temperature with New Contact

The new contacts had a strongly positive effect on the DC resistance. At room temperature, the power coil resistance reduced from 8.6Ω to 5.3Ω. Multiple measurements have shown that the cumulative resistance of the power coils within the LTCC (Low Temperature Co-fired Ceramic) pieces is close to 5.0Ω, indicating that the contact resistance is now negligible, even at high temperature. This is confirmed with the DC resistance measurement of the RF antenna, which has had its resistance reduced from 6.7Ω to 0.7Ω. Again, this indicates that the DC contact resistance reduced to approximately zero.

At temperatures of 400°C, therefore, the resistance is much more in line with other independent measurements of the internal LTCC line resistance without external wires. This is strong evidence that the contact resistance now remains negligible across the entire temperature range from 25°C to 500°C. Also note that the resistance returns to the low initial value after the temperature test.

Using the new contacts, a full power, full temperature 16 hour duration test was performed on the stator. Power consumption, current, power transfer, and RF signal to noise was measured while the stator was powered and at 400°C. Once the stator assembly was fully heat soaked to 400°C, the drive power was held constant and relevant inputs and outputs were monitored for changes which might indicate any degradation. Comparisons are made after heat soak because temperature changes of the circuit have an expected impact on the circuit resistance, and any changes before heat soak are not indicative of permanent degradation. Table 13 shows the results from this test.

Time After Heat Soak	Input Power (Held Constant)	Input Current	Power Transfer Voltage	RF Signal to Noise (dBm)
0 hours	410 Watts	801 mA	25.50 Volts	37dBm
8 hours	410 Watts	800 mA	25.48 Volts	38dBm
16 hours	410 Watts	800 mA	25.47 Volts	40dBm

Table 13: Inductive Power System 400 °C Full Power Duration Test Results

As can been seen in Table 13, the 400 °C continuous power test showed that after heat soak, there was no degradation in input current or power transfer with time. The RF signal to noise ratio needs to stay above 5 dBm for good signal recovery. The measured signal to noise ratio of 37-40 dBm is well above requirements. The 16 hour duration of this test reflects the fact that a system in an engine situation is likely to be powered continuously for a maximum of 8 hours.

Radio Frequency (RF) Data Transmission Testing

Another functionality of the rotating antenna and inductive power ring is the transmission and reception of a radio frequency (RF) telemetry signal from the rotating wireless telemetry board to outside the engine via the ring. The wireless telemetry board is connected to a monopole antenna embedded in the rotating antenna. The rotating antenna transmits the RF telemetry data to an RF antenna embedded in the inductive

power ring. This embedded ring antenna is connected to a cable which leads out of the turbine.

RF transmit power of the wireless telemetry board is -20dBm, and a typical RF telemetry signal frequency is 70MHz. Therefore -20dBm of power at 70MHz was injected into the rotating antenna. The stator ring RF output was measured through 3.5m long shielded, grounded cables to simulate the cables which would connect the stator ring to the outside of the engine. The goal is to have a signal which is more than 3dBm above the noise floor. The noise floor was measured to be at -63dBm (see Figure 107).

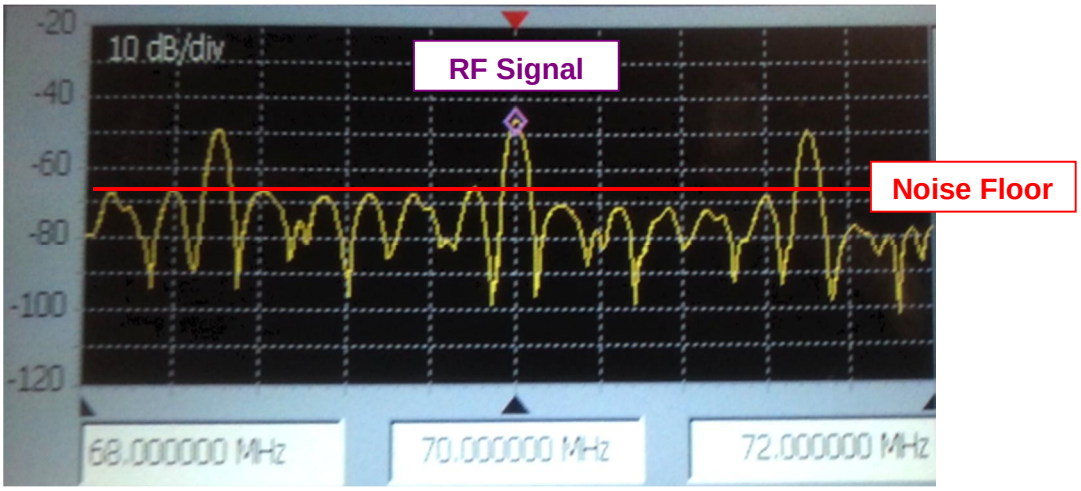

Figure 107: Input Power to Get 30VDC Out vs. Frequency

The power level of the received RF telemetry signal vs. temperature is shown in Figure 108, with the noise floor indicated by a red line. The noise floor did not rise above the level of -63dBm at any temperature.

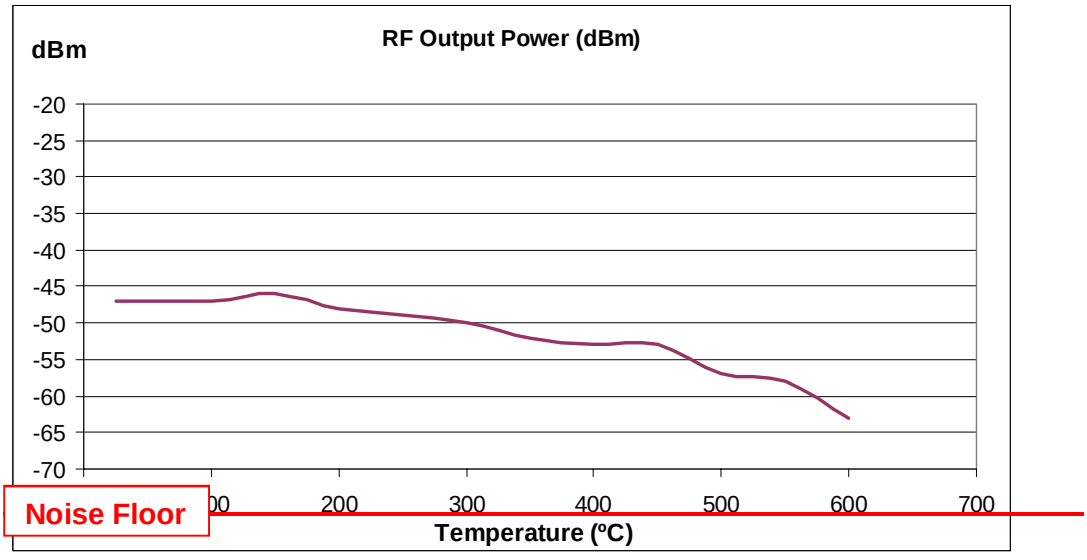

Figure 108: RF Output Power vs. Temperature

In order for the telemetry signal to be detected, the received signal must stay above the sensitivity of the amplifier/receiver (-90dBm) and stay above the noise floor. The above graph shows that the received signal stayed significantly above the noise floor to temperatures of almost 600ºC. In the temperature region we are most interested it, at 350ºC to 450ºC, the signal level was at least 10dBm above the noise floor, resulting in a signal to noise ratio (SNR) of 10dBm, which is a linear ratio of 10:1. This is well within operating parameters.

Extreme Temperature Testing

Before and after tests to 500ºC and 600ºC, the key electrical parameters of the power inducing ring and the power receiving antenna were measured. After cool down, almost no difference in these key parameters of resistance and inductance were measured. The largest change (18%) was in the resistance of the power receiving antenna, and this was in a positive (lower resistance) direction. Table 14 shows the differences.

Electrical Parameter	Before Test	After 500C Test	After 600C Test	Max % Change
Ring Resistance	78.8	78.8	80.4	+2%
Ring Inductance	85.4	85.5	86.0	+0.7%
Antenna Resistance	50.6	45	41.4	-18%
Antenna Inductance	85.6	84.7	83.7	-2%

Table 14: Key Parameters of Power Induction System Before and After Temperature Tests

This is an important set of data because it shows that even when heated to 600ºC, no significant permanent changes to materials or electrical connections are observed. Measurements of these parameters at these elevated temperatures were also made. The inductance increased marginally, and the resistance increased markedly, but this is expected behavior. While efficiency does suffer at higher temperatures (see Figure 8), no discontinuities in material performance or electrical connection performance were observed. In these tests, all the materials are identical to what would be installed in the engine. This temperature test article also contained 36 electrical connections, none of which failed at any point in the test.

Vibration Testing Results

Vibration tests were performed on inductive power ring elements. The test article was vibrated in the direction perpendicular to the ring coils and in the two directions parallel to the plane of the coils for 5 hours in each of the three directions direction. The 60 Hz vibration magnitude ($30m^2/s$) is four times the expected vibration and is higher than the vibration at which the engine would automatically shut down. In addition to the 60Hz tone, a vibration sweep from 10 to 240Hz was simultaneously induced to account for

other lower level vibrations observed in gas turbine engines. Figure 109 shows the magnitude and frequencies of the two five-hour tests. This test was carried out at room temperature.

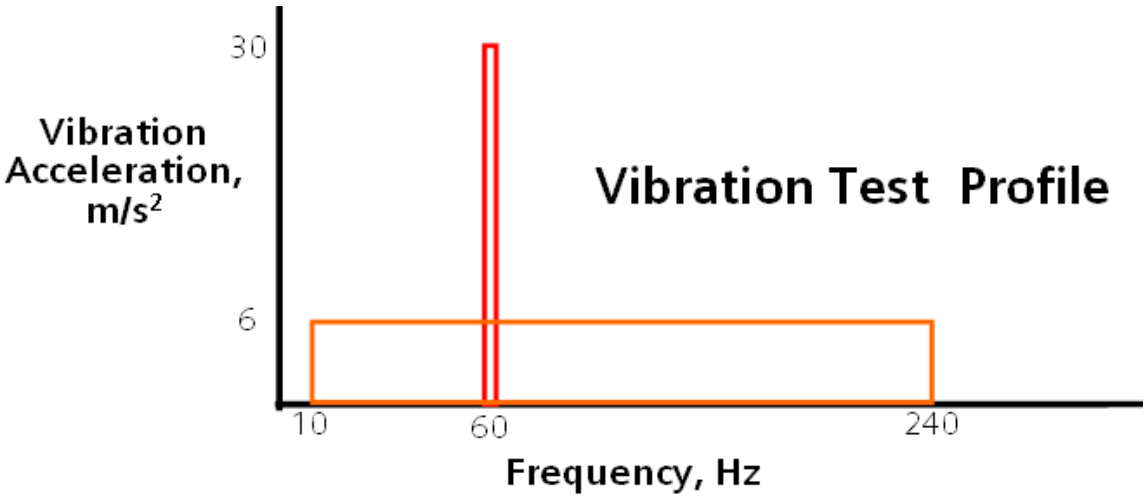

Figure 109: Vibration Test Profile

The conductivity of the eight electrical connections in the test article was measured continuously during the test, and no open or degraded connections were observed. After the test, the vibration article was disassembled, and no cracking, erosion, or other significant changes in the components was observed.

As described above, Siemens demonstrated a novel power induction system which functions to 450ºC. At a lower efficiency, the system functions marginally to 550ºC. This system has been shown to be vibration and temperature resistant.

Extensive vibration testing was done on a large LTCC piece of the power inducing stator. This piece was bolted to a metallic plate in the same manner that it will be bolted to an engine component. This piece was then vibrated at appropriate frequencies to simulate the engine environment (based on internal Siemens vibration measurements). The amplitude of the vibration during these tests was four times the maximum engine shutdown vibration, and the test lasted 10 hours at room temperature. Figures 110 and 111 show the vibration article on the vibration table, indicating the directions of vibration.

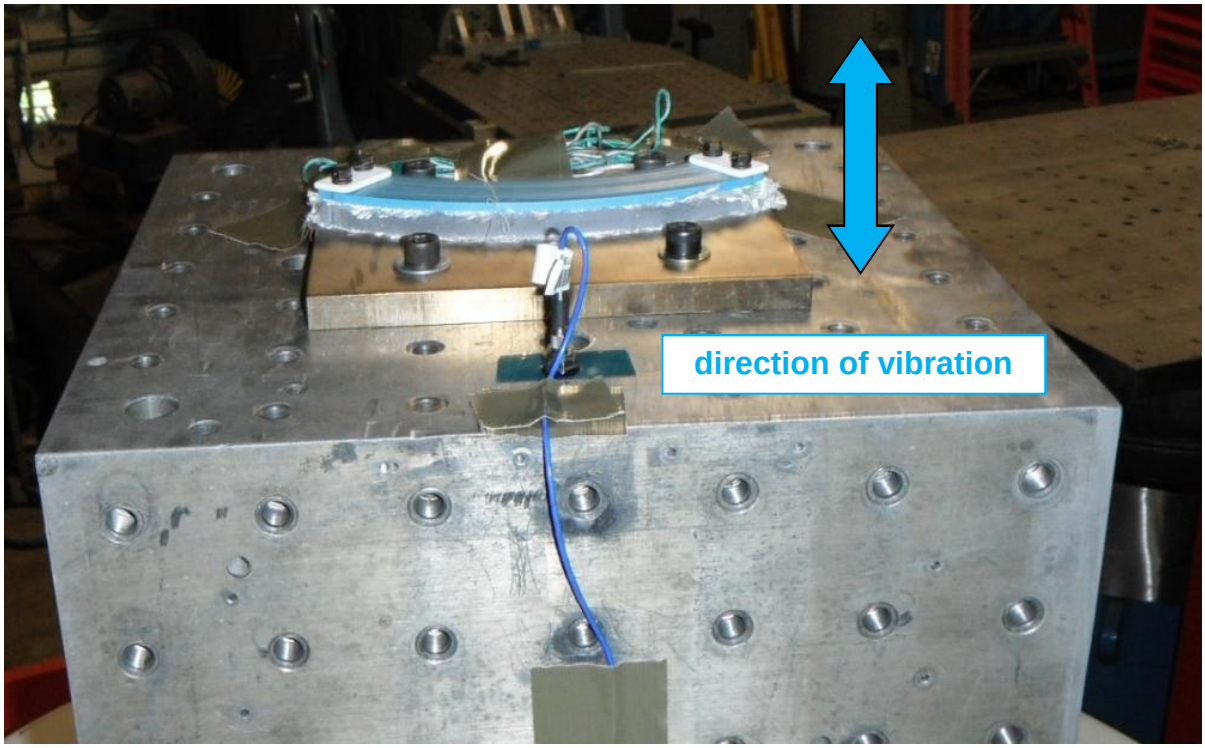

Figure 110: Stator Vibration Test – Axial Direction

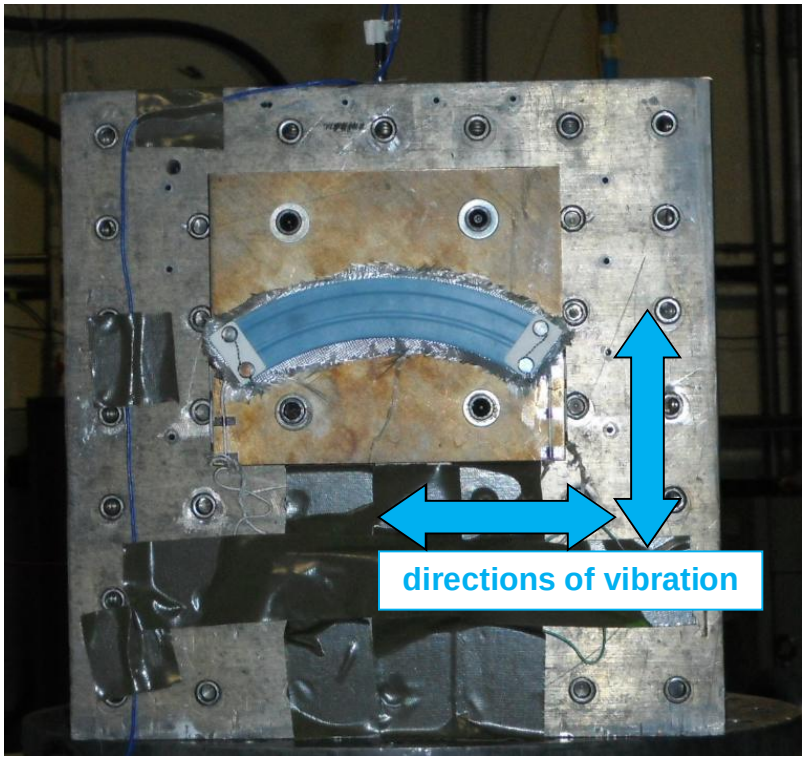

Figure 111: Stator Vibration Test – Two Radial Directions

Visual inspections of the vibration article after testing and disassembly revealed no cracks, chipping, rubbing, or other defect. Electrical tests indicated no functional degradation. This is the third vibration test performed on planar LTCC stators, for a total of 30 hours of vibration testing. To date, no negative effects of vibration testing have been observed.

Integrated Full System Heated Spin Test Results

In the winter of 2014, the spin rig power induction ring was assembled. Two rotating antennas, each of which rotates next to the electronics boards, were also assembled. The rotating antennas wirelessly receive power from the stationary power induction ring and provide that power to the electronics board. The RF carrier from the electronics board is transmitted by each rotating antenna wirelessly to the power induction ring. Below is a description of how each component faired during the spin rig test.

The rotating antennas performed nominally throughout the spin test. Electrical tests before and after the spin test showed no degradation in the resistance or inductance of the rotating antennas. The ceramic boxes which enclose the antennas showed no cracking, chipping, or other mechanical issues. The external pins showed excellent durability and minimal bending. Electrical connections were maintained throughout the test. These rotating antennas, which see the highest temperatures and g-loads in the spin rig and engine, are functionally and mechanically fully operational. Figures 112-115 show the pins before and after the spin test, along with pictures of the spin disk assembly. No pin breaks or elongations occurred. No bending of the pins occurred. This is a first time these pins have survived without significant bending, which is remarkable given that this portion of the spin disk experienced over 14,500g at 350ºC for well over an hour. As can be seen in the after spin test pictures, the light application of the white cement (used for electrical insulation) did experience some chipping and cracking. No short circuits to the underlying metal occurred.

Figure 112: Rotating Antenna Pins before Spin Test

Figure 113: Rotating Antenna Pins before Spin Test, Side View

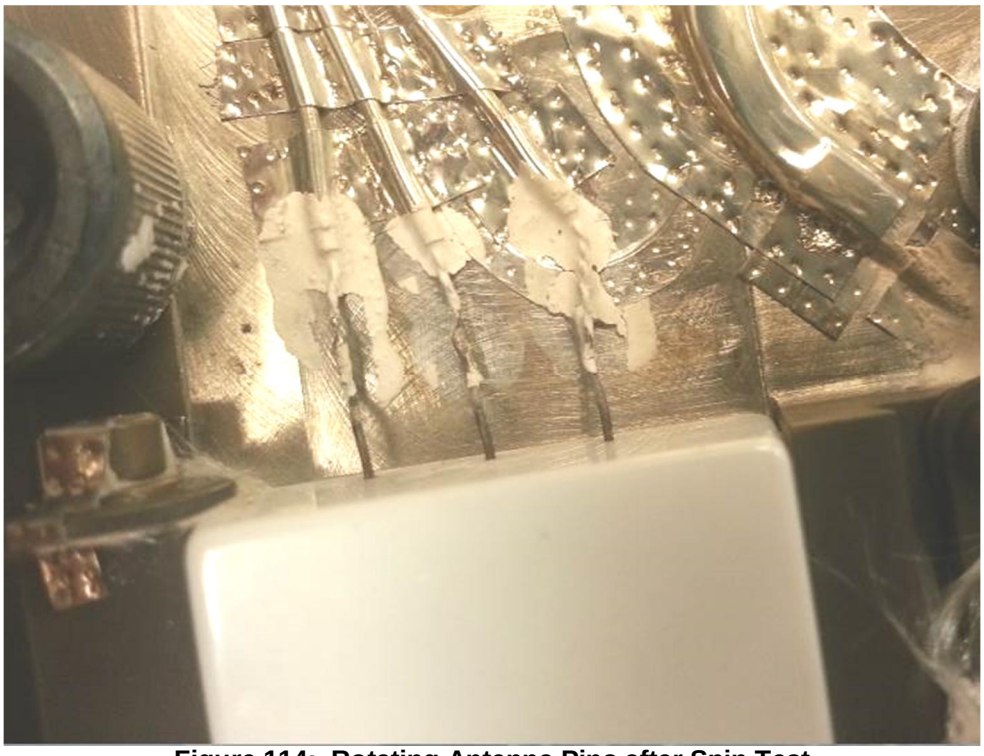

Figure 114: Rotating Antenna Pins after Spin Test

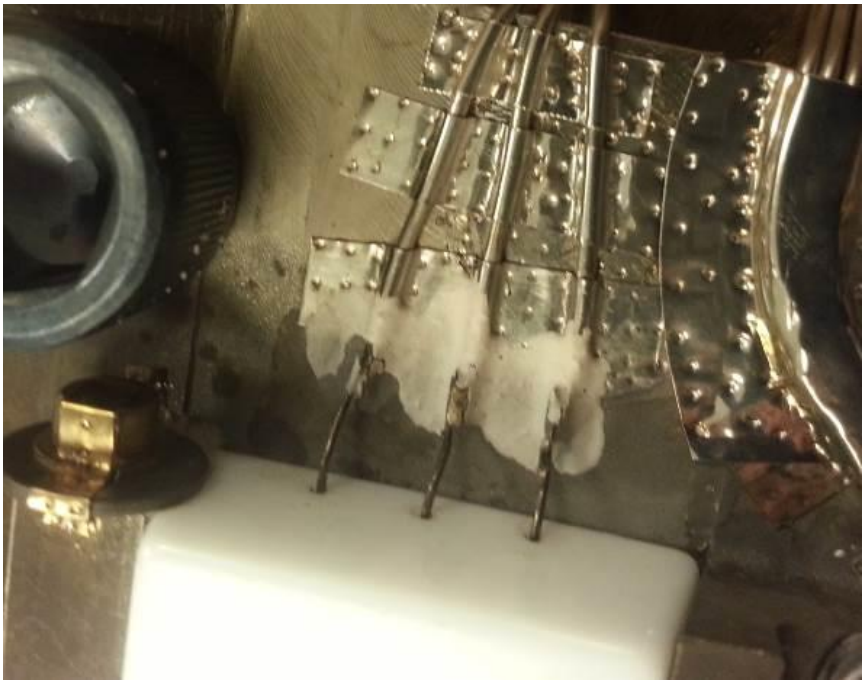

Figure 115: Rotating Antenna Pins after Spin Test

The stationary inductive power ring, shown in Figure 116, provided power sufficient to power the electronics boards over the full temperature range of the test. This ring of ceramic-embedded coils also received the RF carrier signal and sent the signal outside the rig on specialized high temperature cables.

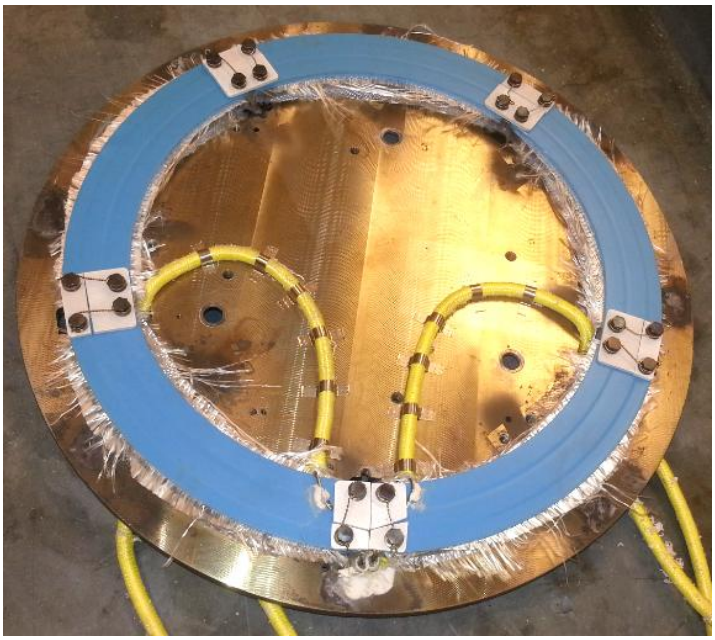

Figure 116: Inductive Power Ring after Spin Test

Three functional issues occurred with the inductive power ring during the spin test:

1) The ring's power transfer varied greatly along its circumference, with variations greater than 50% (expected 20%)
2) The RF carrier signal received was measured at -68dBm, while lab tests showed the signal was measured at -39dBm
3) There was an arcing event between the power circuit and the RF circuit

The ring's design inherently causes some power transfer drop as the rotating antenna passes over the bolts which hold the pieces together. This ring is comprised of five ceramic arced segments. Extensive lab tests were carried out to characterize this power variation. Seal plate assemblies were created with a rotating antenna connected to a rectifier circuit of the same electronic geometry as that used on the electronics board. The presence of additional metallic backing and electrical grounding were included. In these lab tests, the transferred power drop between the ring segments was about 20%. This is an acceptable power variation for the electronics boards to deal with. Between the ends of the segments, the power transfer is stable and flat. The power transfer is also consistent from segment to segment (within a few percent).

On the rig, the power variation was considerably worse. Once the rig was assembled, the spinning disk containing the rotating antennas and electronic boards was rotated very slowly by hand as the rectified voltage was measured via the slip ring. The same variation was seen on each rotating antenna/electronics board pair, about 55% between peak and low power transfer. The variation in power transfer at the midpoints of different segments also varied by up to 20%. A separate seal plate containing a rotating antenna with a rectifier circuit was passed over the power induction ring at a consistent distance once the spin rig was opened. This seal plate was grounded to the spin rig. This test showed a power transfer variation of 20% between peak and low power transfer, and only a few percentage points of variation between midpoints of segments. The cause of this discrepancy is currently unknown. The rotating segment of the rig has been sent to Siemens for lab tests in order for this problem to be characterized and resolved.

There is a significant negative impact of this higher power variation. When the power transferred to the electronics board drops below a certain point, the center frequency of the RF carrier is changed. This variation causes a change greater than what can be automatically dealt with by the RF demodulation system. Additionally, the sensor data is coded into the RF carrier as change in frequency. This power variation can, therefore, interfere dramatically with data recovery. To mitigate this effect, a high speed data recorder was used to recover the demodulated waveform. Strain and thermocouple data can be recovered from the short periods of power stability, even at high speeds. Demodulated data was recovered in real time during the test, as shown in Figure 6.

In lab tests, the RF carrier signal was simulated with a function generator transmitting at a power identical to the electronics board transmissions. Cabling, grounding, seal plate geometry, and temperature were all designed to simulate the rig/engine environment as closely as possible. In these lab tests, the RF carrier was received at -39dBm, with a noise floor at -70dBm, resulting in an excellent signal ratio of 31dB. At the spin test, the

RF carrier was measured at -68dBm, and the noise floor was approximately -80dBm, resulting in a signal to noise ratio of 12dB. Additionally, the extremely low signal level of 68dBm made recovery more challenging (though feasible). The cause of this degraded RF transmission is currently unknown, but lab tests with spin rig equipment are planned in order to characterize this discrepancy.

The failure which ended the test was an arcing event between the power circuit and the RF circuit on the power inducting ring. At high powers, the voltage on the ring segment coils causes current to arc to the RF ring at the outside circumference of the ring (still within the same ceramic piece). When this happens, power transfer suffers and the RF carrier signal is overwhelmed with harmonics. This failure mode was also observed during lab tests. The mitigation was to attach a 10pF capacitor at exposed RF nodes, such as the ends of the RF cables coming from the inductive power ring.

While troubleshooting the low RF carrier signal issue during the spin test, one of the RF cables was intentionally cut and left in place. The end of this cable eventually came to rest in contact with grounded metal near the spin rig. This provided the ground path between the segments and ground, and current arced from the power coils to the RF antenna in the segments, and out the cut cable to where it was touching the grounded metal. Troubleshooting during the spin test campaign (which lasted a week) revealed a damaged segment, which exhibited visual artifacts of the arcing event (see Figure 16). The DC resistance of this segment was 1.5Ω. This was much lower than the nominal segment resistance value of 3.2Ω, and was further evidence that shorting from an arc event had occurred. A segment next to this one was also measured to have lower than expected resistance (1.8Ω), but no visual evidence of arcing.

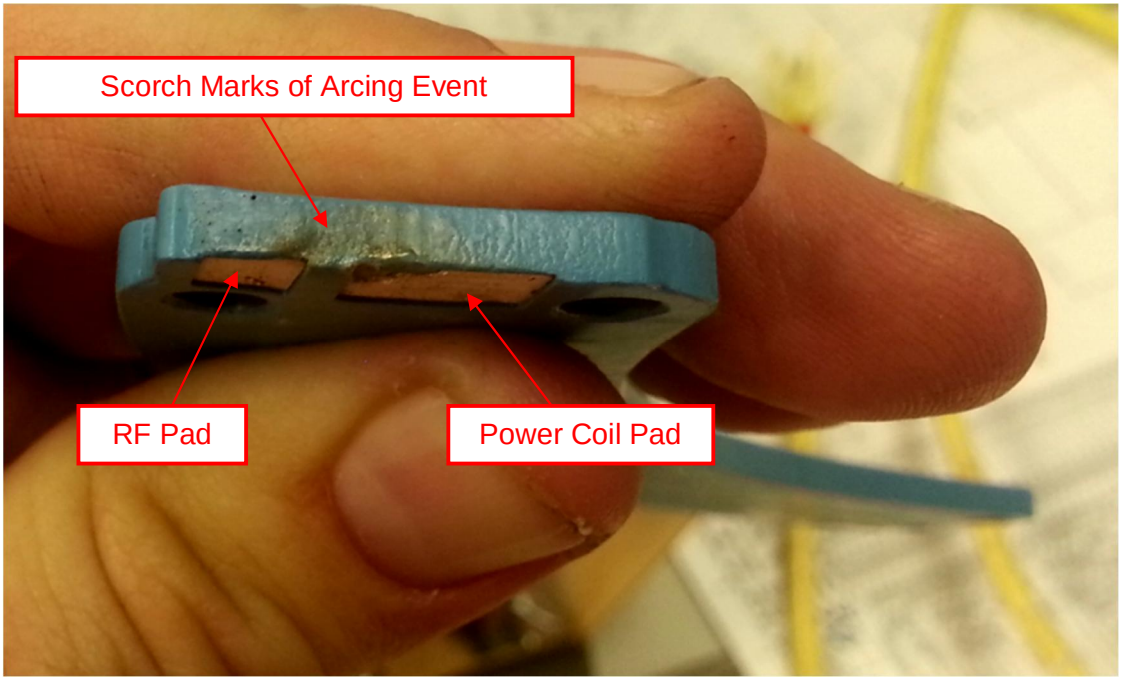

Figure 117: Stator Segment Exhibiting Evidence of Power to RF Arcing Event

The segment with the lower resistance and visible arcing was replaced with a spare. If two spares were available, both segments would have been replaced because of the resistance reading. The ring functioned nominally for one more day of spin testing. Toward the end of that day, evidence of further arcing occurred, and the test was ended an hour early. It is very likely that the original arcing event damaged two stator segments, and this second, un-replaced segment had a latent failure which manifested at the end of the test. If that is the case, then both the arcing issues were caused by the one case of leaving the unprotected RF cable end near grounded metal, and is not indicative of a new failure mode. This problem can be mitigated in two ways: ensure protection of all RF conductors at all times and lower the overall power through the power coils by future power transfer efficiency increases.

Even with these issues, the test was a significant improvement over previous spin tests. Except the arcing event, the power transfer remained fairly consistent over the full temperature range, which was a very large problem with the previous system iterations. The electrical connections between segments and from segments to external wires remained consistent throughout the test across the entire temperature range. These no-weld, no-cement connections allowed an intrusive field repair which took 10 minutes to perform. Disassembly after the integrated spin test shows no degradation in the electrical connections or non-arced stator pieces. No cracks, chips, or other issues were observed, indicating strong vibration resistance. Note that the Aerodyn rig produces vibrations similar in displacement and magnitude to those seen in a large gas turbine.

2.5 - TASK 5: ROBUST ADVANCED SILICON CARBIDE DEVICES RESULTS

Task 5 develops and fabricates advanced SiC devices, matched transistor pairs, and integrated circuits. Siemens partnered with the University of California at Berkeley to develop advanced silicon carbide (SiC) devices. Currently, the Berkeley team produced two generations of Zener diodes. This second generation, illustrated in Figure 118, is planned to be incorporated into the wireless transmitter board design in the near future. Additionally, the team at Berkeley is designing transistors, and prototypes will be available in the coming months. These will be configurable in matched transistor pairs, and are the first step toward creating SiC integrated circuits.

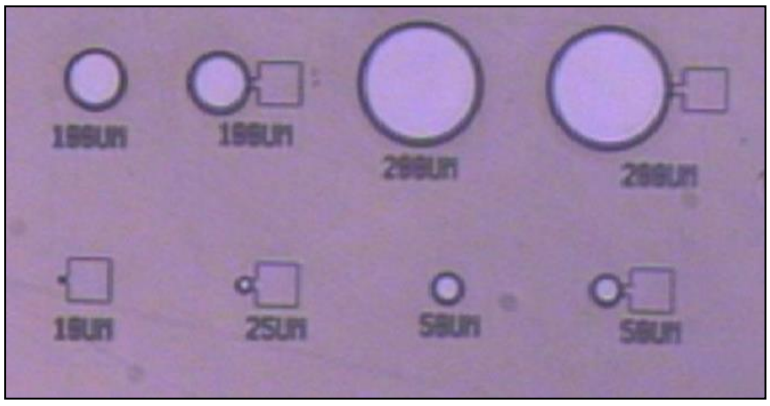

Figure 118: Micrograph of Second Generation Zener Diode Structures

Silicon carbide technology is, for the most part, still in the discrete component development stage. However, some research groups are working on integrated SiC circuitry. In order to miniaturized and add features to our wireless telemetry circuit board, we need to develop and incorporate SiC integration technologies.

Siemens, along with our subcontracted wireless telemetry circuit board developer, APEI, documented the requirements of the following components: Zener diode, advanced transistors and energy scavengers. In addition to temperature environment specifications (continuous operation at 450^{o}C+ for >100 hours), extensive electrical specifications have also been shared with the Berkeley team. Also, die metallization, packaging, and device profiles have also been jointly developed. For the energy scavengers, space requirements and profiles were generated. Additionally, blade pressure amplitude and period profiles were simulated and shared with Berkeley.

Silicon Carbide Zener Diodes

High temperature Zener diodes are a highly desirable component for use in the wireless electronics boards. The current methodology used for power regulation involves a number of transistors and capacitors configured to simulate the functionality of a diode circuit. This results in ripple on the rectified power signal (affecting telemetry stability) than would be rectified by a Zener diode. The use of a Zener diode also reduces the overall size of the electronics board and the number of connections required. Currently available diodes are not capable of functioning at temperatures above 150 ºC. Table 15 lists the benefits of incorporating the Zener diode into our electronics boards.

Issue/Parameter	Without Zener	With Zener	Resulting Benefits
Power Regulation	Considerable variation	Much more stable	Significantly increased measurement accuracy
JFET use	Need 4-5 JFETs	Need 1-2 JFETs	Reduced impact of JFET temperature/age drift results in increased measurement accuracy
			Increased space on board
			Lower number of connections (Points of Failure)

Table 15: Benefits of Incorporating Zener Diode into Telemetry Board

In late 2011, the University of California at Berkeley delivered their first generation of Zener diodes. These were evaluated by Arkansas Power Engineering for use in their

wireless telemetry boards. Electrically, these 1st generation Zener diodes were superior, and provided significant functionality improvements over the existing power regulation designs. For power rectification circuits, the less ripple the better. APEI designed and constructed a power regulators based on JFETs and Zener diodes. Figure 119 depicts the input and output of a power rectification circuits built from JFETs. Its output ripple is 1.6V when operated at 450°C. Figure 120 depicts the input and output of a power rectification circuits built from a Zener diode. Its output ripple is 0.8V when operated at 450°C, a 50% improvement.

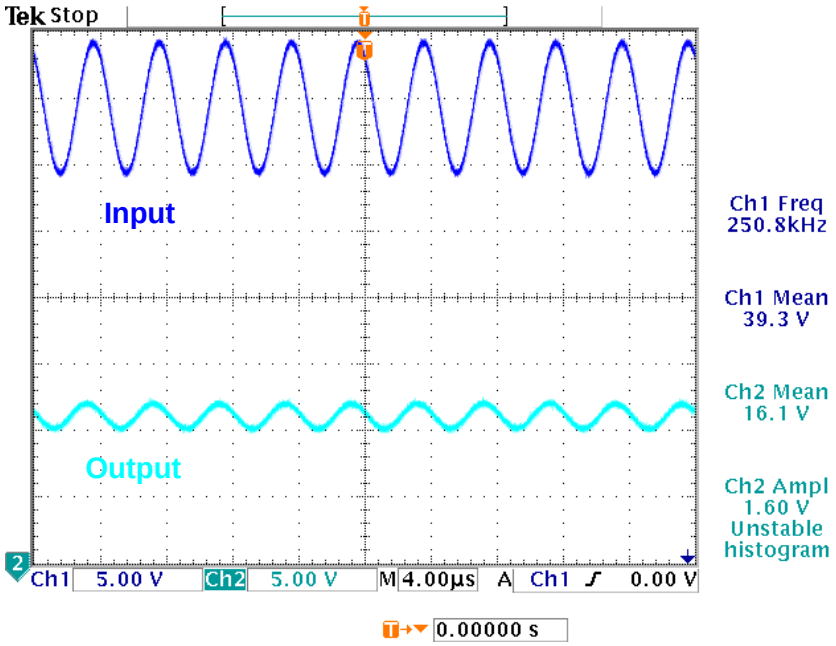

Figure 119: Input and Output of SiC JFET voltage regulator at 450ºC

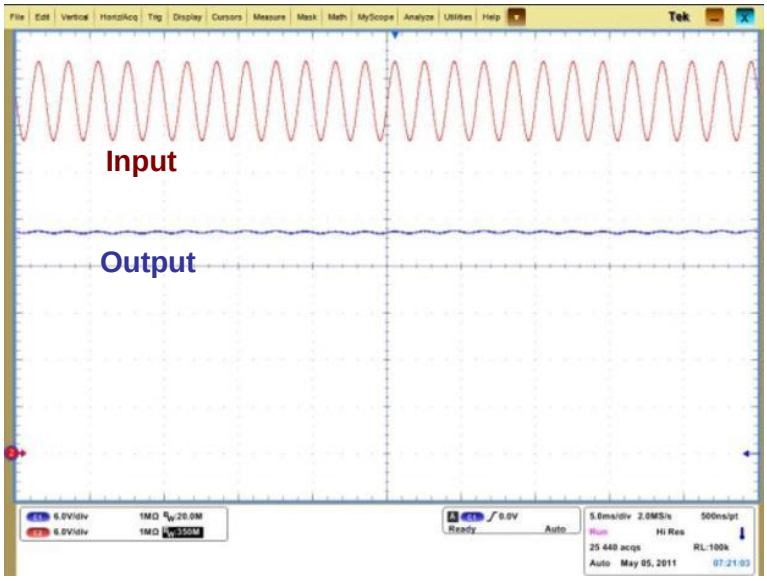

Figure 120: Input and Output of SiC Zener Diode Voltage Regulator at 450°C

Unfortunately, the 1st generation Zener diodes could not be utilized in telemetry boards, because their bond pad metallization proved incompatible with the telemetry board construction. Berkeley delivered their 2nd Generation Zener diodes to APEI. Their construction was coordinated with APEI to ensure the bond pad metallization was compatible with APEI's board construction methods. These Zener diodes will very likely be incorporated into the next generation of the electronics boards (outside time frame of this project.)

Harsh Environment Piezoelectric Energy Scavenger

Berkeley fabricated functioning piezoelectric, high temperature diaphragms for use in energy scavenging devices. They subjected these diaphragms to pressure pulses with the same amplitude, period, and width of pressure pulses seen in Siemens gas turbines. Currently, the resonant frequency of the devices is higher than the period of the engine pressure pulses, resulting in relatively low resonance. However, direct measurements of power induced have been made for non-resonant situations, and significant increases in power have been observed. These devices currently could not be used to produce the power needed to drive the wireless telemetry circuit board, but significant progress is being rapidly made on this energy scavenging project. Once the resonant frequency is made to match the pressure pulse frequency, the output power will scale with the resonant factor (Q-factor). Higher Q-factors are expected, which may result in a functional energy scavenging device capable of producing sufficient power in the space available in a gas turbine.

In late 2012, a new design of the pressure-wave energy scavenging device was implemented. The device was subjected to pressure waves in the 1-2kHz frequency range at pressures near 2 psi. Energy transfer was seen at these frequencies and pressures, which are relevant to the environment within a gas turbine hot gas path. Additionally, temperature testing up at 30^{o}C, 162^{o}C, and 320^{o}C was performed. The energy transferred degraded by half at 162^{o}C, but the recovered to the room temperature levels at 320^{o}C. This indicates that while the design is temperature dependent, it may be possible to optimize it for different temperature operating points.

In early 2013, the pressure-wave energy scavenging device was characterized. The device was subjected to pressure waves in the range of 630Hz at 50% and 20% duty cycles. The resonance frequency of the transducer is approximately 13kHz, so the energy transfer was not optimal. The expected duty factor in a gas turbine engine is, however, expected to be far from 50%, so this test is an important testing milestone. Figure 121 shows the results of varying the duty factor from 50% to 20%.

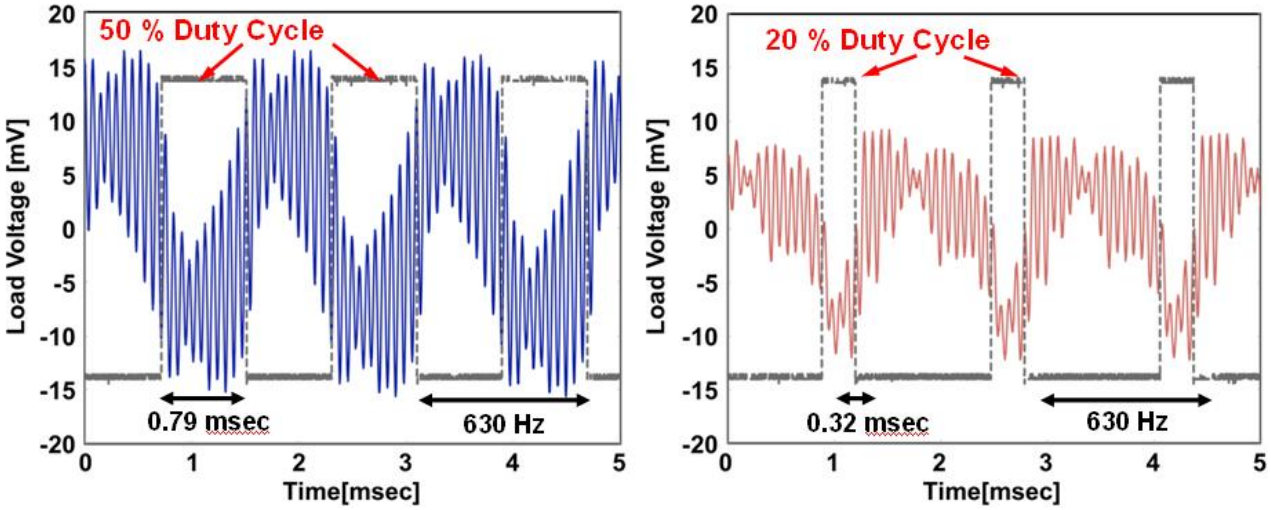

Figure 121: Energy Harvester Transduction at Different Duty Cycles

An effort was then made to lower the resonant frequency of the energy scavenging devices. To lower the frequency to the optimal range of 1-2kHz, the diaphragm must be made less stiff. Different ways to accomplish this are underway, but each of them involves weakening the outer edge of the diaphragm. Testing has shown that this affects the manufacturability and robustness of the devices.

In late 2013, the pressure-wave energy scavenging device was further characterized at pressure wave frequencies realistic to the interior of a gas turbine. The device was subjected to pressure waves in the range of 1 kHz at 50% and 20% duty cycles at pressures expected in a gas turbine engine. The devices were connected to a rectifier circuit (see Figure 122).

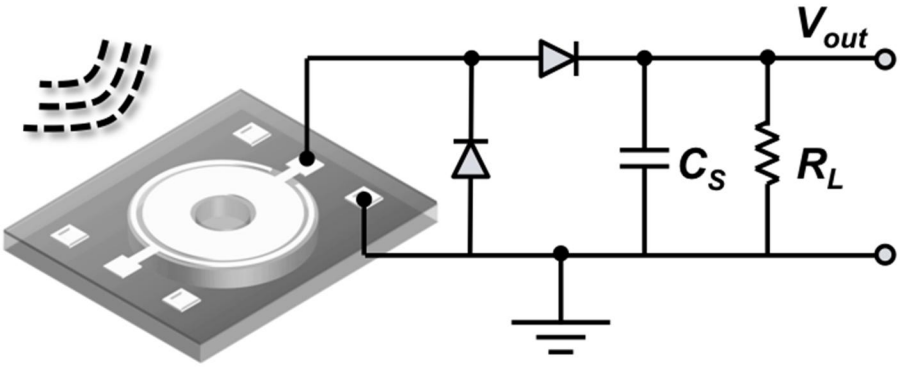

Figure 122: Rectifier Circuit Connected to Pressure Energy Harvester

The energy scavenger devices tested are in the size range of ~ 1mm^2. As seen in Figure 123, the energy per device at room temperature was on the order of 1μW. Thus, the maximum possible energy density for a reasonably sized energy harvester bank of the size of 100 square cm is about 5mW. Currently, the Q is measured at about 160. In order to replace the current power induction system, the efficiency of this system would

need to increase by a factor of 25, and needs to be further demonstrated at higher temperatures.

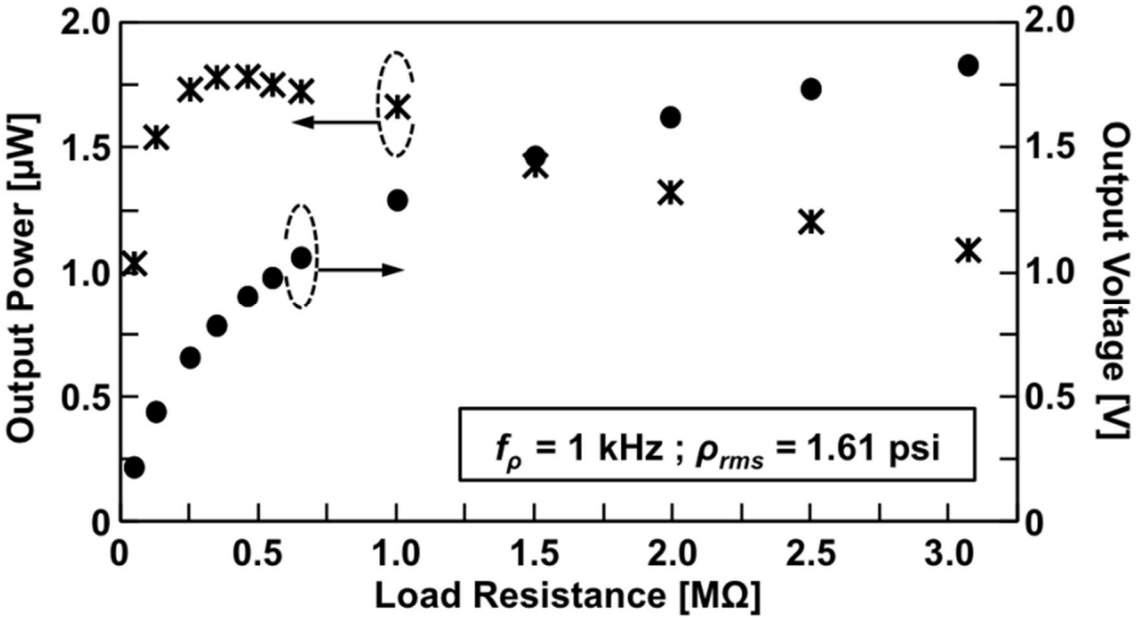

Figure 123: Energy Harvester Efficiency

Simulation of proposed designs of the high temperature silicon carbide pressure energy scavengers was also completed. New designs were compared in an advanced simulation environment, with a focus on the maximum allowable stresses and their impacts on power density (microwatts per centimeter). Power densities were calculated to exceed 250 µW/cm^2. The simulated power densities assume a quality factor (Q) of 1. Q acts as a linear multiplier of power density, and expected actual values of Q exceed 200. The power densities of the next build may, therefore, exceed 50mW/cm^2.

A significant discovery was made by the University of California at Berkeley that may increase the power scavenging by several fold. By etching the sidewalls of the cavities at an angle less than 90º (see Figure 124), lower resonant frequencies, higher vibration quality factors, and higher stress thresholds can be realized. Figure 125 shows the estimated power enhancement factor, which looks to be a factor of seven at reasonable etching dimensions.

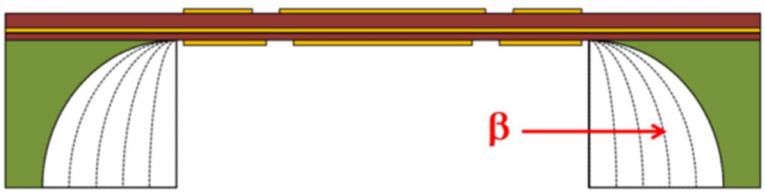

Figure 124: Sidewall Etching Angles Under a SiC Pressure Transducer

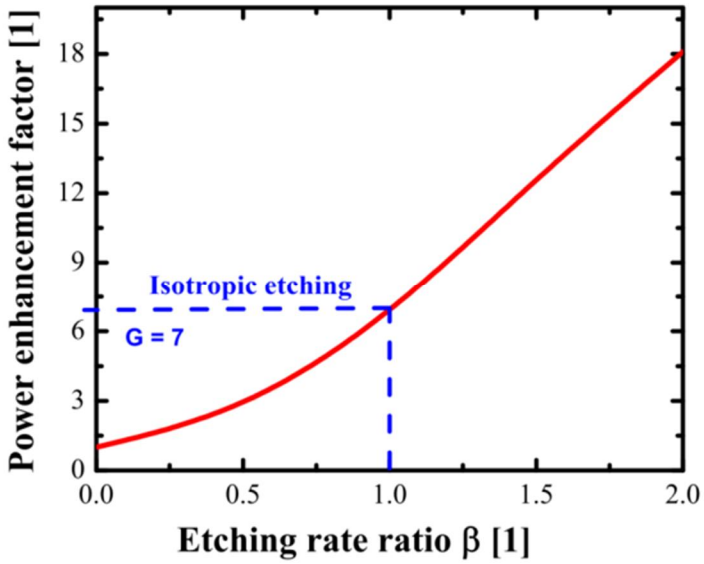

Figure 125: Effect of Sidewall Etching on Power Enhancement Factor

Multiple sets of characterization revealed a wider principle of frequency optimization for these silicon carbide energy scavenging devices. It appears that the most efficient target frequency is approximately 0.7 of the device resonant frequency. This is an unexpected, but welcome result. Due to size and stress limitations, it is difficult to make devices which are large enough to have low frequency responses on the order of 1-3 kHz, which is optimal for in-engine energy harvesting. But this realization of the optimum frequency being 0.7 of the resonant frequency, along with the gains realized by the angling of the cavity walls, brings this technology closer to practical utility.

PN and Schottky Diode Rectifiers

Silicon carbide diodes are useful devices that can be used in the wireless system electronics boards as rectifiers for transforming the AC voltage produced by the inductive power system into the DC voltage required to run the instrumentation and RF electronics. Berkeley is currently fabricating silicon carbide diode rectifiers of multiple sizes and types (PN diode rectifiers and Schottky diode rectifiers) in order to find the best possible performance over temperature. Figure 126 shows the devices approximately halfway through the fabrication process. Working rectifier devices were not realized during the timeframe of this project.

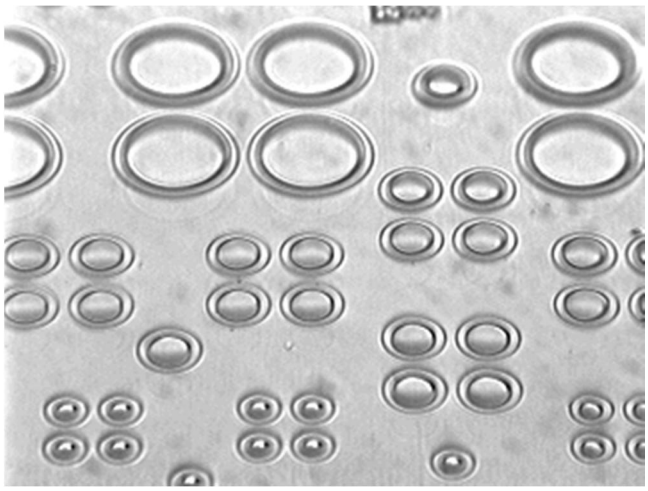

Figure 126: Silicon Carbide Rectifiers Under Fabrication

Silicon Carbide Transistors (JFETs and BJTs)

Significant progress has been made by the University of California at Berkeley, in partnership with Siemens, in silicon carbide JFETs and Bipolar Junction Transistors (BJTs). These devices being developed by Berkeley are in the early prototype stage, but many fabrication hurdles have been overcome on the last two years. High temperature p-type and n-type contact metallization were developed, and difficulties in reliably etching silicon carbide were overcome. Siemens, as the major funding source for this effort, shared target parameters with the Berkeley team in hopes of producing devices which can be incorporated into existing high temperature instrumentation, such as the wireless telemetry board in this project. Berkeley's production of both p-type and n-type JFETs, if accomplished, will be a boon to the effort toward miniaturizing the wireless telemetry board. Much more electrically robust, simpler, smaller circuits can be designed if both p-type and n-type JFETs are available. Additionally, Berkeley's approach will allow both devices to be integrated into one die, decreasing related circuit sizes by an order of magnitude over current technology. The BJT technology would also allow for significant reduction in size, especially for analog aspects of the circuitry.

In early 2012, Siemens initiated contact between APEI and the U. C. Berkeley team to ensure that the parameters of the Berkeley devices would be useable in future APEI wireless telemetry boards. A significant amount of guidance was provided to Berkeley concerning the device parameters, especially for the junction field effect transistors and bipolar junction transistors. Conversely, APEI gained significant knowledge of the potential capabilities of Berkeley's devices along with existing device test results, which may significantly impact future wireless telemetry board design.

In early 2013, new fabrication runs of the integrated SiC JFETs were tested. The sample appeared very rough after the contact metallization annealing was performed. Electrical tests showed that device contacts were very high in resistance, effectively making all the n-type JFETs inoperable, along with the majority of the p-type JFETs. In order to

overcome this new obstacle, a thermal cap is being investigated which will be deposited over the contact metallization during subsequent fabrication runs. The next fabrication run with this new thermal cap was completed in mid-2013

In the late summer of 2013, full device characterization of the latest fabrication runs of the N-type SiC JFETs were completed up to 600°C. At this temperature, gains up to 86 were achieved, with an off resistance better than 800kΩ. This is superior to other known 600°C devices. Still, a challenge remains in producing a device with a stable gain over temperature, which would be preferable for instrumentation projects. The gain reduces by 85% between room temperature and 600°C, and the off-state leakage current degrades from 10^{-9} to 10^{-7} amps (smaller is better). While this variation is not ideal, it can be dealt with via system calibration. More importantly, 90 hour aging tests show that the transconductance (another measure of gain) does not degrade significantly at 540°C as shown in Figure 127.

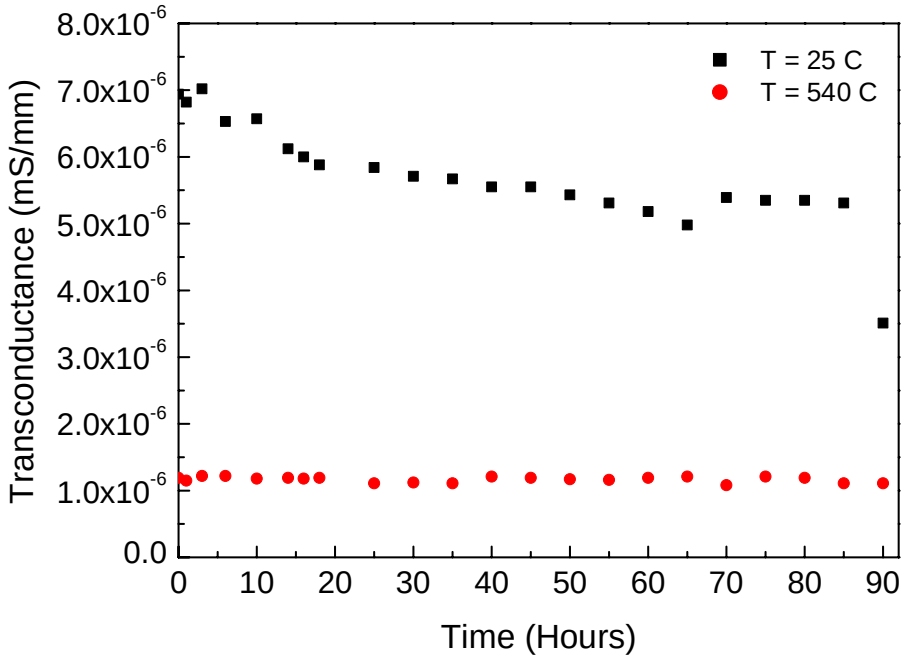

Figure 127: N-Type JFET Transconductance Over 90 Hours at 25 °C and 540 °C

In spring of 2013, a run of SiC BJTs were characterized. At room temperature, a gain of 5600 was achieved. Unfortunately, current gain at high temperature was inhibited by the presence of interface defects between silicon dioxide (insulator) and silicon carbide (semiconductor) interfaces. The presence of these interface defects strongly affected the gain of the transistors, reducing the current gain from an expected value of greater than 100 to an actual value of less than 15. A literature review showed that these interface defects can be neutralized by performing high temperature annealing in a 1000ºC nitrogen-rich environment. This must be done during, not after, the fabrication process. A new mask was being designed, and the next fabrication run was the following months.

Tests on that second generation of silicon carbide bipolar junction transistors (BJTs) show promise. Testing up to 400ºC showed relatively stable current-voltage curves (see Figure 128). These devices can be used in many (but not all) of the places currently planned for the JFETs in the wireless telemetry boards.

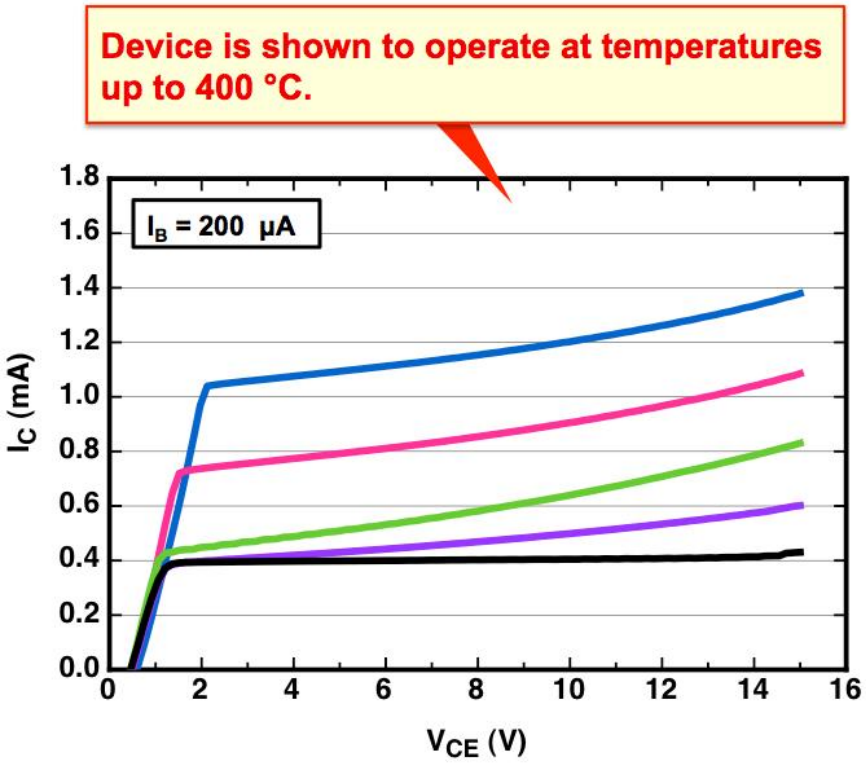

Figure 128: I-C curves of SiC BJTs Over Up to 400ºC

2.6 - TASK 6: SYSTEM INTEGRATION AND VALIDATION TESTING RESULTS

Task 6 prepares and perform demonstration test of the system components. Siemens target was to install components in an H-class engine. Design reviews were held to allow installation of stator and rotor components in the H-Class Berlin test engine. In parallel with the H-class installation execution, Siemens organized Technology Readiness Level (TRL) 5 level spin tests of individual wireless telemetry components and integrated systems. Details of spin test and H-Class validation activities accomplished are described below.

Spin Tests of 1st Generation Wireless Power Induction System

In order to perform high temperature, high g-load spin testing, Siemens contracted the services and facilities of Aerodyn, Inc. They have the capability to subject test articles to g-loads exceeding 20,000G while simultaneously exposing them to temperatures above 450°C (Figures 129 and 130). This test rig simulates well the 14,500g, 450°C engine environment.

Figure 129: Aerodyn Spin Rig

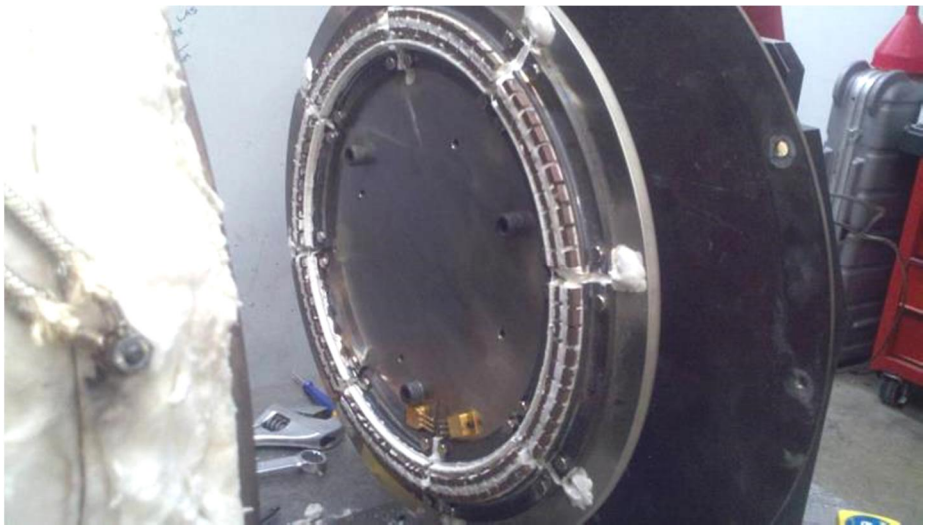

Figure 130: Aerodyn Spin Rig, Showing the Stationary Power Inducing Stator Ring

Extensive testing of individual components was accomplished. Tests that are executed on functional components are referred to as "functional spin tests." Other tests were performed to examine structural integrity, but not functionality. These tests are referred to as "mechanical spin tests." In some of thesis cases the functionality of the test article is tested before and after the spin test, but not during that test. The results of spin testing and how it was used to improve the design of individual components were described in prior sections.

The spin tests were instrumental in defining the developed status and needs of components of the wireless system. Table 16 summarizes the spin tests that occurred before the major system redesign of the power induction system that began in February 2012.

In order to perform fully functional integrated spin tests, a special stationary power-inducing stator ring was created for the Aerodyn spin test (shown in Figure 130). This allows the rotating power receiving antenna to wireless provide power to the rotating wireless telemetry circuit boards. This test is the closest simulation to an engine test possible. Such a test was attempted in January 2012. For the first time, RF telemetry was received from wireless-powered telemetry boards at full g-load.

Before the temperature could be ramped up, unfortunately, wire issues external to the rotating power-receiving antennae occurred. The g-load caused wires to break on the blade bracket. Other wire break issues occurred at the pins of the wireless telemetry circuit board. Repairs were attempted, but subsequent tests showed wire connections degraded significantly, and testing was discontinued. Investigations showed that the wire breaks at the rotating power-receiving antennae were caused by issues with the method used to bond the antenna's wires to the blade bracket. The methodology of crafting these seal plate connections was later improved. The spring 2014 spin test validated these improvements, as described near the end of this section.

Date	Rotating Antenna	Telemetry Board	Mechanical Only	Functional Test	Results/ Accomplishments
4/27/2011	X	X		X	- Cracked Telemetry Board - Cracked Rotating Antenna - No functionality after 4000 rpm
4/29/2011	X	X		X	- Telemetry Board non-functional, but did not crack @ 12,000g & 400C - Rotating Antenna functioned partially at 12,000g & 400C, showed cracking
6/1/2011		X	X		- Four telemetry boards all passed mechanical test at 12,000g and 450^{o}C, no cracking.
7/1/2011		X		X	- Thermocouple telemetry board non-functional before test - Stain gauge telemetry board functioned for 1.5 hours at 12,000g & 450^{o}C, then experienced lifted wire bond.
11/5/2011	X	X	X		- Two redesigned rotating antennae passed mechanical spin test at 14,500g & 450^{o}C - Two telemetry boards experienced minor bond wire lifting during same test; functioned nominally after bond repair.
1/31/2012	X	X		X	- Four rotating antenna survived 14,500g & 450^{o}C test, though external wiring failed. - Two telemetry boards functioned at 14,500g, then experienced external wire failure - Two transmitter boards experienced inductor delamination and loss of function. - Telemetry boards not tested at temperature due to external wire failures

Table 16: Summary of Spin Rig Tests Occurring Before System Redesign in February 2012

Installation of System into H-Class Gas Turbine

Early in this project, the wireless system was installed into an H-class engine. Siemens prepared all drawings and specifications for a wireless component test in an H-class engine located in Berlin. Extensive design reviews were held on stationary and rotating components. The design reviews passed and approval was granted to install the wireless components in an H-class engine. The schedule developed was to install the stator components in December 2010, and the rotor components would then follow with an installation in spring to summer of 2012. Stator elements were successfully installed. Unfortunately, after installation design validation tests exposed that the initial stator designs were limited in their ability to transmit adequate power at temperatures above 250^{o}C. Nonetheless, we monitored used the installed stators and their performance during engine validation testing. As the H-class engine operated over various design points, the stator instillation degraded to the point that we knew we could not transfer power with them and use then in the wireless validation tests. H-Class validation testing with these components was, therefore, discontinued and we proceeded to redesign the power induction system.

Failure of the 1st Generation Power Induction System

Stator components were installed in the H-class engine. As this engine began to be run at full temperature in September 2011, however, issues began to arise with the stationary components of wireless system. The power inducing stator degraded at temperature and could not transmit power.

The first issue with the installed H-class power inducing stators was actually an issue with the high-temperature power wire. The insulation on this wire failed at high temperature and vibration, causing the power from the external power supply to be shorted to engine instead of supplying the stators. Upon repair of this wire, further engine activities occurred, followed by further stator electrical tests. Those tests showed further degradation of the stators. Boroscope inspections revealed significant damage to those stator pairs (Figure 131).

The cause of the damage is unknown; it may be foreign object debris damage or the result of high temperature and vibration. It was not possible to repair this damage or replace the non-functional stator pairs. Two RF telemetry antennae are embedded in the stators. Each stator's RF antenna is connected to adjacent stators such that each RF telemetry antenna spans three or four stator pairs. Boroscope inspections showed that both installed RF telemetry antenna were damaged and could not be repaired. Without functional RF telemetry antennae, no sensor data could be obtained from the wireless telemetry system.

Figure 131: Damage to Installed Power Inducing Stator Segments

The wire breaks on two of the stator pairs result in those two stator pairs being completely non-functional. As the rotating power-receiving antenna swept past those stator pairs, its received power drops to zero, and then goes back to higher levels as it sweeps past the remaining functional stator pairs, as illustrated in Figure 132.

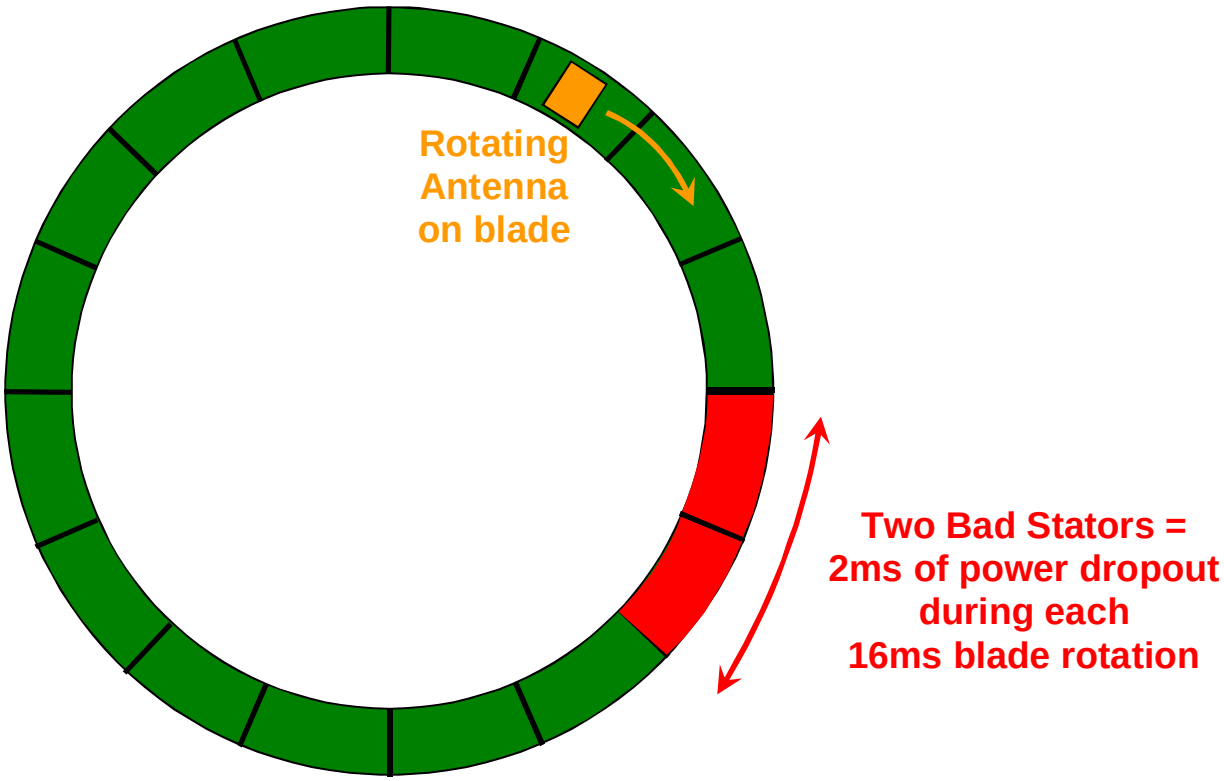

Figure 132: Impact of One Non-functional Stator Pair on Power Induction

This rapid, 60 Hz ringing in the power going to the wireless telemetry board would overwhelm its power conditioning circuitry, allowing the ringing to manifest itself at the output of the power conditioning block. Simulated data from APEI shown in Figure 133 indicated that an unacceptable amount of voltage ripple is induced at the output of the rotating antenna. This high voltage ripple strongly interferes with the function of the wireless telemetry board.

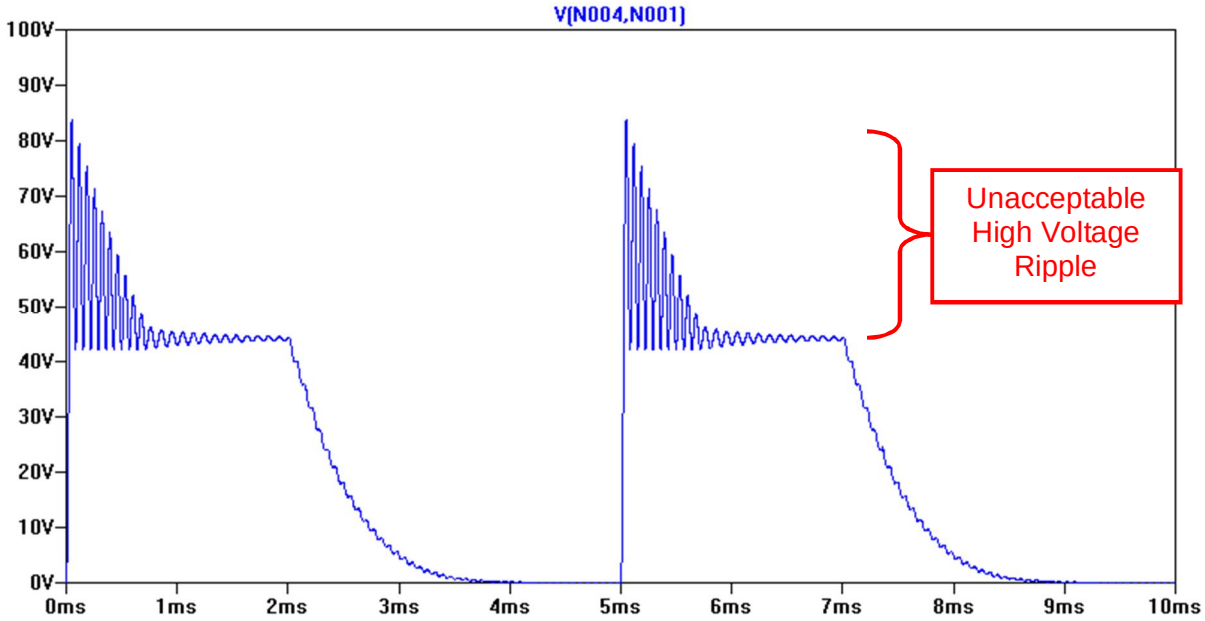

Figure 133: Circuit Simulation of Power Regulation Circuit

The output of the power conditioning block should be a constant voltage, with no frequency components. These unwanted on-board frequency components making reliable sensor interfaces and RF modulation impossible. Additionally, the occurrence of multiple issues with the stators with only moderate engine activity implied that further issues were likely to occur. Table 17 summarizes the issues with the power-inducing stators and the high temperature power wire and the effects these issues had on the system.

Based on the impacts of the issues delineated above, the H-class engine test of the full wireless system had to be effectively cancelled. Because there was no chance that telemetry could be relayed from the rotating sensing system, the decision was made not to install the wireless telemetry board or the instrumented blades. Instead, further development was made in the wireless telemetry circuit boards in preparation for the next engine test. The strain gauge blades were to be instrumented with conventional strain gauges because the spray-on strain gauge technology was not deemed ready for engine test implementation. Once the issues were discovered with the stators, instrumentation of these strain blades was halted.

Issue	Impact on Test	Repairable?
Shorted Power Wire	Little or no power going to stators; wireless system becomes non-functional.	**Yes; Repaired**
Open Stator Power Wires & Coils	No power going to two of eight stator pairs; partial or total telemetry loss	**No**
Open Stator RF Antenna	No telemetry available from wireless system.	**No**
Risk of Future Wire Breaks	Unknown combination of above effects. Likelihood for further issues high.	**Unknown**

Table 17: Impact of Stator and Power Wiring Issues

At the time of the evaluation of the stator issues described in Table 17 above, one power inducing stator pair remained to be installed in the H-class engine. Because of the issues encountered with the other stators, this stator pair was instrumented with accelerometers and thermocouples in order to more accurately assess the environment in which the stators must function. This vibration and temperature data was used to set environmental specifications for further lab tests of redesigned components.

Siemens used the lessons learned from the initial stator design to develop a more robust second generation design, and we developed engine validation opportunities with smaller industrial engine frames to continue the development and validation of wireless components.

Delays in Full System Integrated Spin Test

Key components for the fabrication of the wireless telemetry boards experienced significant delivery delays. The new silicon carbide transistors were needed, and the boards were redesigned for robustness. Delays in the supply of redesigned telemetry boards and the second generation inductive power supply development significantly delayed the ability to perform an integrated spin test with the new wireless system.

Preliminary testing of the strain gage wireless telemetry board was completed in the fall of 2013. An over-temperature RF telemetry test was completed, and showed a signal-to-noise ratio of 15dBm at 400ºC. This is significantly better than the needed signal-to-noise ratio of 3dBm.

A full system spin test was planned to measure system robustness and accuracy in a fully simulated engine environment. Testing temperatures will reach 400ºC and g-loads will reach 16,200g. Table 18 below gives the two target environments, reflecting the environments of two different engine installation targets.

Parameter	Target Engine Environment 1	Target Engine Environment 2
Max Temperature	325ºC	400ºC
Max G Load	16,200g	14,500g
Vibration	15mm/s^2	15mm/s^2
Wireless Power Spacing	10-18mm	12-20mm

Table 18: Spin Test Environment Targets

Integrated Full System Heated Spin Test

In late 2013, a peer review was held on the designs for implementing this wireless system in a Siemens industrial turbine. This paved the way for the fully integrated heated spin test.

A full system spin test was performed in the spring of 2014. In this section, an overview of the testing is provided. Detailed performance of the electronics boards and the inductive power system are described in Section 2.3 and 2.4. Details of the spin rig experimental methodology are given in Sections 1.3, 1.4, and 1.6.

In the final, integrated spin test, two sets of seal plate assemblies were mounted on the spin disk. Each seal plate assembly is comprised of either the thermocouple or strain gage electronics board and a white rotating power antenna (see Figure 134). This spin disk is then connected to a slip ring, which allows electrical connections to be made from the spinning electronics boards to outside the rig. These connections were used to introduce simulated sensor signals to the electronics boards and to monitor their rectified received voltages. The electrical connection diagram of the seal plate is shown in Figure 135.

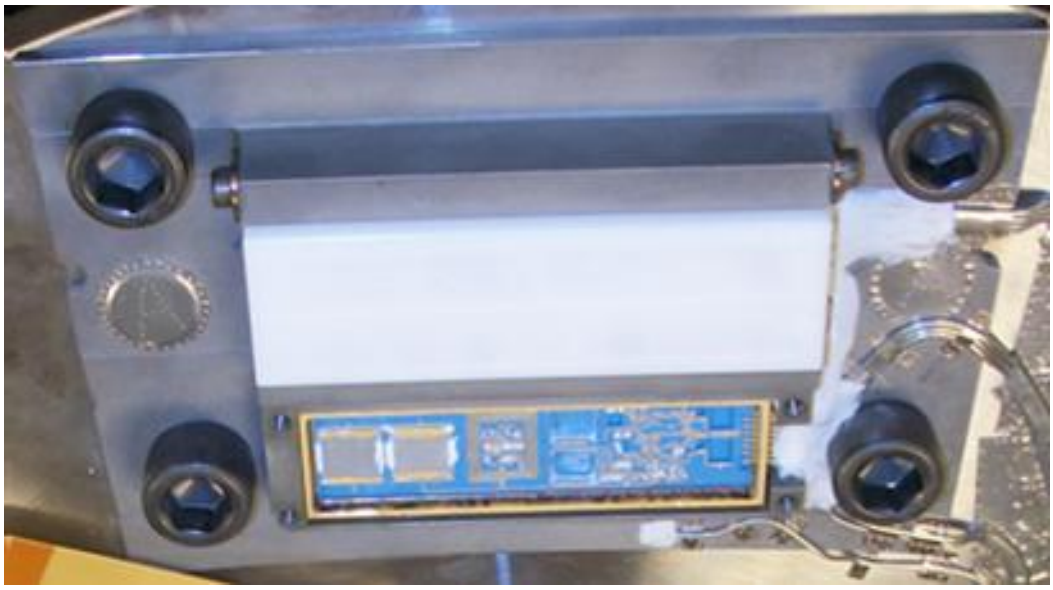

Figure 134: Seal Plate Assembly for Spin Test

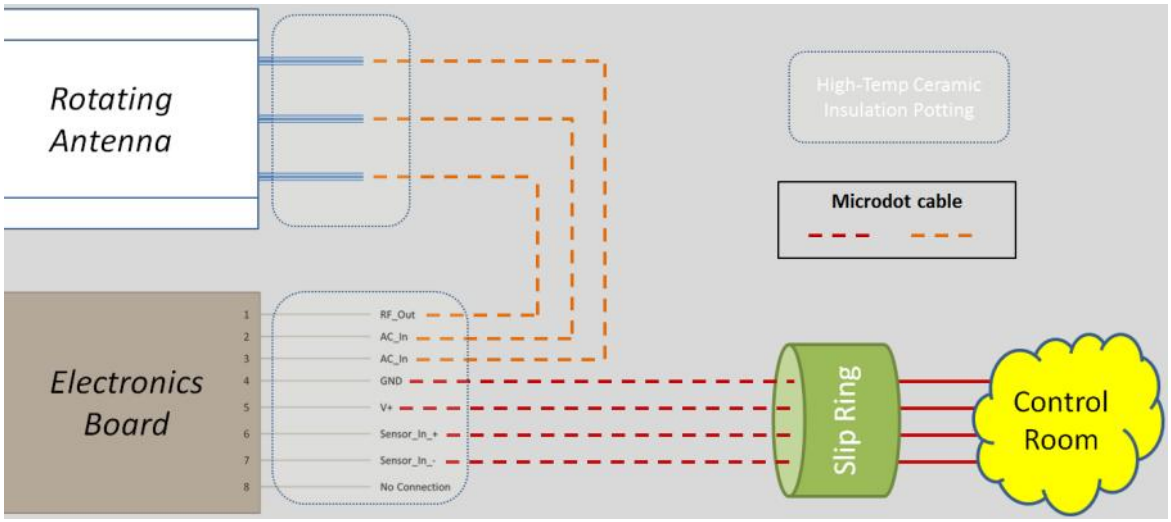

Figure 135: Seal Plate Assembly Connection Diagram

The power induction ring is mounted on the metallic ring of the spin rig, such that it faces the spinning disk. High temperature power cables and RF cables connect this power induction ring to the power electronics which drive the ring and the RF demodulation equipment which reads the data from the RF carrier. The power is supplied by an RF amplifier connected to a signal conditioning box which contains a transformer and a matching circuit.

Early in the test run large, fast power variations were seen. This is discussed in detail in Section 2.3. Recording equipment was used to recover demodulated data for the very short periods (several milliseconds at a time) of stable power.

During the first day of testing, the thermocouple board showed issues with modulation. It correctly produced the RF carrier signal, but its data was not modulated properly. The strain gage board functioned nominally. Both boards functioned at 350ºC with no spinning.

On the second day, the rig was heated to above 300ºC and then spun at increasing speed. At 3000rpm (1,500g), the strain gage board stopped producing an RF carrier. The TC board functioned nominally. The spin test was halted to resolve the strain gage board issues.

On the third day, the TC board was the focus, though the strain gage board was also still on the slip ring. During that test, the TC board functioned nominally up to an air temperature of 450ºC and a seal plate temperature of over 300ºC. The spin disk reached speeds of 4500rpm (3,200g), and the TC board stopped producing a carrier. Power to the ring was increased in hopes of providing more power to the board to cause the RF carrier to appear. Harmonics appeared on the RF line, indicating leakage of power from the power coils to the RF line. Testing was halted, and the ring was taken off the rig. As described in Section 1.4, a bad segment was discovered and replaced.

On the fourth and last day of testing, the strain gage board was powered via the slip ring. When this was done, the strain gage board functioned. While no RF signal was seen on the RF line, this signal was seen on the DC power line, and it could be modulated. Thus, the board was missing two functions: incoming power rectification, and final sending of the RF signal. As described in detail in Section 1.3, these were explained in post-test inspection by a burned out capacitor and an errant bond wire. The strain gage board stopped functioning completely at 1,500g that day. No further signal was seen from that board. In lab testing after the test, adding DC power to the board while removing the stray bond wire resulted in the production of an RF carrier on its RF output pins.

On the fourth day of testing, the thermocouple board functioned properly up to 1,500g and above 300ºC. It then stopped functioning until the g-load got to 10,500g. It then continued to function nominally up to 14,500g and 300ºC for an hour. At this point, another arcing even occurred in the power induction ring, and all testing was halted.

Detailed analysis of post-test inspections is included in Sections 1.3 and 1.4 of this report.

This spin test showed the best performance for this wireless system has performed. It is not yet ready for installation into a gas turbine engine, but the design concepts have been shown to function at full engine environment for an hour. Further refinements are required, along with subcomponent advancements (capacitors and silicon carbide transistors), but all these are possible in the short term.

For the first time, an electronics board was powered wirelessly, collected data, and transmitted that data wirelessly at 14,500g and 350ºC.

3. CONCLUSIONS

Conclusions for each task are described in the following sections, and that is followed by a summary of the project conclusions.

3.1 - TASK 1: DEVELOP CBM APPROACH FOR TURBINE BLADES

A methodology for implementing a Condition Based Monitoring (CBM) system based on using wireless sensors to obtain accurate point measurements of blade characteristics to calibrate existing global measurements was developed. For example,
IR camera and wireless point temperature sensors will be used to develop 2D blade temperature maps. Similarly, tip timing data will be enhanced with wireless strain gauge data to provide 2D strain maps of rotting blades. Existing 2D blade mapping software can be calibrated via the point sensors provided by this wireless blade monitoring system. Using this calibrated data, Remaining Useful Life (RUL) models that exist at Siemens can be improved with operational data input. These models are currently updated via global engine conditions and material and components computer modelling. The addition of empirical sensor data from the wireless telemetry system is expected to increase the accuracy of the component life monitoring system.

A method was also invented to interface the wireless blade monitoring system with the existing control and data collection system used by Siemens. Off-the-shelf technology can easily be integrated with existing control and monitoring systems to make this data widely available and useable for the above CBM and RUL systems.

3.2 - TASK 2: SCALE-UP AND MANUFACTURING OF SPRAYED SENSORS

Siemens successfully applied spray on thermocouple technology to large H-class turbine blades. The cost of these sensors is currently prohibited, however, and the accuracy is not as good as existing thermocouples. The lifetime of these sensors is, however, expected to be an order of magnitude higher than conventional sensors, so they have application advantages.

Spray-on strain gage sensors with acceptable resistive stability were not successfully realized. At this time, Siemens does not have the technology to implement a sufficiently functional spray on strain sensor.

3.3 - TASK 3: ROBUST 450^{O}C WIRELESS TELEMETRY CIRCUIT BOARD

Siemens and APEI demonstrated wirelessly powered, high temperature electronics that are capable of modulating a sensor signal onto a radio frequency carrier at higher temperatures (400ºC) than any other reported in literature. In addition, these electronics are capable of withstanding g-loads in excess of 14,000g and vibrations expected inside large gas turbines. This is a significant accomplishment and a unique milestone for harsh environment sensors and telemetry.

The lack high temperature capacitors and transistors inhibits the development of miniaturized, robust versions of these wireless telemetry boards. Based on surveys of vendors, it appears that these high temperature capacitors and transistors may be available in the next 6-12 months. When combined with the increased robustness of the integrated boards demonstrated in our spin testing, future electronic boards may become an economic and flexible option for instrumenting gas turbines for validation and long-term monitoring.

3.4 - TASK 4: ROBUST 450^{O}C WIRELESS TELEMETRY SYSTEM

Siemens created a novel, high temperature, high g-load, vibration-resistant wireless power system which is capable of functioning in the presence of grounded metal. We know of no other system that functions to temperatures above 300ºC; this system functions at temperatures up to 600ºC. The 20mm gap across which energy is transferred is many times larger than typical wireless power transfer gaps of 1-2 mm. It is a significant technological advancement to be able to transfer 500mW wirelessly across such a large gap, especially at these elevated temperatures.

The power receiver is capable of functioning at g-loads up to 15,000g continuously with no degradation. It ceramic, magnetically-transparent casing is unique in high g-load magnetic systems.

The electrical connections devised for this high temperature telemetry system are also unique. Based on compression and temperature-stable systems, these connections have proven to be long-term reliable in multiple vibration and temperature tests. They are also field removable and replaceable, and involve no soldering or brazing.

3.5 - TASK 5: ROBUST ADVANCED SILICON CARBIDE DEVICES

The University of California at Berkeley team made significant progress in high temperature Zener diodes that function to 450ºC. Independent component analysis at APEI indicates that these diodes are applicable for future generations of the wireless telemetry board. Using the Zener diodes may decrease board size by 30%, while also reducing the required input power by as much as 40%.

Progress was also made in the production of high temperature transistors, other diodes, and energy scavengers, but they are not yet ready for system integration. Berkeley appears to be a potential near-future source of integrated silicon carbide transistors that will enable financially feasible implementations of these devices into wireless telemetry boards and the wireless system as a whole.

3.6 - TASK 6: SYSTEM INTEGRATION AND VALIDATION TESTING

Early in this project, the first generation wireless system was installed in an H-class engine. Initial *in situ* testing indicated, however, that the engine environment damaged the power inducing stators beyond repair, so the test was cancelled. A full redesign of the wireless system was then accomplished during this program.

Following this redesign, extensive lab testing, including oven, vibration, and electrical testing was performed on each component of the system and the system successfully past TRL 4 criteria. Sub-component testing in ovens and spin rigs were also performed for parts of the electronics board and the power induction system.

A total of 16 spin rig tests were performed on the second generation wireless system and/or its subcomponents. The last spin test was a full system integrated spin test. During this integrated spin test, sensor data was wirelessly transmitted and recovered using an electronics board which was wirelessly powered. This entire system functioned properly at 350ºC and 14,500g continuously for one hour. Because the system did not exhibit sufficient durability, it did not meet the full TRL 5 requirements, and is not deemed ready for engine installation.

The unique accomplishment of wirelessly transmitting sensor signals across a 20mm gap via wirelessly-powered electronics operating at 350ºC and 14,500g validates this system approach, and shows the value of continuing the development of a wireless blade condition-based monitoring system.

3.7 - SUMMARY

In this project, Siemens developed an integrated wireless electronic system that can transmit sensor data from rotating gas turbine components across a 20mm gap at 350ºC and 14,500g for one hour. Two major component innovations were achieved. Arkansas Power Electronics, Inc. developed a high temperature electronics board capable of withstanding 14,500g and temperatures in excess of 350ºC. To supply power to this rotating wireless electronics board, Siemens developed a new wireless power transfer system. This wireless power system is capable of operating at temperatures up to 600ºC, that is more than 350ºC higher than existing commercially available wireless power transfer systems.

These wireless sensor systems were validated in extensive bench, furnace, vibration, and spin rig tests. A Technology Readiness Level 4 was reached, and all TRL 5 requirements were met except for long-term durability.

The high temperature wireless telemetry boards created for this project show the promise of high frequency silicon carbide electronics. Currently, these electronics are available only in single-transistor form, which makes too complex to be sufficiently durable. Integrated silicon carbide devices are expected to become available in the very near future, allowing for miniaturization and increased durability of these high temperature electronic boards.